MERGING SYNTHETIC AND NATURAL COMPONENTS INTO FUNCTIONAL POLYMER ZWITTERIONS

MERGING SYNTHETIC AND NATURAL COMPONENTS

INTO FUNCTIONAL POLYMER ZWITTERIONS

A Dissertation Presented

By

Le Zhou

Submitted to the Graduate School of the
University of Massachusetts Amherst in partial fulfillment
of the requirements for the degree of

DOCTOR OF PHILOSOPHY

May 2023

Polymer Science and Engineering

MERGING SYNTHETIC AND NATURAL COMPONENTS

INTO FUNCTIONAL POLYMER ZWITTERIONS

A Dissertation Presented

By

Le Zhou

Approved as to style and content by:

Todd Emrick, Chair

Reika Katsumata, Member

Shelly Peyton, Member

David A. Hoagland, Department Head
Polymer Science and Engineering

DEDICATION

To my friends and family

ACKNOWLEDGEMENTS

I sincerely appreciate Professor Todd Emrick for taking me as his student and for his mentoring throughout my way to Ph.D. The first email I got from you after being accepted into the group said, *Ph.D. work is not easy but is greatly rewarding when done with energy and focus*, and you have helped me to stay energetic and enthusiastic for my research with your continuous patience, encouragement and guidance throughout the highs and lows of graduate school. You provided valuable and creative scientific suggestions and supported me to try all different kinds of things, which led to this thesis work and my growth as a scientist. I am also truly grateful for the time you spent with me writing and editing the papers, which greatly improved my scientific writing and communicating ability. You have been the person I look up to for the past five years, and your work attitude and personality will continue to inspire me in my future career.

I would like to thank my committee members, Professors Reika Katsumata and Shelly Peyton. Thank you for your time and efforts to help me reach the Ph.D. milestones and providing valuable advice for this thesis work. I would like to thank the collaborators: Alexandria Triozzi and Dr. Zhefei Yang from the Emrick group, K.P. Sonu from the Peyton group in Chemical Engineering Department at UMass, Janelle W. Salameh and Shreya Kumar from the Figueiredo group at Purdue University, and Dr. James Quirk from the Washington University School of Medicine. I thank the Polymer Science and Engineering department for accepting me as a Ph.D. student and I appreciate the work from PSE staff that have made PSE an enjoyable environment to study and work. I would like to thank Dr. Weiguo Hu, Dr. Steve Eyles, and Dr. James Chamber for their great efforts keeping the NMR, Biophysical Characterization, and Optical Microscopy facilities running. I would also like to thank Professors Liming Jiang, Jun Ling and Binyang Du at Zhejiang University, who introduced me to polymer science and supported my application to PSE.

I appreciate the funding sources that have made this thesis work possible: the National Institutes of Health (AR069079 and CA196947) and Army Research Office (W911NF1910388).

I would like to particularly thank my friends Dr. Liz Stubbs and Dr. Hazel Davis. Thank you for your company in and outside Conte. Graduate school would be tough without the happy time spent with you and the constant care, support, and encouragement from you. Importantly, you have shown me the value of serving as active members of the community and being a positive and supportive team member. I would like to thank Chris Cueto and James Pagaduan for being my friends, and I really enjoyed the time we spent together in lab and office. I would also like to thank the Emrick group members, Dr. Cristiam F. Santa Chalarca, Dr. Ashlin Sathyan, Dr. Marcel Brown, Dr. Hyunki Kim, Hong-Gyu Seong, Eva Morgenthaler, Dr. Liz Stubbs, Chris Cueto, James Pagaduan, Dr. Zhefei Yang, Professor Akifumi Kawamura, Conny Meissner, Brian Montz, Deborah Snyder, Dr. Ryan Selhorst, Dr. Marcus Cole, Dr. Dylan Barber, Dr. Sarah Ward and Steve Rosa, for working together and supporting each other. I thank my friends Hsinjung Yu, Hao Wan, and Weiyue Xin, for spending time and exploring new things outside work with me. I would also like to thank my classmates Ipek Sacligil and Ria Ghosh for their care and encouragement. I would like to give a special thank you to my friend Dr. Xinning Zhang, for staying connected over the years and across the distance.

I would like to express my deepest love and gratitude to my family — especially my parents and grandparents for their endless love, care, understanding, and support.

ABSTRACT

MERGING SYNTHETIC AND NATURAL COMPONENTS
INTO FUNCTIONAL POLYMER ZWITTERIONS

MAY 2023

LE ZHOU, B.ENG., ZHEJIANG UNIVERSITY

M.S., UNIVERSITY OF MASSACHUSETTS AMHERST

PH.D., UNIVERSITY OF MASSACHUSETTS AMHERST

Directed by: Professor Todd Emrick

Polymer zwitterions represent an emerging class of materials with enormous potential to advance technologies closely related to people's lives, such as biomedical development and electronic applications. This thesis exploited innovative synthetic designs to incorporate useful functionalities into polymer zwitterions, particularly fluorinated and reactive groups, and successfully expanded their properties and applications. The core of this thesis relies on the development of novel fluorinated choline phosphate (FCP) monomers, in which the fluorocarbons are directly embedded into the zwitterionic moieties. These novel FCP monomers, in combination with conventional zwitterionic monomers and fluorinated monomers, allow the construction of a library of fluorinated polymer zwitterions with well-controlled compositions and architectures. The FCP polymers proved advantageous for applications ranging from 19F magnetic resonance imaging to fluid-fluid interface stabilization and antifouling coatings. The unique combination of fluorocarbon and zwitterions inspired further study to gain a deeper understanding of the surface properties of FCP polymers. Zwitterionic, FCP, and fluorinated polymer brushes were grafted from Au substrates using surface-initiated atom transfer radical polymerization, and comprehensive wettability and surface energies study

were conducted with these functionalized surfaces, with results demonstrating a distinct responsiveness of FCP polymers to the contacting fluid environment. Remarkably, these dynamic FCP coatings afforded similar or better resistance to protein fouling in comparison to conventional zwitterionic or fluorinated polymer-modified surfaces. Furthermore, the FCP polymers were used in a polymer-based DNA packaging system, which was built on previous work on DNA delivery in the Emrick group. The presence of FCP polymers imparted the DNA packaging system with desirable colloidal stability under biologically relevant conditions, partially screened the cationic charge that might cause cytotoxicity, and enabled the tuning of binding affinity for DNA. This polymeric vector formulation holds great potential to improve the safety and efficacy of gene delivery, which is currently the major challenge of field. In addition to fluorinated polymer zwitterions, novel reactive polymer zwitterions containing 1,2-dithiolanes and alkenes were synthesized and used to prepare hydrogels with strain-stiffening properties that are of interest for tissue engineering. Overall, this thesis successfully prepared an array of functional polymer zwitterions with unique designs that hold promise for imaging, therapeutic delivery, and coating applications. Importantly, the novel monomers and polymers established here inspire opportunities and interests to pursue the development of new materials and advance fundamental understanding of their properties.

TABLE OF CONTENTS

Page

LIST OF TABLES

LIST OF FIGURES

CHAPTER 1

INTRODUCTION: POLYMER ZWITTERIONS: FROM SYNTHETIC DESIGNS TO FUNCTIONAL MATERIALS

1.1 Polymer Zwitterions

Biocompatible polymers play an essential role in advancing medicine and biotechnologies. Such polymers maybe composed of natural materials and or may rely upon the ability of chemists to replicate or mimic Nature's functionalities with synthetic variants. As a result, polymers have become critically important components of materials in biomedical and pharmaceutical applications, with utility as therapeutic delivery vectors,[1] medical device coatings, and implantable structures.[2–4] Zwitterions, defined as inner-salts with equal numbers of oppositely charged ions within its covalent framework, are recognized as crucial components of biological systems. For example, phosphorylcholine (PC) lipids constitute the cell membrane surface, while betaine and taurine have important functions in metabolic activity and cell protection.[5,6] Synthetic chemists, inspired by these natural molecules and integrated zwitterionic moieties into synthetic monomers to create polymer zwitterions (Figure 1-1). The zwitterionic

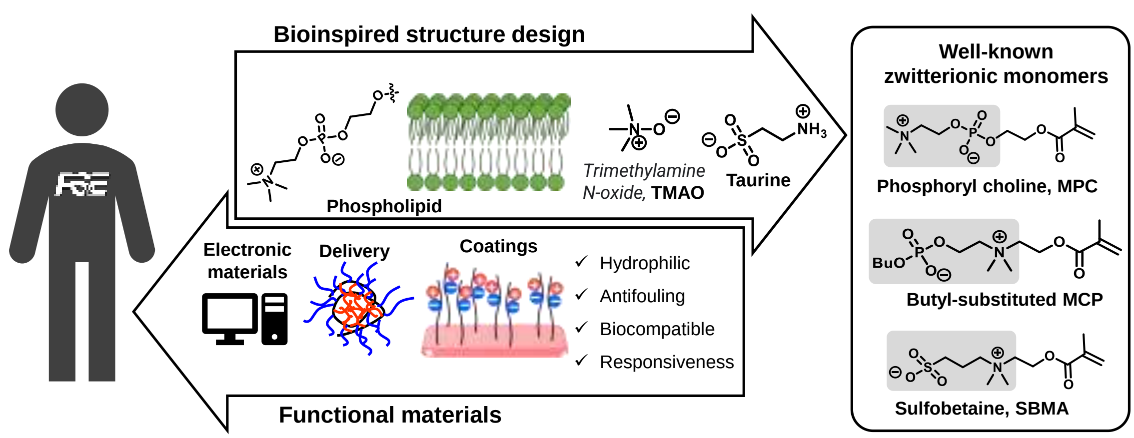

Figure 1-1. Bioinspired polymer zwitterions as functional materials.

structures confer a number of useful properties to the polymers, including substantial hydrophilicity, fouling resistance, and pH responsiveness, generating novel structures that comprise an important class of growing interest for bio-related applications.

PC, sulfobetaine (SB), and carboxybetaine (CB) represent the most commonly used zwitterionic moieties in polymeric structures;[7] indeed, just this three zwitterions comprises thousands of published papers focusing on the chemistry, physics, or material performance of polymer zwitterions. Zwitterionic polymers have been prepared in various forms, ranging from soluble linear polymers to crosslinked networks,[8] to nanoparticles,[9] to surface grafted brushes[10]. Moreover, detailed studies have been conducted with polymer zwitterions to probe their interaction with water, thus providing better understanding of their antifouling properties. Distinct from polyethylene glycol (PEG), which interacts with water *via* hydrogen bonds, the hydrophilicity of polymer zwitterions is attributed to ion-dipole interactions with water, forming a tighter and denser hydration layer at the polymer-fluid interface.[11] The hydration layer acts as an effective barrier against adsorption of proteins, cells, and bacteria, and since polymer zwitterions exhibit superior antifouling properties, they are considered promising materials for biomedical applications as alternatives to PEG. For example, Li, *et al.* reported that poly(carboxybetaine) (PCB)-conjugated proteins induced negligible anti-PCB antibodies, whereas quantitative correlation of anti-PEG antibody with immunogenicity of the protein was observed for PEG-conjugated proteins.[12] While many applications-oriented studies of zwitterionic polymers are still in the early stages, such promising outcomes speak to their potential for significant impact in medicine and pharmaceutical science. For example, Kawaguchi and coworkers grafted ploy(2-methacryloyloxyethyl phosphorylcholine) (PMPC) brushes on polyethylene (PE) surfaces by photoinitiated polymerization, and this technology is used to modify the PE surface of hip acetabular liners of the joint replacement product, Aquala®. The hydrophilicity of PMPC brushes greatly enhances the lubricity and wear resistance of this implant.[13,14] Recently, Zhang *et al.* showed that poly(carboxybetaine acrylamide) (PCBAA) afforded better prevention of post-operative adhesion of the injured sites relative to Interceed (oxidized regenerated cellulose; FDA-approved solid antiadhesion films; Johnson & Johnson) in three challenging clinically relevant models.[15]

The library of polymer zwitterions continues to expand by employing new anion/cation species, varying separation distances between charged moieties, and differing dipole orientation (Figure 1-2).[16,17] Some of these novel structures exhibited superior antifouling properties compared to conventional polymer zwitterions, while others generated new features. For example, Li, *et al.* described trimethylamine *N*-oxide (TMAO)-based zwitterionic polymers, which achieved ultralow protein fouling against undiluted blood plasma (<0.3 ng/cm^2).[18] In another example, polymers containing sulfonium sulfonate zwitterions were reactive and showed strong interzwitterion interactions, such that sticky droplets and droplet-based fibers could be produced.[19–21] More recently, Brown, *et al.* presented the first example of phosphonium-containing zwitterionic monomers, with tunable solubility of the resultant polymers (in water and

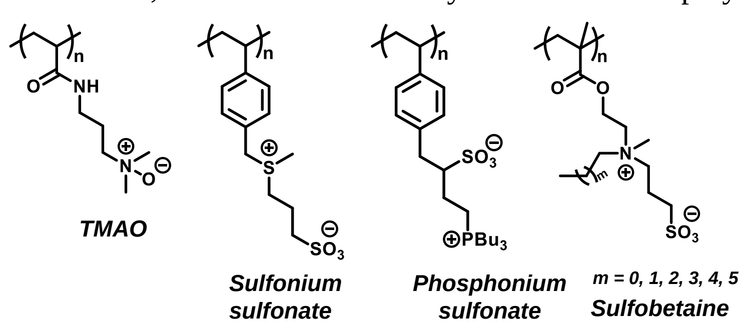

Figure 1-2. Recently developed new polymer zwitterions.

organic solvents) enabled by selection of the substituents on the phosphonium cation.[17] Additionally, the impact of spacer length between the charged groups, substituents on the cations, and dipole orientation on solution behaviors and antifouling properties were described for SB based polymers.[22–24] Overall, the chemical versatility of polymer zwitterions offers a platform to examine new structures and construct advanced materials, with even further potential realized when merging with other types of chemical structures, opening opportunities for widespread of implementation and technological breakthroughs.

1.2 Synthetic strategies to functional polymer zwitterions

A variety of synthetic strategies have been employed to incorporate reactive and stabilizing moieties into polymer zwitterions, all of which rely on the development of novel monomers and initiators, as well as advanced polymerization techniques (Figure 1-3). Progress in polymer chemistry has introduced numerous monomers that are available commercially or can be prepared readily at an appreciable scale, and which enable control over the composition and architecture of polymer products, such as by controlled polymerization techniques and especially atom transfer radical polymerization (ATRP) and reversible addition fragmentation chain transfer (RAFT) polymerization.[25,26] Therefore, copolymerizing zwitterionic monomers with other functional monomers presents a convenient and common method to synthesize functional polymer zwitterions and has yielded materials with applications spanning both the biological sciences and electric materials. For example, Pagaduan, *et al.* prepared copolymers consisting of methyl methacrylate (MMA) and sulfobetaine methacrylate (SBMA) units, which as polymer films modulated the work function of graphene; moreover, incorporation of benzophenone units enabled spatial control over work function using lithographic patterning techniques.[27] When incorporating reactive groups, the polymers can be further converted to impart desirable functionalities including crosslinks and therapeutic molecules, *via* post-polymerization modification or even during polymerization, offering a route to incorporate structures not normally compatible with polymerization conditions. For example, Chen, *et al.* synthesized PMPC-doxorubicin and PMPC-camptothecin prodrugs by one pot ATRP/click chemistry, where the presence of CuBr enabled polymerization also induced TMS-deprotection, liberating alkynes for cycloaddition with azide-modified drugs.[28,29] In another example, post-polymerization reaction of dopamine and polycyclooctenes containing PC units and pentafluorophenyl esters yielded polymer zwitterions functionalized with catechol groups. When these polymers were employed to stabilize fluid droplets, they exhibited an unusual property to transport nanoparticles *via* a "pickup and drop-off" process under fluid-driven flow.[30]

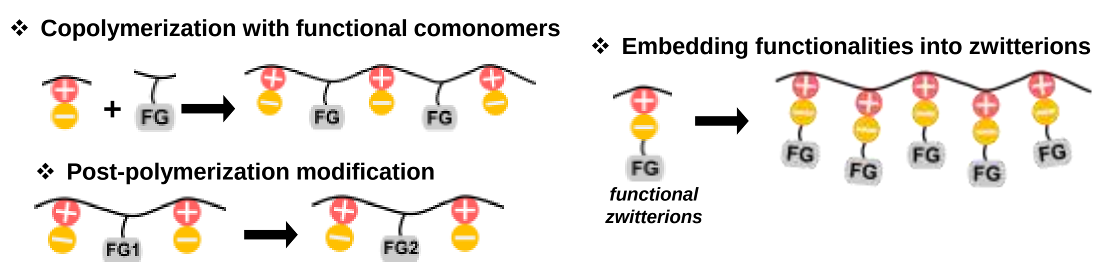

Figure 1-3. Examples of synthetic strategies to achieve functional polymer zwitterions.

In addition to having the zwitterionic unit and functional groups in separate monomer units of the polymers, an alternative design is to embed functionalities directly into the zwitterionic moieties, which can be achieved by 1). post-polymerization modification and 2). synthesizing novel functional zwitterionic monomers. The later approach is the only feasible route to 100% functional group incorporation and effectively combines the properties of each structure. In one example, Chang, *et al.* synthesized allyl substituted 1,3-propanesultones, which reacted with dimethylamino ethyl methacrylate (DMAEM) to yield SBMA containing unsaturated pendent groups. Homopolymers made by RAFT polymerization of allyl-functionalized SBMA were aqueous soluble and distinctly salt responsive with respect to surface activity, whereas copolymers of SBMA and n-butenyl methacrylate showed no salt-responsive behavior.[31] While incorporating functional groups into the chain-end quaternary ammonium group of PC structures is not trivial, the choline phophosphate (CP) structure (i.e., an inverted PC), opens opportunities to achieve such structural variability and therefore has been examined in several studies. Functional CP methacrylates (MCPs) are prepared by ring-opening of substituted cyclic phosphates with DMAEMA giving access to MCPs with methyl, n-butyl, and n-butenyl substituents on the phosphate group. Polymers prepared from methyl substituted MCP purportedly induced aggregation of red blood cells (RBCs), whereas MCP polymers (polyMCP) with n-butyl pendant groups caused no such RBC aggregation.[32,33] Moreover, polyMCP with n-pentenyl or alkynyl groups provided accessibility to material crosslinking and drug conjugation, and the alkenes can be converted to other functionalities such as epoxide and halogenated groups.[34] Notably, the ring opening reaction of the cyclic phosphate with DMAEMA can occur through an exocyclic pathway that produces salt byproducts, or an endocyclic pathway that gives the desirable MCP monomers. The substituents on the cyclic phosphates largely determine the preference of the reaction pathways as discussed further in Chapter 2.[33]

These synthetic strategies have generated a number of functional polymer zwitterions, each of which possess their own potential advantages. *Copolymerization of* *zwitterionic monomers with other functional monomers* provides a facile route to expand the library of available polymer structures with readily available monomers, though some structures may not tolerate specific polymerization conditions. *Post-polymerization modification* confers a route to include structures incompatible with polymerization conditions; however, limited solubility of polymer zwitterions may constrain the variety of applicable chemistry and the degree of functionality is unlikely to be controlled as precisely as in copolymerization pathway. Importantly, *directly attaching organic functional groups to zwitterionic moieties* provides access to novel structures that retain the features of zwitterions and presents new opportunities to advance application areas. As will be described, my thesis work employed PC, CP, and SB-based polymer zwitterions, using synthetic strategies that yield a series of new polymers, and hydrogels, and surface coatings.

1.3 Fluoropolymers: biological utilities and remediation

A major part of this thesis examined the synthesis and properties of novel fluorinated polymer zwitterions (FPZs). To date, fluorinated polymers have been instrumental materials in a myriad of technologies, ranging from fluoropolymers such as Teflon™ and Nafion™, to polymers with fluorinated side chains. This class of polymers includes those that fall into per- and polyfluoroalkyl substances (PFAS) category and which have come under scrutiny for environmental and health concerns.[35,36] Nonetheless, fluorination has been found to be an essential component of materials design for a number of biological applications, including molecular imaging, therapeutic delivery, and tissue engineering.[37–40] For example, ^{19}F magnetic resonance imaging (MRI) is a powerful technique in preclinical biomedical research and can complement ^{1}H MRI to enhance diagnostic capabilities.[37,41] Perfluorocarbon (PFC) emulsions used today as ^{19}F MRI probes have disadvantages regarding stability, heterogeneity, and *in vivo* accumulation.[42] Polymeric MRI agents can overcome these challenges, with added advantages that include targeting and drug moieties for therapeutic purposes. However, aggregation of fluorocarbon groups in aqueous environments may attenuate the desired signal and thus require new designs to improve the aqueous solubility of fluoropolymers.[37] In addition, amphiphilic fluorinated polymers can stabilize PFC emulsions, making them useful for ultrasound imaging and as artificial blood substitutes.[43,44] Remarkably, several reports on fluorinated polymers for gene delivery show preservation of efficient delivery and transfection in the presence of serum, attributed to their ability to resist protein adsorption, and thus enhancing cell uptake and endosomal escape, while influencing the binding strength with DNA. [45–47] However, the authors note that the detailed mechanisms of polyplex internalization, and polymer-DNA interactions, requires more detailed investigation.[42]

As research continues to reveal the importance of fluoropolymers for a breadth of essential applications, concerns over the accumulation of PFAS in animals and humans are escalating, and significant effort is now devoted to discovering methods to eliminate PFAS from environment.[48] Methods employed today to remove PFAS from water include treatment with granular activated carbon, ion exchange resin, or membrane filtration.[49] However, each of these treatments lacks specificity and has limited removal efficiency (i.e., loading capacity). New reports describe cases where the hydrophobic F-F interactions allows fluorinated materials to function as effective sorbents.[50] For example, Dichtel and coworkers prepared cyclodextrin networks that were crosslinked with fluorinated molecules, and the obtained adsorbent removed perfluorooctanoic acid (PFOA), a notorious PFAS, under environmentally relevant conditions, reducing its concentration from 1 μg/L to 10 ng/L.[50] More recently, Leibfarth and coworkers crosslinked DMAEMA using a fluorinated dimethacrylate, and the resultant ionic fluorogel resins exhibited high affinity for PFAS, with removal efficiency over 80% for PFOA, perfluoro-1-octanesulfonic acid (PFOS), and perfluoro-2-propoxypropanoic acid (GenX).[51] In addition, a number of studies have utilized fluoropolymers to capture PFAS from aqueous environments, and ^{19}F nuclear magnetic resonance (NMR) and molecular dynamic simulations identified the importance of both F-F interactions and electrostatic forces between PFAS compounds and polymers.[52,53] Overall, use of fluoropolymers remains essential to applications that span from industrial engineering, medicine and electronic materials, while the concerns about persistence and effects on health grow. Going forward, development of novel fluoropolymers that are benign to the environment and human health will alleviate the current dilemma between essential utility and the drawbacks. In Chapter 2 of this thesis, the preparation of a library of fluorinated polymer zwitterions is described as the first example of inserting fluorocarbon groups directly into zwitterions. The utility of these polymers in ^{19}F MRI, surface modification, and DNA packaging are discussed in Chapters 2-4, respectively.

1.4 Polymeric vectors for nucleic acid delivery

Gene therapy strategies using DNA and RNA, with the objective of correcting or altering genetic malfunction, continue to evolve as researchers seek safe and efficient methods for encapsulation and delivery of genetic material.[54,55] The ultimate success of nucleic acid-based medicine will largely depend on the safety and effectiveness of the delivery system, and as such a vast literature is devoted to delivery vectors—both viral and nonviral—with evaluation of their toxicity and ability to deliver genetic material of interest *in vitro* and *in vivo*.[56] According to the Gene Therapy Clinical Trials Worldwide database (provided by *The Journal of Gene Medicine*), viral vectors are used in over 60% of current clinical trials, the large majority of which involve adenovirus, adeno-associated virus (AAV), retrovirus, and lentivirus.[57] However, consistently problematic issues associated with viral vectors include their toxicity, which stems from immunogenic response that compromises therapeutic efficacy,[58] as well as their genotoxicity that arises from insertional mutagenesis (where an exogenous DNA sequence integrates within the genome of a host organism), which may lead to leukemia and, in severe cases, death.[59] Other issues hindering wide clinical adoption of viral vectors include difficulties associated with targeting to certain tissues in systemic treatments.[60] Therefore, loading capacity in terms of nucleic acid size is limited,[61,62] and the cost of production and quality control are high.[63] Further investigation into the fundamental features of viral capsids is needed to optimize all aspects of gene therapy – from vector design to encapsulation efficiency to production technology.[64] Nonetheless, recent progress is encouraging, such as for the gene therapy products Luxturna and Zolgensma that have been approved by the U.S. Food and Drug Administration (FDA) for treating retinal and spinal disease, respectively.[65]

Ongoing clinical gene therapy trials using nonviral vectors,[66] such as lipids, nanoparticles, and polymers, represent alternatives to viral vectors with advantages of reduced immunogenicity, easier preparation and scalability, and accessibility to large payloads. With nonviral vectors, synthetic design strategies often borrow structural features of proteins and peptides to retain characteristics of viral systems but in simpler synthetic constructs. Moreover, synthetic routes to non-viral vectors open opportunities to rationally design their structure-property relationships, with the goal of optimizing cell entry and in many cases nuclear localization. Currently, research activities involving nonviral vectors are dominated by lipids and polymers. Lipid-based gene delivery is the most thoroughly examined of nonviral delivery system, with distinct advantages—biocompatibility, biodegradability, and amenability to surface functionalization—countered by drawbacks of short shelf-life and low transfection efficiency.[67] Notably, the recent application of lipid nanoparticles in SARS-CoV-2 mRNA vaccines reflects major progress in lipid-enabled delivery, which is likely to motivate further research and clinical translation.[68]

Cationic polymers represent another major class of nonviral gene therapy vectors, with a wide variety of chemical designs investigated to date. Especially prominent are poly(ethylenimine) (PEI), poly-L-lysine (PLL), and polyamidoamine (PAMAM) dendrimers – just this small group of polymers comprises thousands of reports on gene delivery.[69,70] Detailed cell culture experiments and animal studies have been conducted with these polymers, with focus on structure-property relationships leading to the development of "benchmark" polycationic vectors, such as SuperFect® (PAMAM dendrimer), PEI 25k (PEI with Mw of 25000 g/mol), and jetPEI®.[69] Such amine-rich polymers, when protonated, form complexes with nucleic acids by electrostatic interactions that are typically referred to as 'polyplexes'. This polycation/polyanion combination is described experimentally by defining the N:P stoichiometric ratio, which refers to the number of protonated amines from the polymer relative to the number of phosphate groups in the nucleic acids. During experimental optimization of a particular delivery system, the literature describes use of systems comprising a wide range of N:P ratios. N:P values will be greater than 1 to ensure complete complexation of the genetic cargo and impart on the polyplex a net positive charge. Most typically, polyplexes are formed at higher N:P ratios (greater than 2 and often greater than 5), which may be advantageous for producing polyplexes of smaller size with minimized propensity to aggregate into undesirably large structures. While the excess cations of polyplexes facilitate cell internalization and endosomal escape, cell membrane damage and an inability to release cargo lead to cytotoxicity and insufficient therapeutic effects.[71] Therefore, cationic polymer delivery vectors face their own dilemma associated with an efficiency/toxicity tradeoff, and are not nearly optimized for widespread clinical use.

Researchers are actively pursuing synthetic designs to improve the safety and efficacy of polyplexes, through tuning of polymer architecture and composition, which in turn impacts the binding strength between polycations and nucleic acids, and the interactions of polyplexes in complex biological environments *in vitro* and *in vivo*. The effect of polycation structure on polyplex performance has emerged through numerous studies, with particular focus on macromolecular architecture as well as the chemical composition of the hydrophobic and hydrophilic sub-units of the polymer. Such studies have significantly expanded the library of polymers available for transfection experiments going far beyond the frequently investigated PLL and PEI structures. Previous work by the Emrick group has developed oligolysine-grafted polycyclooctenes as safe and efficient DNA carriers, giving comparable to better transfection as commercial benchmark agents with high cell viability (>80%), with incorporation of zwitterions and nucleus-targeting peptides influencing the binding strength and cell internalization to further improve transfection results (Figure 1-4).[72–74]

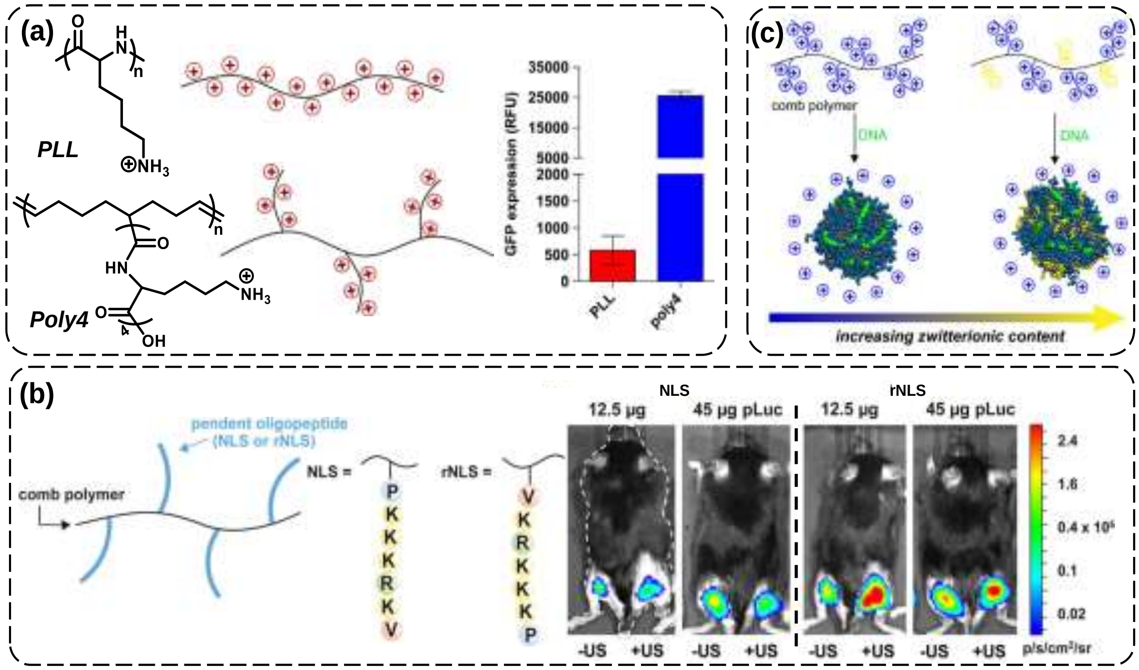

Figure 1-4. Examples of oligopeptide grafted polycyclooctenes developed by Emrick and coworkers for gene delivery: (a) reconfiguration of PLL into tetralysine-grafted polycyclooctene greatly improved transfection; Reprinted from Biomaterials, 32, Sangram S. Parelkar, Delphine Chan-Seng, and Todd Emrick, Reconfiguring polylysine architectures for controlling polyplexbinding and non-viral transfection, 2433, Copyright (2011), with permission from Elsevier; (b) *In vivo* ultrasound-assisted DNA delivery using polycyclooctene with pendent rNLS oligopeptides. Reprinted with permission from ref. 73. Copyright (2014) American Chemical Society. (c) Incorporation of zwitterions into the polycations weakened binding strength with DNA which facilitated release. Reprinted with permission from ref. 74. Copyright (2016) American Chemical Society.

Recently, fluorination has emerged as a powerful strategy to improve the delivery efficiency of cationic polymer vectors. The F-F interaction and low surface energy characteristics of the fluorocarbons are thought to contribute to polyplex stability in biological conditions and facilitate penetration through biological barriers. Inspired by these exciting results and building on the previous synthetic platform of the Emrick group, work in Chapter 4 describes the synthesis of polycyclooctenes containing both oligopeptide and fluorinated pendant for encapsulating DNA and investigating the impact of FPZs on the properties of the polyplex system.

1.5 Thesis outline

This thesis focuses on the synthesis of novel functional materials by merging synthetic chemistry with Nature-inspired zwitterionic structures to produce functional polymer zwitterions. Novel fluorinated CP monomers were prepared, in which the fluorinated groups were embedded directly into the zwitterionic moieties. Constructing fluorinated polymer zwitterions with the FCP monomers yielded polymers viewed to be applicable as ^{19}F MRI imaging agents, surfactants, and surface coatings. In combination with polyolefins containing both fluorinated and oligopeptide pendent groups, the utility

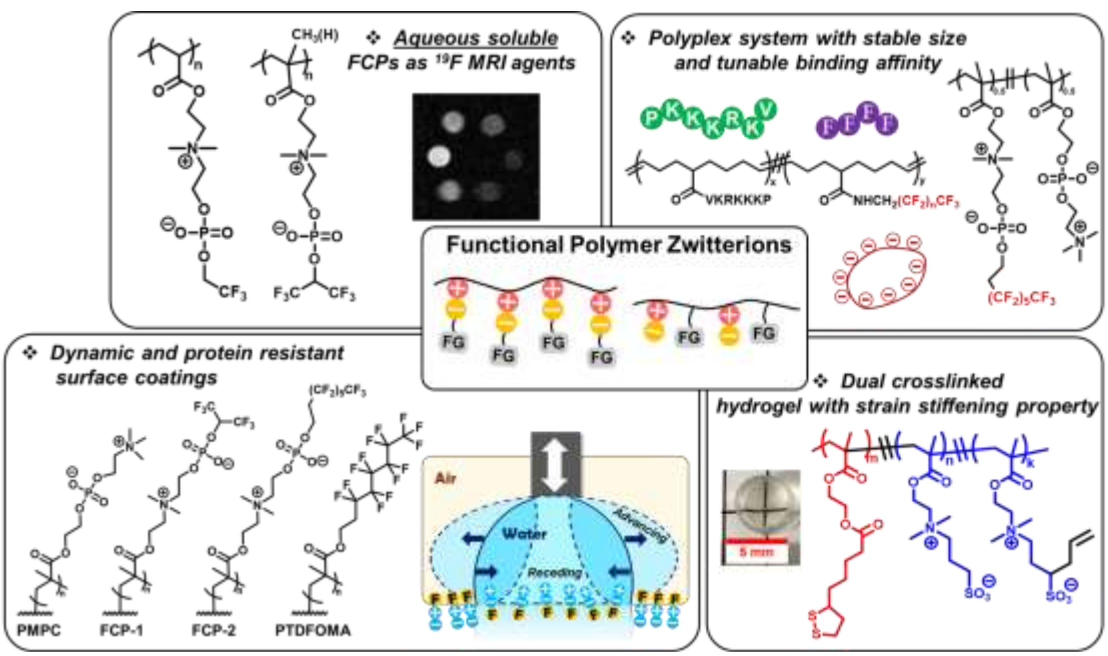

Figure 1-5. Overview of research presented in this dissertation centering on functional polymer zwitterions; including fluorinated polymer zwitterions for bioimaging (top left), DNA complexation (top right) and surface coatings (bottom left), fluorinated cationic poly(cyclooctenes) for DNA complexation (top right), and alkene/disulfide containing polymer zwitterions for making dynamic hydrogels.

of fluorinated polymer zwitterions augmented DNA packaging strategies. In addition, polymer zwitterions were functionalized with crosslinking groups to afford hydrogels with strain-stiffening properties. *Each of these synthetic objectives hinges on the ability to successfully integrate useful and desirable functionality into polymer zwitterions, via syntheses that extend well beyond the conventional methods known today.*

Chapter 2 describes the attachment of fluorinated alkyl groups to CP moieties, yielding fluorinated zwitterionic monomers that proved amenable to controlled free radical polymerization and the production of a new set of CP-containing fluorinated polymers, as well as copolymers with phosphorylcholine (PC) zwitterions. This combination of fluorinated hydrocarbons and zwitterions affords novel, water soluble polymer amphiphiles that were then examined at fluid interfaces, as coatings, in cell culture, and in magnetic resonance imaging.[75]

In Chapter 3, the impacts of fluorinated CP polymers on surface properties were investigated further by conducting surface grafting (i.e. "grafting-from" chemistry) using fluorinated polymer zwitterions by surface-initiated atom transfer radical polymerization (SI-ATRP). The resultant polymer-coated metal substrates exhibited wetting characteristics intermediate between those of zwitterionic and fluorinated brushes, with unusually large contact angle hysteresis values indicative of surface rearrangement in response to the contacting fluidic environment. Surfaces functionalized with fluorinated polymer zwitterions exhibited impressive resistance to fouling from aqueous protein solutions, such as bovine serum albumin and lysozyme.

Chapter 4 expanded the application of fluorinated polymer zwitterions to DNA packaging, which is envisaged as useful in future gene therapy strategies.

Polycyclooctenes containing both fluorinated and oligopeptide pendent groups were prepared and used in DNA complexation to form polyplexes. The presence of fluorinated polymer zwitterions, and adjustable fluorocarbon length and incorporation ratio in the polycyclooctenes, were found to influence the size and binding strength of the polyplexes, both of which are key factors to the success of transfection. These strategies allowed formulating the polyplexes system into PFC nanoemulsions that augment this delivery platform with desirable characteristics such as imaging ability and ultrasound responsiveness.

Chapter 5 describes novel synthetic functional polymer zwitterions containing 1,2-dithiolane and alkene moieties, which produced hydrogels that exhibit strain-stiffening behavior. Irreversible crosslinking induced by thiol-ene chemistry yielded hydrogel networks with well-defined moduli without the need for addition of an external crosslinking component. The availability of residual thiol groups confers a route to secondary crosslinking through interchain disulfide bond formation, which was facilitated when subjected to mechanical strain thereby stiffening the polymer network. These strain-stiffening hydrogels were studied in a collaboration with Professor Shelly Peyton (UMass Chemical Engineering), represent potential biomaterials that benefit from mechano-responsive behavior, which is needed in emerging applications of tissue engineering. Finally, Chapter 6 documents experimental procedures for the synthetic and characterization work performed to complete this thesis.

1.6 References

1. Machtakova, M., Therien-Aubin, H. & Landfester, K. Polymer nano-systems for the encapsulation and delivery of active biomacromolecular therapeutic agents. *Chem. Soc. Rev.* **51**, 128–152 (2022).

2. Ralls, A., Kumar, P., Misra, M. & Menezes, P. L. Material Design and Surface Engineering for Bio-implants. *JOM* **72**, 684–696 (2020).

3. Etayash, H. & Hancock, R. E. W. Host Defense Peptide-Mimicking Polymers and Polymeric-Brush-Tethered Host Defense Peptides: Recent Developments, Limitations, and Potential Success. *Pharmaceutics* **13**, (2021).

4. Chopra, A. M. *et al.* Polymer coating embolism from intravascular medical devices — a clinical literature review. *Cardiovasc. Pathol.* **30**, 45–54 (2017).

5. Arumugam, M. K. *et al.* Beneficial Effects of Betaine: A Comprehensive Review. *Biol. 2021, Vol. 10, Page 456* **10**, 456 (2021).

6. Ripps, H. & Shen, W. Review: Taurine: A “very essential” amino acid. *Mol. Vis.* **18**, 2686 (2012).

7. Zhou, L. Y. *et al.* Novel zwitterionic vectors: Multi-functional delivery systems for therapeutic genes and drugs. *Comput. Struct. Biotechnol. J.* **18**, 1980–1999 (2020).

8. Dong, D. *et al.* High-strength and fibrous capsule–resistant zwitterionic elastomers. *Sci. Adv.* **7**, eabc5442 (2022).

9. Fujii, S., Kozuka, S., Yokota, K., Ishihara, K. & Yusa, S. I. Preparation of Biocompatible Poly(2-(methacryloyloxy)ethyl phosphorylcholine) Hollow Particles Using Silica Particles as a Template. *Langmuir* (2022). doi:10.1021/acs.langmuir.2c00423

10. Yan, W. *et al.* Growing Polymer Brushes from a Variety of Substrates under Ambient Conditions by Cu0-Mediated Surface-Initiated ATRP. *ACS Appl. Mater. Interfaces* **11**, 27470–27477 (2019).

11. Zhou, L. Y. *et al.* Novel zwitterionic vectors: Multi-functional delivery systems for therapeutic genes and drugs. *Computational and Structural Biotechnology Journal* **18**, 1980–1999 (2020).

12. Li, B. *et al.* Revealing the Immunogenic Risk of Polymers. *Angew. Chemie Int. Ed.* **57**, 13873–13876 (2018).

13. Moro, T. *et al.* Surface grafting of artificial joints with a biocompatible polymer for preventing periprosthetic osteolysis. *Nat. Mater. 2004 311* **3**, 829–836 (2004).

14. Ishihara, K. Highly lubricated polymer interfaces for advanced artificial hip joints through biomimetic design. *Polym. J. 2015 479* **47**, 585–597 (2015).

15. Zhang, E. *et al.* Fouling-resistant zwitterionic polymers for complete prevention of postoperative adhesion. *Proc. Natl. Acad. Sci. U. S. A.* **117**, 32046–32055 (2020).

16. Schönemann, E. *et al.* Synthesis of Novel Sulfobetaine Polymers with Differing Dipole Orientations in Their Side Chains, and Their Effects on the Antifouling Properties. *Macromol. Rapid Commun.* **41**, 1900447 (2020).

17. Brown, M. U., Triozzi, A. & Emrick, T. Polymer Zwitterions with Phosphonium Cations. *Cite This J. Am. Chem. Soc* **143**, 6532 (2021).

18. Li, B. *et al.* Trimethylamine N-oxide–derived zwitterionic polymers: A new class of ultralow fouling bioinspired materials. *Sci. Adv.* **5**, eaaw9562 (2019).

19. Santa Chalarca, C. F. & Emrick, T. Reactive polymer zwitterions: Sulfonium sulfonates. *J. Polym. Sci. Part A Polym. Chem.* **55**, 83–92 (2017).

20. Santa Chalarca, C. F. *et al.* Building Supracolloidal Fibers from Zwitterion-Stabilized Adhesive Emulsions. *Adv. Funct. Mater.* **28**, 1804325 (2018).

21. Letteri, R. A. *et al.* Forming Sticky Droplets from Slippery Polymer Zwitterions. *Adv. Mater.* **29**, 1702921 (2017).

22. Lewoczko, E. M. *et al.* Effects of N-Substituents on the Solution Behavior of Poly(sulfobetaine methacrylate)s in Water: Upper and Lower Critical Solution Temperature Transitions. *ACS Appl. Polym. Mater.* **3**, 867–878 (2021).

23. Higaki, Y. *et al.* Effect of Charged Group Spacer Length on Hydration State in Zwitterionic Poly(sulfobetaine) Brushes. *Langmuir* **33**, 8404–8412 (2017).

24. Schönemann, E. *et al.* Synthesis of Novel Sulfobetaine Polymers with Differing Dipole Orientations in Their Side Chains, and Their Effects on the Antifouling Properties. *Macromol. Rapid Commun.* **41**, 1900447 (2020).

25. Matyjaszewski, K. Atom Transfer Radical Polymerization (ATRP): Current status and future perspectives. *Macromolecules* **45**, 4015–4039 (2012).

26. Perrier, S. 50th Anniversary Perspective: RAFT Polymerization - A User Guide. *Macromolecules* **50**, 7433–7447 (2017).

27. Pagaduan, J. N. *et al.* Electronic Tuning of Monolayer Graphene with Polymeric 'zwitterists'. *ACS Nano* **15**, 2762–2770 (2021).

28. Chen, X., Parelkar, S. S., Henchey, E., Schneider, S. & Emrick, T. PolyMPC–Doxorubicin Prodrugs. *Bioconjug. Chem.* **23**, 1753–1763 (2012).

29. Chen, X., McRae, S., Parelkar, S. & Emrick, T. Polymeric Phosphorylcholine−Camptothecin Conjugates Prepared by Controlled Free Radical Polymerization and Click Chemistry. *Bioconjug. Chem.* **20**, 2331–2341 (2009).

30. Bai, Y. *et al.* Functional droplets that recognize, collect, and transport debris on surfaces. *Sci. Adv.* **2**, (2016).

31. Chang, C.-C., Letteri, R., Hayward, R. C. & Emrick, T. Functional Sulfobetaine Polymers: Synthesis and Salt-Responsive Stabilization of Oil-in-Water Droplets. *Macromolecules* **48**, 7843–7850 (2015).

32. Yu, X., Yang, X., Horte, S., Kizhakkedathu, J. N. & Brooks, D. E. ATRP synthesis of poly(2-(methacryloyloxy)ethyl choline phosphate): a multivalent universal biomembrane adhesive. *Chem. Commun.* **49**, 6831–6833 (2013).

33. Hu, G., Parelkar, S. S. & Emrick, T. A facile approach to hydrophilic, reverse zwitterionic, choline phosphate polymers. *Polym. Chem.* **6**, 525–530 (2015).

34. Hu, G. & Emrick, T. Functional Choline Phosphate Polymers. *J. Am. Chem. Soc.* **138**, 1828–1831 (2016).

35. Lohmann, R. *et al.* Are Fluoropolymers Really of Low Concern for Human and Environmental Health and Separate from Other PFAS? *Environ. Sci. Technol.* **54**, 12820–12828 (2020).

36. Zhang, C. *et al.* Biological Utility of Fluorinated Compounds: from Materials Design to Molecular Imaging, Therapeutics and Environmental Remediation. *Chem. Rev.* **122**, 167–208 (2022).

37. Fu, C. *et al.* Low-Fouling Fluoropolymers for Bioconjugation and In Vivo Tracking. *Angew. Chemie* **132**, 4759–4765 (2020).

38. Patra, D., Kumar, P., Pal, D., Chakraborty, I. & Shunmugam, R. Unique Random-Block Polymer Architecture for Site-Specific Mitochondrial Sequestration-Aided Effective Chemotherapeutic Delivery and Enhanced Fluorocarbon Segmental Mobility-Facilitated 19F Magnetic Resonance Imaging. *Biomacromolecules* (2022). doi:10.1021/acs.biomac.2c00188

39. Wijekoon, A., Fountas-Davis, N. & Leipzig, N. D. Fluorinated methacrylamide chitosan hydrogel systems as adaptable oxygen carriers for wound healing. *Acta Biomater.* **9**, 5653–5664 (2013).

40. Lv, J. & Cheng, Y. Fluoropolymers in biomedical applications: state-of-the-art and future perspectives. *Chem. Soc. Rev.* **50**, 5435–5467 (2021).

41. Tirotta, I. *et al.* 19F magnetic resonance imaging (MRI): From design of materials to clinical applications. *Chem. Rev.* **115**, 1106–1129 (2015).

42. Lv, J. & Cheng, Y. Fluoropolymers in biomedical applications: state-of-the-art and future perspectives. *Chem. Soc. Rev.* **50**, 5435–5467 (2021).

43. Huang, Y. *et al.* Polymer-stabilized perfluorobutane nanodroplets for ultrasound imaging agents. *J. Am. Chem. Soc.* **139**, 15–18 (2017).

44. Hu, H. *et al.* Perfluorocarbon-based O2 nanocarrier for efficient photodynamic therapy. *J. Mater. Chem. B* **7**, 1116–1123 (2019).

45. Wang, M., Liu, H., Li, L. & Cheng, Y. A fluorinated dendrimer achieves excellent gene transfection efficacy at extremely low nitrogen to phosphorus ratios. *Nat. Commun. 2014 51* **5**, 1–8 (2014).

46. Lv, J. *et al.* Fluorination on polyethylenimine allows efficient 2D and 3D cell culture gene delivery. *J. Mater. Chem. B* **3**, 642–650 (2015).

47. Wang, X. *et al.* In Vivo Tracking of Fluorinated Polypeptide Gene Carriers by Positron Emission Tomography Imaging. *ACS Appl. Mater. Interfaces* **12**, 45763–45771 (2020).

48. Lohmann, R. *et al.* Are Fluoropolymers Really of Low Concern for Human and Environmental Health and Separate from Other PFAS? *Environ. Sci. Technol.* **54**, 12820–12828 (2020).

49. PFAS Treatment in Drinking Water and Wastewater – State of the Science | US EPA. Available at: https://www.epa.gov/research-states/pfas-treatment-drinking-water-and-wastewater-state-science. (Accessed: 8th August 2022)

50. Zhang, C. *et al.* Biological Utility of Fluorinated Compounds: From Materials Design to Molecular Imaging, Therapeutics and Environmental Remediation. *Chem. Rev.* **122**, 167–208 (2022).

51. Kumarasamy, E., Manning, I. M., Collins, L. B., Coronell, O. & Leibfarth, F. A. Ionic Fluorogels for Remediation of Per-and Polyfluorinated Alkyl Substances from Water. *ACS Cent. Sci.* **6**, 487–492 (2020).

52. Tan, X. *et al.* Revealing the Molecular-Level Interactions between Cationic Fluorinated Polymer Sorbents and the Major PFAS Pollutant PFOA. *Macromolecules* **55**, 1077–1087 (2022).

53. Tan, X. *et al.* Amphiphilic Perfluoropolyether Copolymers for the Effective Removal of Polyfluoroalkyl Substances from Aqueous Environments. *Macromolecules* **54**, 3447–3457 (2021).

54. Caffery, B., Lee, J. S. & Alexander-Bryant, A. A. Vectors for glioblastoma gene therapy: Viral & non-viral delivery strategies. *Nanomaterials* **9**, 105 (2019).

55. Pardi, N., Hogan, M. J., Porter, F. W. & Weissman, D. mRNA vaccines-a new era in vaccinology. *Nat. Rev. Drug Discov.* **17**, 261–279 (2018).

56. Dunbar, C. E. *et al.* Gene therapy comes of age. *Science (80-.).* **359**, eaan4672 (2018).

57. GTCT (FMS19). Available at: https://a873679.fmphost.com/fmi/webd/GTCT. (Accessed: 27th May 2022)

58. Shirley, J. L., De Jong, Y. P., Terhorst, C. & Herzog, R. W. Immune Responses to Viral Gene Therapy Vectors. *Mol. Ther.* **28**, 709–722 (2020).

59. Wu, C. & Dunbar, C. E. Stem cell gene therapy: the risks of insertional mutagenesis and approaches to minimize genotoxicity. *Front. Med. 2011 54* **5**, 356–371 (2011).

60. Bulcha, J. T., Wang, Y., Ma, H., Tai, P. W. L. & Gao, G. Viral vector platforms within the gene therapy landscape. *Signal Transduct. Target. Ther.* **6**, 53 (2021).

61. Kotterman, M. A., Chalberg, T. W. & Schaffer, D. V. Viral Vectors for Gene Therapy: Translational and Clinical Outlook. *Annu. Rev. Biomed. Eng.* **17**, 63–89 (2015).

62. Waehler, R., Russell, S. J. & Curiel, D. T. Engineering targeted viral vectors for gene therapy. *Nat. Rev. Genet.* **8**, 573–587 (2007).

63. Srivastava, A., Mallela, K. M. G., Deorkar, N. & Brophy, G. Manufacturing Challenges and Rational Formulation Development for AAV Viral Vectors. *J. Pharm. Sci.* **110**, 2609–2624 (2021).

64. Bouard, D., Alazard-Dany, N. & Cosset, F. L. Viral vectors: From virology to transgene expression. *Br. J. Pharmacol.* **157**, 153–165 (2009).

65. Approved Cellular and Gene Therapy Products | FDA. Available at: https://www.fda.gov/vaccines-blood-biologics/cellular-gene-therapy-products/approved-cellular-and-gene-therapy-products. (Accessed: 27th May

2022)

66. Ginn, S. L., Amaya, A. K., Alexander, I. E., Edelstein, M. & Abedi, M. R. Gene therapy clinical trials worldwide to 2017: An update. *J. Gene Med.* **20**, e3015 (2018).

67. Buck, J., Grossen, P., Cullis, P. R., Huwyler, J. & Witzigmann, D. Lipid-based DNA therapeutics: Hallmarks of non-viral gene delivery. *ACS Nano* **13**, 3754–3782 (2019).

68. Tenchov, R., Bird, R., Curtze, A. E. & Zhou, Q. Lipid Nanoparticles from Liposomes to mRNA Vaccine Delivery, a Landscape of Research Diversity and Advancement. *ACS Nano* **15**, 16982–17015 (2021).

69. Malloggi, C. *et al.* Comparative evaluation and optimization of off-the-shelf cationic polymers for gene delivery purposes. *Polym. Chem.* **6**, 6325–6339 (2015).

70. Piotrowski-Daspit, A. S., Kauffman, A. C., Bracaglia, L. G. & Saltzman, W. M. Polymeric vehicles for nucleic acid delivery. *Adv. Drug Deliv. Rev.* **156**, 119–132 (2020).

71. Monnery, B. D. Polycation-Mediated Transfection: Mechanisms of Internalization and Intracellular Trafficking. *Biomacromolecules* **22**, 4060–4083 (2021).

72. Parelkar, S. S., Chan-seng, D. & Emrick, T. Reconfiguring polylysine architectures for controlling polyplex binding and non-viral transfection. *Biomaterials* **32**, 2432–2444 (2011).

73. Parelkar, S. S. *et al.* Polymer-peptide delivery platforms: effect of oligopeptide orientation on polymer-based DNA delivery. *Biomacromolecules* **15**, 1328–1336 (2014).

74. Ghobadi, A. F. *et al.* Dispersing Zwitterions into Comb Polymers for Nonviral Transfection : Experiments and Molecular Simulation. (2016). doi:10.1021/acs.biomac.5b01462

75. Zhou, L., Triozzi, A., Figueiredo, M. & Emrick, T. Fluorinated Polymer Zwitterions: Choline Phosphates and Phosphorylcholines. *ACS Macro Lett.* **10**, 1204–1209 (2021).

CHAPTER 2

FLUORINATED POLYMERZWITTERIONS: CHOLINE PHOSPHATES AND PHOSPHORYLCHOLINES

2.1 Introduction

Polymer zwitterions, such as poly(2-methacryloyloxyethyl phosphorylcholine) (polyMPC), have proven exceptionally useful in applications where biocompatibility, hydrophilicity, and non-fouling effects are desired.[1] Combining early reports of phosphorylcholine (PC)-based polymer syntheses, such as by Nakabayashi and Ishihara,[2] with advances in controlled free radical polymerization of hydrophilic monomers,[3–5] has afforded new routes to polymer-drug conjugates,[6,7] polymer-grafted substrates,[8,9] and aqueous polymer assemblies.[10] The bio-friendly, non-fouling properties of PC and other zwitterions are derived from the extensive hydration associated with the zwitterionic groups,[11] while copolymerization methodology involving zwitterionic monomers lends rich chemical versatility beyond that of conventional hydrophilic polymers, such as poly(ethylene oxide).

Most polymer zwitterions reported to date integrate zwitterionic moieities from biology directly into the polymer sidechain, such as PC, sulfobetaine (SB), and carboxybetaine (CB)-containing structures.[12] One drawback to these structures is a lack of direct accessibility to functional group integration. However, recent reports by us and others described the preparation of polymers with “inverted” PC groups, referred to as choline phosphate (CP) structures, that readily lend themselves to functional group incorporation.[13–16] The preparation of CP-substituted methacrylates consists of: (i) conversion of ethylene chlorophosphate to functional cyclic phosphates and (ii) ring-opening of the phosphate with methacrylate-containing nucleophiles (endocylic reaction) while avoiding undesired salt formation (exocyclic reaction) (**Figure 2-1**). The preference for endo *vs.* exocyclic reaction mechanisms is influenced by steric and electronic factors associated with the R-substituent of the cyclic phosphate; in cases where a product mixture is obtained, the undesirable salt by-product must be removed (for example by ion exchange chromatography).[17]

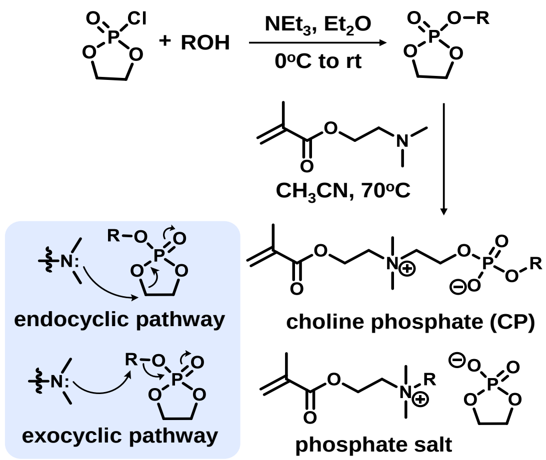

Figure 2-1. Reaction pathways for CP-monomer syntheses.

Prior work by Emrick and coworkers showed that the CP-synthetic strategy represents an opportunity to prepare novel CP-polymers with embedded alkenyl and alkynyl groups, affording polymer zwitterions which retain their desired hydrophilicity and biocompatibility and that are amenable to attachment of drugs and other moieties without sacrificing their zwitterionic character.[15,16] Here, our synthesis of fluorinated

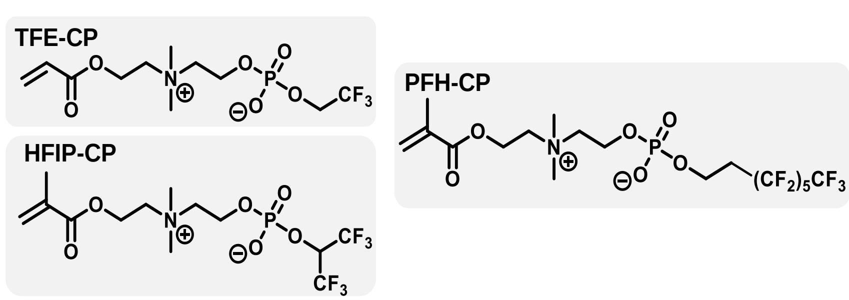

Figure 2-2. Chemical structures of fluorinated CP monomers described in this Chapter.

choline phosphate (FCP)-substituted methacrylates, shown in **Figure 2-2**, gives access to a novel array of fluorinated polymer zwitterions as described below.

We recognize this CP-synthetic strategy as an opportunity to prepare novel polymers that combine zwitterions and fluoroalkanes within each subunit of the polymer structure. Like hydrophilic polymers, fluorinated polymers tend towards non-fouling surface properties, but for reasons associated with surface energy rather than hydrophilicity.[11,18] Using fluorinated polymers in water is of interest biologically for ^{19}F magnetic resonance imaging (^{19}F MRI) contrast agents (CAs), though aggregation of the fluorinated units in water is problematic since this causes depletion of the signal. Recent activity along these lines is highlighted by the preparation of water soluble fluorinated sulfoxide polymers, as well as fluorinated poly(2-oxazoline) that possess favorable MRI contrast properties.[19–21] Perfluorocarbons, such as perfluorobutane (PFB) and perfluoro-*n*-octyl bromide (PFOB), are commonly used CAs for ^{19}F MRI and ultrasound imaging. Encapsulation of perfluorocarbons as the oil phase in emulsions requires small molecule or polymer surfactants, many of which are themselves fluorinated amphiphilic polymers.[22–24]

With this motivation to combine zwitterions with fluorinated moieties, we sought to prepare novel fluorinated CP monomers, and following from that a series of fluorinated CP/PC-substituted polymers, such as illustrated in **Figure 2-3**. While fluorinated hydrocarbons are rarely combined with zwitterions in polymer structures,[25,26] we anticipate that new syntheses that directly embed fluorine character into zwitterionic units hold promise across a breadth of both materials and biological applications.

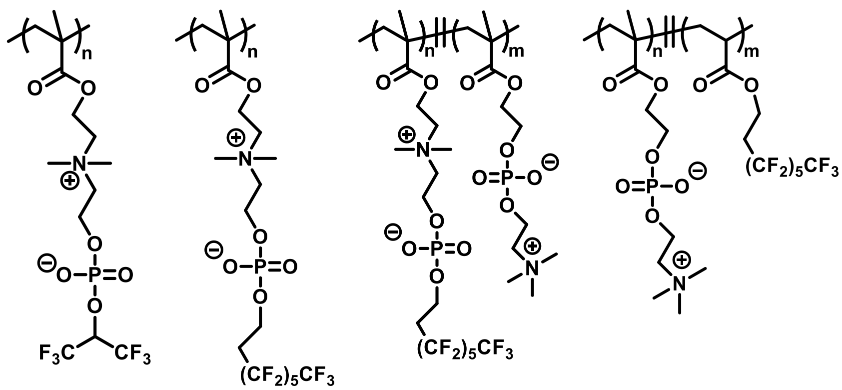

Figure 2-3. Chemical structures of CP- and PC-containing fluorinated zwitterionic polymers, **P1-P4**, described in this Chapter.

2.2 Monomer Synthesis

Fluorinated CP monomers **TFE-CP**, **HFIP-CP**, and **PFH-CP** were prepared in multigram scale using the synthetic route shown in **Figure 2-1**. First, ethylene chlorophosphate was reacted with a fluorinated alcohol (R-OH) in the presence of triethylamine, yielding the fluorinated cyclic phosphate product in high yield (~75-90%) after isolation by filtration and solvent evaporation. The ^{31}P NMR spectra of these products showed a single, clean resonance at ~17 ppm. Ring-opening with dimethylaminoethyl methacrylate (DMAEMA) in acetonitrile yielded the fluorinated CP monomers in up to 70% yield after precipitation and purification by several washing/centrifugation cycles using acetonitrile and ether. Performing the reactions under anhydrous conditions was essential to avoiding by-product formation, while the presence of 4-methoxyphenol prevented premature radical polymerization. The isolated monomers, obtained as white solids, produced clean NMR spectra in solution, as shown in **Figure 2-4a** for monomer **HFIP-CP**, with ^{1}H NMR spectroscopy showing the characteristic methacrylate olefin signals as well as the methine proton peak of the hexafluoroisopropyl group (5.27 ppm), and the ^{31}P spectrum showing a single resonance at -3.12 ppm (shifted slightly from the resonance of MPC which appears at -0.44 ppm). A trace amount of the salt by-product was observed in the ^{31}P NMR spectrum (19.10 ppm) of the crude product following the synthesis of monomer **PFH-CP**; this was completely removed during purification, as confirmed by ^{31}P NMR spectroscopy (**Figure 2-4b**). High-resolution mass spectrometry also confirmed the formation of the desired products (**HFIP-CP**: $C_{13}H_{20}F_6NO_6P$, calcd $[M+Na]^+$, 454.0825; found 454.0829; **PFH-CP**: $C_{18}H_{23}F_{13}NO_6P$, calcd $[M+Na]^+$, 650.0949; found 650.0947). The fluorinated CP monomers proved soluble in both polar and fluorinated solvents, including pure water, methanol, 1,1,1-trifluoroethanol (TFE) and 1,1,1,3,3,3-hexafluoroisopropanol (HFIP).

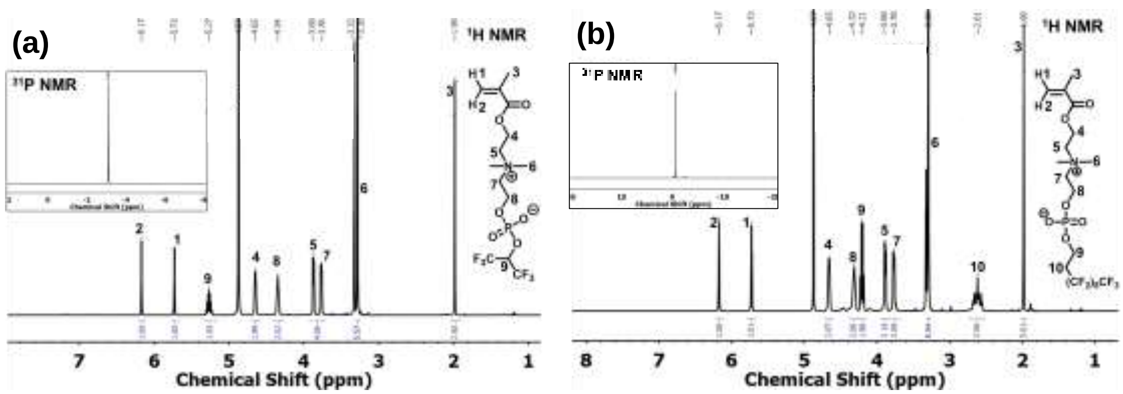

Figure 2-4. ^1H NMR and ^{31}P NMR (insets) spectra of (a) HFIP-CP and (b) PFH-CP in CD_3OD (signals at 3.32 ppm and 4.87 ppm arise from residual CH_3OH).

2.3 Polymer synthesis

Polymerization of the fluorinated CP monomers was performed by reversible addition–fragmentation chain-transfer (RAFT) polymerization in TFE at 70 °C using 4-cyano-4-(phenylcarbonothioylthio)pentanoic acid (CPPA) as the chain-transfer agent and 4,4'-azobis(4-cyanovaleric acid) (ACVA) as initiator. Under these conditions, polymerization of **HFIP-CP** was well-controlled, as indicated by plotting $\ln([M]_0/[M]_n)$ as a function of time, shown in **Figure 2-5a** for a typical reaction where $[M]_0 = 0.8$ M and $[M]_0:[CTA]_0:[I]_0 = 50:1:0.2$. Following a short incubation period, propagation proceeded at a constant rate until high monomer conversion was reached. By ^{1}H NMR evaluation of aliquots taken from the reaction mixture, monomer conversion reached or exceeded 90% at t = 4 h (**Figure 2-5b**). Polymer molecular weight was determined by gel permeation chromatography (GPC) equipped with refractive index (RI) detection, using TFE as the mobile phase and PMMA calibration standards. The GPC traces shifted to higher molecular weight (shorter retention time) as the reaction proceeded (**Figure 2-5c**), and molecular weight increased nearly linearly with monomer conversion, while the polydispersity index (Đ, defined as M_w/M_n) was maintained in the 1.2-1.3 range (**Figure 2-5d**). By ^{1}H NMR spectroscopy, the degree-of-polymerization (DP) was calculated to be ~25-115, as judged by integrating the methine resonance (-CH(CF_3)$_2$) at 5.29 ppm against the aromatic chain-end (this DP value correlated closely to the monomer-to-CTA feed ratio). After the polymerization, purification by precipitation, dialysis, and

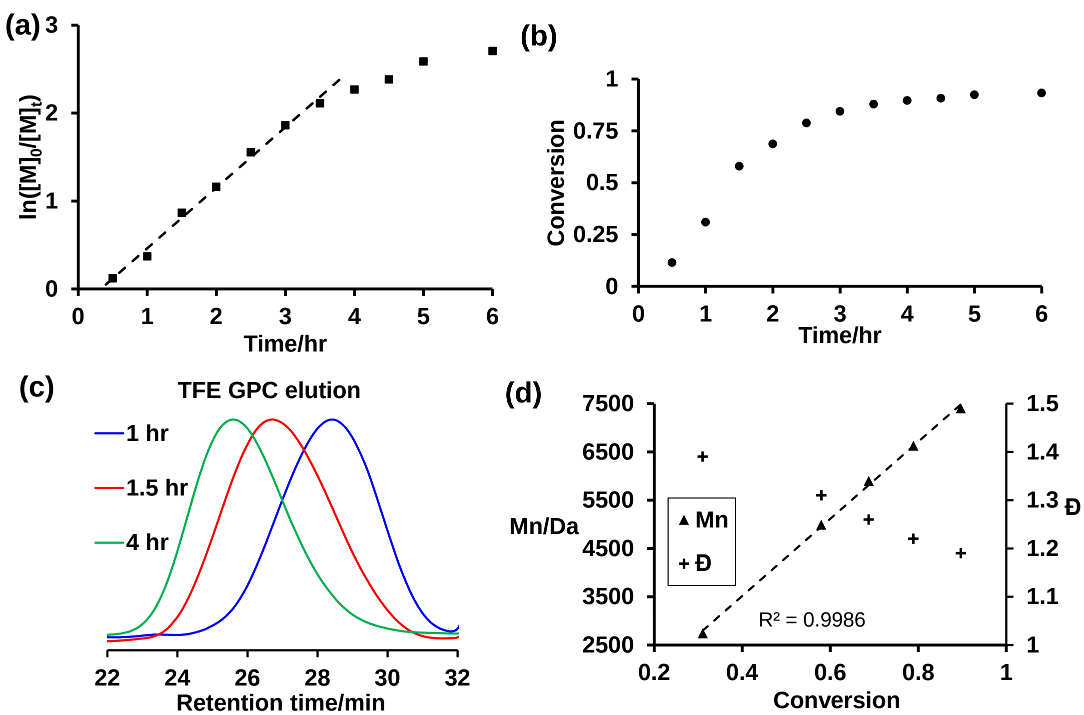

Figure 2-5. Homopolymerization of HFIP-CP: (a) first kinetic plot; (b) monomer consumption as a function of time; (c) GPC traces for poly (HFIP-CP) eluting in TFE at t = 60 min, 90 min, and 4 h; and (d) Mn and Đ at different conversions.

lyophilization afforded **P1** in ~80% yield with M_n of 2-15 kDa. FCP **P1** proved readily soluble in polar protic solvents (water and methanol) as well as fluorinated solvents (TFE and HFIP). The GPC-estimated M_n, recorded in TFE, was significantly lower than the M_n derived from the DP calculated by the ^{1}H NMR spectroscopy (**Table 2-1**). That the NMR and GPC-derived molecular weights differ significantly is not surprising in light of the unusual structure of these polymers (containing both the zwitterionic and fluoroalkyl groups) and their potential impact of polar interactions with the stationary phase on GPC measurements.

RAFT polymerization of **PFH-CP** proceeded similarly to that of **HFIP-CP** (**Figure 2-6**) and in high monomer conversion and isolated yield. Monomer conversion reached 84% at t = 6 h while polymer molecular weight increased almost linearly with conversion. Polymers were obtained in ~65-70% yield after purification by precipitation and vacuum drying, with M_n values of 11-13 kDa estimated by GPC and 18-44 kDa

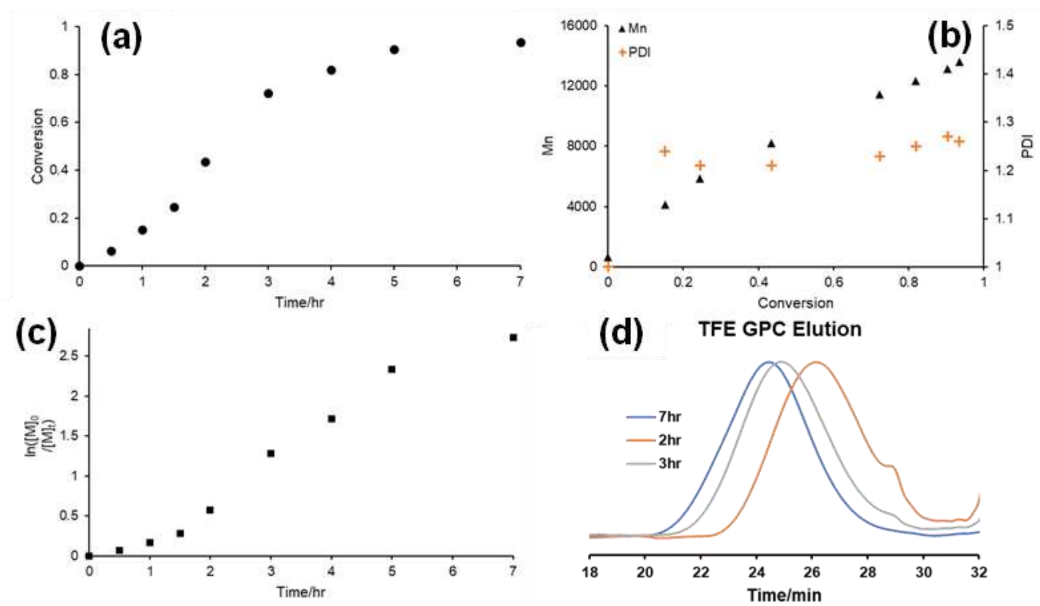

Figure 2-6. RAFT homopolymerization of PFH-CP: (a) monomer conversion as a function of time, (b) M_n and Đ at different extents of monomer conversion, (c) first order kinetic plot, (d) GPC elution traces at different time points.

calculated by [1]H NMR spectroscopic integration. Interestingly, the higher fluorine content of **P2** (relative to **P1**) made it sparingly soluble in methanol and insoluble in water, while both **P1** and **P2** were readily soluble in TFE and HFIP. To this point, we have observed chemical stability of **P1** in pH 7.4 PBS buffer, with no sign of hydrolytic degradation that would release small molecule PFAS structures.

Table 2-1. Characterization data of homopolymers **P1** and **P2**.

Polymer	Conv (%)	$M_{n,NMR}$	$M_{n,GPC}$	Đ
	80	10.8	2.2	1.27
P1	94	21.5	6.7	1.25
	88	49.6	15.5	1.23
P2	96	18.8	11.6	1.14
	88	43.9	13.1	1.23

Polymerizations involving PC, CP, and fluorinated monomers proved exceptionally versatile for preparing random copolymers **P3** and **P4** and, as illustrated in **Figure 2-7**, block copolymers **P5-P7**. For example, RAFT copolymerization of MPC and monomer **PFH-CP** proved successful for the preparation of random and block copolymers. Samples of random copolymer **P3**, with narrow Đ (1.1-1.2), were obtained

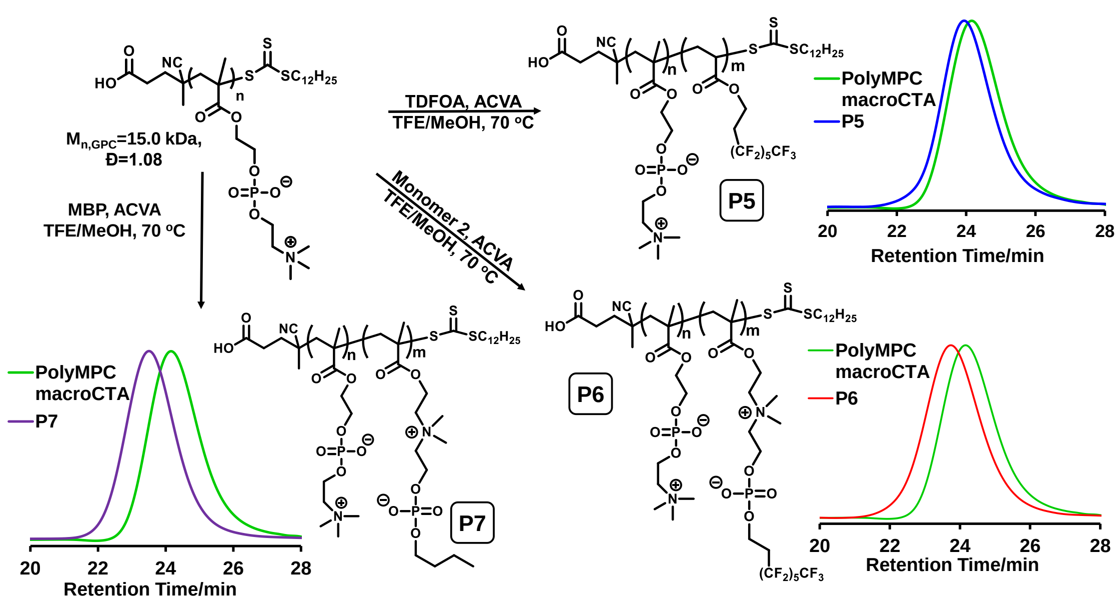

Figure 2-8. GPC traces of polyMPC macroCTA before and after chain extension reactions for the preparation of block copolymers **P5**, **P6**, and **P7**.

by copolymerization of **PFH-CP** and MPC in TFE to achieve 20-80 mole percent incorporation of **PFH-CP**. These polymers formed homogenous solutions in water with up to 50 mole percent incorporation of **PFH-CP**. Block copolymers **P5-P7** were also prepared in order to deepen our understanding of structure-property relationships of polymers containing zwitterionic (PC or CP) and fluorinated units. These were made from a common polyMPC macroCTA ($M_{n,GPC}$ 15 kDa) with the corresponding chain-extending monomer, targeting a 1:1 molar ratio of the MPC blocks and the additional block. The preparation of **P5** utilized a commercially available fluorinated acrylate, 1H,1H,2H,2H-tridecafluoro-*n*-octyl acrylate (TDFOA), as the second block. According to the first order kinetic plot (**Figure 2-8**) of the chain extension, propagation occurred at a constant rate, over about three hours, to reach about 80% conversion. The ^{1}H NMR spectrum of **P5** in CD_3OD confirmed the incorporation of TDFOA, with the monomer ratio calculated by integrating methylene resonances from 4.53-3.96 ppm (for both blocks) and at 3.75 ppm (for the polyMPC block). Notably, the GPC trace of **P5** with TFE as the mobile phase

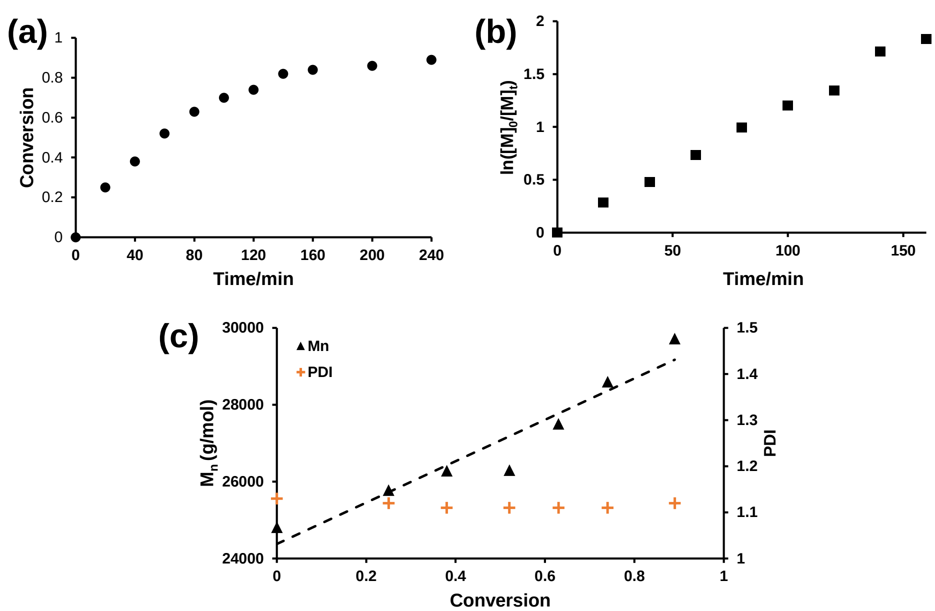

Figure 2-9. Chain-extension of a polyMPC macroCTA with TDFOA: (a)TDFOA conversion as a function of time; (b) evolution of Mn and Đ during the polymerization; (c) first-order kinetic plot.

showed only a slight shift towards higher molecular weight. Block copolymer **P6** was prepared by extension of the macroCTA with **PFH-CP** in 1:1 MeOH:TFE, with GPC analysis confirming successful chain-extension. For both random and block copolymers of MPC and **PFH-CP** (**P3** and **P6**), the incorporation of **PFH-CP** was calculated by integrating the methylene resonance of the CP monomer unit at 2.62 ppm against the MPC methylene signal at 3.74 ppm (or against the backbone protons from 0.68-2.45 ppm), giving results consistent with the monomer feed ratios employed. Moreover, **P7**, a block copolymer was prepared from MPC and the *n*-butyl-substituted CP monomer (MBP),[15] with the GPC trace again shifting significantly towards lower retention volume (higher molecular weight). We speculate that the similar GPC profiles seen for **P5** and its macroCTA precursor may be due to polar interactions between the fluorinated hydrocarbon and the stationary phase, an effect that is eliminated in the all-zwitterionic diblock copolymers **P6** and **P7**. As is typical, these GPC analyses provide estimates of molecular weight that depend in part on the selected calibration standards (PMMA in these cases). Therefore, we also report molecular weights observed by end-group analysis by ^{1}H NMR spectroscopy, by integrating peak intensity of the CTA protons against selected protons of the polymer chain (**Table 2-2**).

Table 2-3. Characterization data of P3-P7.

Polymer	MPC (mol%)		$M_{n,NMR}$	$M_{n,GPC}$	Đ
	target	actual			
P3	20	18	25.6	16.5	1.18
	50	45	30.9	20.5	1.14
	80	82	34.6	20.7	1.14
P4	50	53	20.0	17.3	1.10
PolyMPC macroCTA	100	100	7.8	15.0	1.08
P5	50	46	19.5	16.5	1.10
P6	50	55	20.6	17.7	1.08
P7	50	48	16.9	19.4	1.09

2.4 Fluorinated CP polymers as ^{19}F MRI contrast agents

We anticipate the utility of this combination of zwitterionic and fluorinated groups across a breadth of materials and biological applications. DLS experiments performed on aqueous solutions of **P1** (2 mg/mL) indicated structures of ~7 nm diameter, while ^{1}H NMR spectroscopy showed no attenuation of the signal for the methine proton adjacent to the CF_3 groups (**Figure 2-9a**). Moreover, the fluorine NMR resonances of **P1** were narrow and intense in both D_2O and CD_3OD (**Figure 2-9b**). In contrast, for **poly(MPC-co-TFEMA)** (**Figure 2-9c**), a random copolymer of MPC and trifluoroethyl-

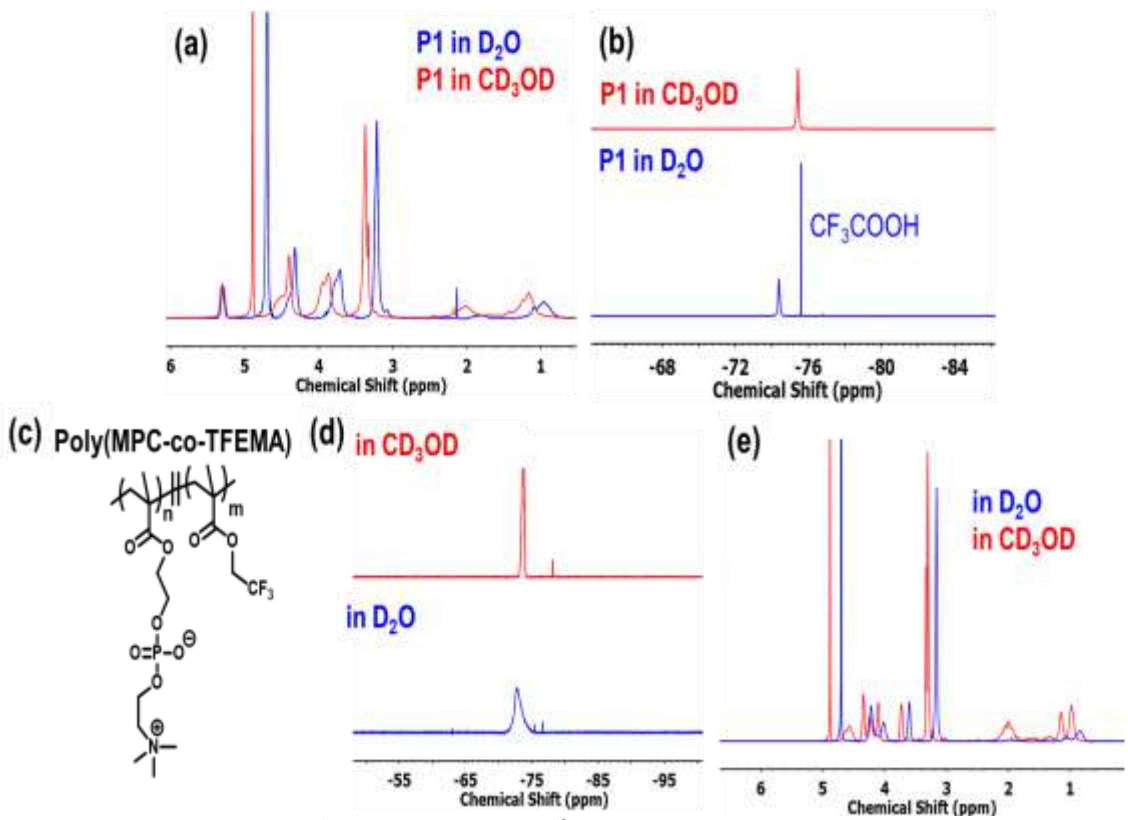

Figure 2-11. Stacked (a) ^{1}H NMR and (b) ^{19}F NMR spectra of **P1** in CD_3OD and D_2O; (c) chemical structure of Poly(MPC-co-TFEMA); stacked (d) ^{19}F NMR and (e) ^{1}H NMR spectra of **poly(MPC-co-TFEMA)** in D_2O and CD_3OD.

substituted methacrylate, the proton resonance of the methylene group nearest the CF_3 diminished greatly in D_2O relative to CD_3OD, and the fluorine signals broadened in D_2O (**Figure 2-9 (d-e)**). Such signal attenuation, suggestive of solution aggregation, is a noted challenge when designing polymeric ^{19}F MRI agents.[19] Thus, the high fluorine content (26 wt%) and water solubility (over 100 mg/mL) of **P1** may be advantageous in this regard. Using inversion–recovery and CPMG pulse sequences,[27,28] spin-lattice (T_1) and

Table 2-5. Relaxation times of **P1** as a function of molecular weight.

Polymer	Conv (%)	$M_{n,NMR}$/kDa	M_n/kDa	Đ	T_1/ms	T_2/ms
	80	10.8	2.2	1.3	442	83
P1	94	21.5	6.7	1.2	420	43
	88	49.6	15.5	1.2	415	32

spin-spin (T_2) values of ~415-442 ms and ~32-83 ms were obtained, respectively, for **P1**, with a molecular weight dependence (**Table 2-3**) that attributed to solution mobility of the polymers.[29,30] In general, shorter T_1 and longer T_2 values are desirable for enhancing signal intensity;[19] among the FCPs prepared in this thesis, the acrylate-based polymers **P8** and **P9**, shown in **Figure 2-10 (a-b)**, appear to have the most favorable magnetic resonance properties. In preliminary studies along these lines, ^{19}F MR imaging of aqueous

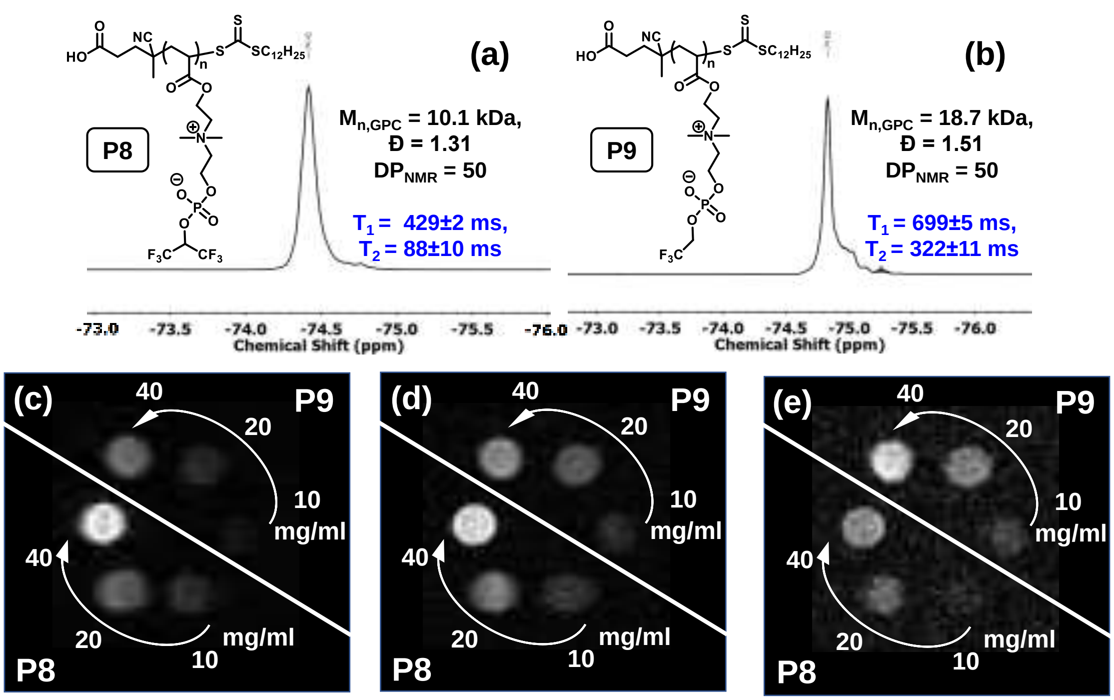

Figure 2-12. ^{19}F NMR spectra and relaxation times of (a) P8 and (b) P9 in D_2O/PBS (1/9 v/v) (10 mg/mL), ^{19}F MR images of solutions of P8 and P9 at different concentrations obtained using (c) fast spin echo sequence, (d) first slice and (e) eleventh slice obtained from multi echo spin echo sequence.

solutions of **P8** and **P9** at different concentrations was performed on a 11.7 T MRI scanner (**Figure 2-10 (c-e)**). Using a fast spin echo sequence, T_1 weighted images of **P8** were brighter images (stronger signal) due to its shorter T_1 and higher fluorine content (**Figure 2-10c**). By a multi echo spin echo sequence, the **P8** image was brighter than **P9** at shorter echo times (**Figure 2-10d**), due to its higher fluorine content, and as echo time increased (weighted towards T_2), the **P9** signal intensified (**Figure 2-10e**).

2.5 Interface stabilization with fluorinated polymer zwitterions

To investigate the surfactant properties of FCP polymers, interfacial tension (IFT) measurements were conducted at the perfluorohexane (PFH)-water interface (45 mN/m) using the pendant drop tensiometry technique (**Figure 2-11a**). With 1 mg/mL polymer solutions, the FCPs **P1**, **P3** and **P6** led to reduction of the initial IFT value to 19, 22 and 17 mN/m, respectively, while MPC-TDFOA copolymers **P4** and **P5** produced relatively modest reduction to 27 and 40 mN/m, respectively (**Figure 2-11b**). The PFH emulsions were prepared by vortexing or sonicating polymer solutions with the oil, producing droplets in the 50-100 micron diameter range as revealed by optical microscopy (**Figure 2-11c**). The droplets remained visibly stable for weeks, distinct from

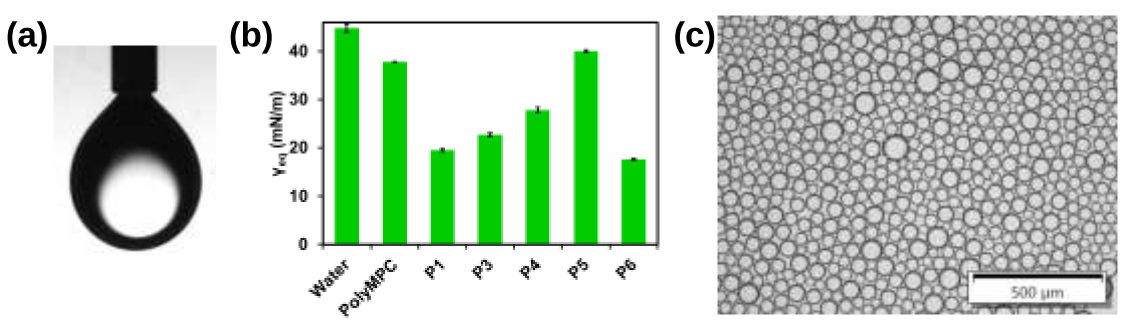

Figure 2-13. Interfacial tension measurements of polymer solutions. (a) Pendant drop tensiometry; (b) mean equilibrium interfacial tension (γeq) of PFH/water at 1 mg/mL (each bar represents an average of three measurements); (c) optical microscope image of PFH droplets in 2 mg/mL **P3** solution prepared by vortexing.

polyMPC itself which is not surface active. In addition, nanoemulsions (*e.g.*,from 20 mL PFH in 4 mL of a 2 mg/mL polymer solution) were prepared using a Branson 150 probe sonicator (40 kHz frequency and 150 W maximum power) at an amplitude of 35-40% for 2-3 min (operating in pulse mode with alternating cycles of 45 seconds on and 30 seconds off). This method produced droplets with an initial z-average diameter of ~200-260 nm and polydispersity index (PDI) below 0.2, as assessed by dynamic light scattering (DLS) (**Figure 2-12a**). Further DLS evaluation probed the change in nanoemulsion size over time.[24] For **P1**, **P4**, **P5**, and **P6**, the droplets coalesced into the micron diameter range upon aging, while **P3**-stabilized droplets grew much more slowly, suggestive of Ostwald ripening.[22] At 2 mg/mL, **P3** produced the most stable structures, increasing from ~200 nm to ~287 nm over one day and up to about 600 nm in two weeks, and repeating the sonication re-established the original size distribution (**Figure 2-12a**). Notably, increasing the concentration of **P3** to 10-20 mg/mL generated smaller droplets (~160 nm diameter) and further slowed growth (~433 nm after two weeks) (**Figure 2-12b**). While the precise structure of these polymers at fluorocarbon-water interfaces is unknown, the

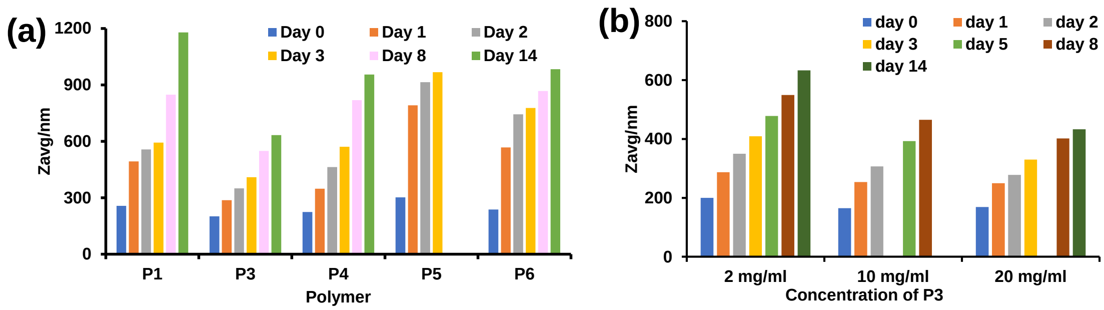

Figure 2-14. (a) Size of the PFH nanoemulsions stabilized by **P1**, **P3**-**P6** (2mg/mL) over time; (b) size of PFH nanoemulsions stabilized by **P3** at different concentrations over time.

enhanced emulsion stability offered by FCP polymers demonstrates one clear benefit of embedding fluorinated groups directly into zwitterionic components of polymers.

2.6 Properties of FCP polymer coatings

The FCP polymers described to this point may exhibit interesting surface properties due to their unusual chemical compositions and the merging of superhydrophilic (zwitterionic) with low surface energy (fluorocarbon) components.[11,31] As a preliminary investigation of such properties, the water insoluble **P2** was applied on a Si wafer by spin-coating from TFE, with comparative property analyses made against a fluorinated methacrylate polymer coating, namely poly(1H,1H,2H,2H-tridecafluoro-*n*-octyl methacrylate) (polyTDFOMA). The wettability of these coated surfaces was probed using water, hexadecane, and perfluorodecalin by contact angle goniometry measurements. The impact of the zwitterion on water contact angle (CA) was evident, with **P2** exhibiting lower CA (~92°) than polyTDFOMA(~114°), while when probed with the organic solvent hexadecane each polymer displayed similar CAs of ~70°. When probed with fluorocarbon liquids, the zwitterion again exhibited significant influence, with perfluorodecalin giving a low but measurable contact angle of ~33° on **P2**-coated Si,

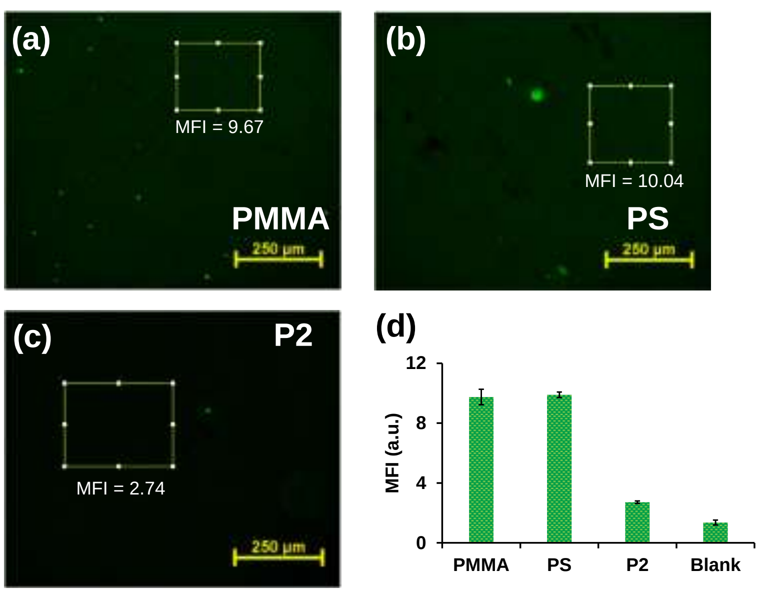

Figure 2-15. Fluorescence microscopy images of (a) PMMA; (b) PS; and (c) P2-coated Si substrates after exposure to FITC-BSA solution and rinsing; (d) MFI values of the images obtained by ImageJ evaluation.

while spreading completely on polyTDFOMA. Thus, the unique FCP design bridges materials properties, tempering zwitterion hydrophilicity with fluorocarbon character and modulating their "fluorophilicity" with zwitterions. The extent to which these distinct components are "switchable" topographically will be probed in future studies. Preliminary results suggest that FCP-coated surfaces resist absorption of FITC-labeled bovine serum albumin (BSA). Immersion of Si substrates coated with the water insoluble **P2** in 1 mg/mL of a PBS solution of FITC-BSA for 20 hours produced little fluorescent signal (minimally greater than a blank control), whereas the same experiment performed on PMMA and PS-coated substrates led to a notably greater fluorescence from absorbed protein (**Figure 2-13**).[32]

2.7 *In vitro* cytotoxicity evaluation

Finally, using aqueous soluble versions of FCP polymers in cell culture indicated low levels of cytotoxicity, at least up to 5 mg/mL levels. As shown in **Figure 2-14**, the percent viability of both human breast cancer cells (MDA-MB-231) and human embryonic kidney 293 cells (HEK293) in the presence of FCP in solution remained high over a 48-hour evaluation time frame, near to that of the control (i.e., no polymer)

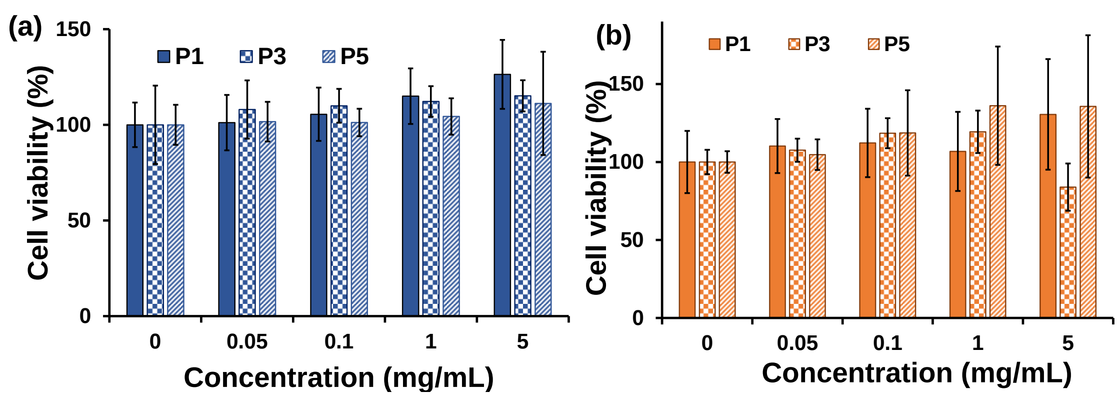

Figure 2-16. *In vitro* cytotoxicity evaluation of **P1** (M_n,GPC = 6.7kDa), **P3** (with 45 mol% incorporation of MPC) and **P6** in cell culture of (a) MDA-MB-231 and (b) HEK293 cells.

samples. With these cell lines, little-to-no negative impact on cell viability was seen, with only a slight reduction in viability (to ~80%) for HEK293 cells at the highest concentration (5 mg/mL) of **P3**. This apparent lack of cytotoxicity in cell culture suggests future potential for using these polymers in diagnostics and therapeutics, as well as materials applications where some fluorinated surfactants have been scrutinized.[33]

In summary, this chapter has described the preparation of fluorinated choline phosphate monomers and examined their controlled free radical polymerization to yield a new library of fluorinated zwitterionic polymers. The combination of fluorinated and zwitterionic units within the same structural moiety holds promise in applications ranging from ^{19}F MRI agents to nonfouling coatings and interface stabilization, which are examined further in Chapters 3 and 4.

Ms. Alexandria Triozzi performed the cell viability tests (section 2.6). Dr. James Quirk performed magnetic resonance imaging in the Small Animal Magnetic Resonance Facility in the Mallinckrodt Institute of Radiology of the Washington University St. Louis School of Medicine.

2.8 References

1. Schlenoff, J. B. Zwitteration: Coating surfaces with zwitterionic functionality to reduce nonspecific adsorption. Langmuir 30, 9625–9636 (2014).

2. Ishihara, K. & Nakabayashi, N. Preparation of phospholipid polymers and their properties as polymer hydrogel membranes. Proc. Control. Release Soc. 22, 787–788 (1996).

3. Hill, M. R., Carmean, R. N. & Sumerlin, B. S. Expanding the Scope of RAFT Polymerization: Recent Advances and New Horizons. Macromolecules 48, 5459–5469 (2015).

4. Perrier, S. 50th Anniversary Perspective: RAFT Polymerization - A User Guide. Macromolecules 50, 7433–7447 (2017).

5. Bhuchar, N., Deng, Z., Ishihara, K. & Narain, R. Detailed study of the reversible addition-fragmentation chain transfer polymerization and co-polymerization of 2-methacryloyloxyethyl phosphorylcholine. Polym. Chem. 2, 632–639 (2011).

6. Chen, X., McRae, S., Parelkar, S. & Emrick, T. Polymeric Phosphorylcholine−Camptothecin Conjugates Prepared by Controlled Free Radical Polymerization and Click Chemistry. Bioconjug. Chem. 20, 2331–2341 (2009).

7. Chen, X., Parelkar, S. S., Henchey, E., Schneider, S. & Emrick, T. PolyMPC–Doxorubicin Prodrugs. Bioconjug. Chem. 23, 1753–1763 (2012).

8. Chen, S.-H., Fukazawa, K., Inoue, Y. & Ishihara, K. Photoinduced Surface Zwitterionization for Antifouling of Porous Polymer Substrates. Langmuir 35, 1312–1319 (2019).

9. Sae-ung, P. et al. Antifouling Stripes Prepared from Clickable Zwitterionic Copolymers. Langmuir 33, 7028–7035 (2017).

10. Ward, S. M., Skinner, M., Saha, B. & Emrick, T. Polymer–Temozolomide Conjugates as Therapeutics for Treating Glioblastoma. Mol. Pharm. 15, 5263–5276 (2018).

11. Xie, Q., Pan, J., Ma, C. & Zhang, G. Dynamic surface antifouling: Mechanism and systems. Soft Matter 15, 1087–1107 (2019).

12. Li, B. et al. Trimethylamine N-oxide–derived zwitterionic polymers: A new class of ultralow fouling bioinspired materials. Sci. Adv. 5, eaaw9562 (2019).

13. Mukai, M., Ihara, D., Chu, C.-W., Cheng, C.-H. & Takahara, A. Synthesis and Hydration Behavior of a Hydrolysis-Resistant Quasi-Choline Phosphate Zwitterionic Polymer. Biomacromolecules 21, 2125–2131 (2020).

14. Wang, W. et al. Tailor-Made pH-Responsive Poly(choline phosphate) Prodrug as a Drug Delivery System for Rapid Cellular Internalization. Biomacromolecules 17, 2223–2232 (2016).

15. Hu, G., Parelkar, S. S. & Emrick, T. A facile approach to hydrophilic, reverse zwitterionic, choline phosphate polymers. Polym. Chem. 6, 525–530 (2015).

16. Hu, G. & Emrick, T. Functional Choline Phosphate Polymers. J. Am. Chem. Soc. 138, 1828–1831 (2016).

17. Mukai, M., Higaki, Y., Hirai, T. & Takahara, A. Separation of endo-cyclic 2-methacryloyloxyethyl choline phosphate by anion exchange approach. Chem. Lett. 47, 1509–1511 (2018).

18. Maan, A. M. C., Hofman, A. H., de Vos, W. M. & Kamperman, M. Recent Developments and Practical Feasibility of Polymer-Based Antifouling Coatings. Adv. Funct. Mater. 30, 2000936 (2020).

19. Fu, C. et al. Low-Fouling Fluoropolymers for Bioconjugation and In Vivo Tracking. Angew. Chemie 132, 4759–4765 (2020).

20. Tennie, I. K. & Kilbinger, A. F. M. Polymeric 19F MRI Contrast Agents Prepared by Ring-Opening Metathesis Polymerization/Dihydroxylation. Macromolecules 53, 10386–10396 (2020).

21. Sedlacek, O. et al. Fluorinated Water-Soluble Poly(2-oxazoline)s as Highly Sensitive 19F MRI Contrast Agents. Macromolecules 53, 6387–6395 (2020).

22. Huang, Y. et al. Polymer-Stabilized Perfluorobutane Nanodroplets for Ultrasound Imaging Agents. 18–21 (2017). doi:10.1021/jacs.6b08800

23. Estabrook, D. A., Ennis, A. F., Day, R. A. & Sletten, E. M. Controlling nanoemulsion surface chemistry with poly(2-oxazoline) amphiphiles. Chem. Sci. 10, 3994–4003 (2019).

24. Day, R. A. et al. Systematic Study of Perfluorocarbon Nanoemulsions Stabilized by Polymer Amphiphiles. ACS Appl. Mater. Interfaces 12, 38887–38898 (2020).

25. Inoue, Y., Watanabe, J., Takai, M., Yusa, S. & Ishihara, K. Synthesis of sequence-controlled copolymers from extremely polar and apolar monomers by living radical polymerization and their phase-separated structures. J. Polym. Sci. Part A Polym. Chem. 43, 6073–6083 (2005).

26. Kasper, J. J. et al. A Library of Fluorinated Electrophiles for Chemical Tagging and Materials Synthesis. J. Org. Chem. 81, 8095–8103 (2016).

27. Carr, H. Y. & Purcell, E. M. Effects of Diffusion on Free Precession in Nuclear Magnetic Resonance Experiments. Phys. Rev. 94, 630–638 (1954).

28. Meiboom, S. & Gill, D. Modified Spin-Echo Method for Measuring Nuclear Relaxation Times. Rev. Sci. Instrum. 29, 688–691 (1958).

29. Couturaud, B. et al. Supramolecular Fluorine Magnetic Resonance Spectroscopy Probe Polymer Based on Passerini Bifunctional Monomer. (2019). doi:10.1021/acsmacrolett.9b00626

30. Zhang, C., Kim, D. S., Lawrence, J., Hawker, C. J. & Whittaker, A. K. Elucidating the Impact of Molecular Structure on the 19F NMR Dynamics and MRI Performance of Fluorinated Oligomers. (2018). doi:10.1021/acsmacrolett.8b00433

31. Xu, B. et al. Semifluorinated Synergistic Nonfouling/Fouling-Release Surface. ACS Appl. Mater. Interfaces 9, 16517–16523 (2017).

32. Ying, P., Yu, Y., Jin, G. & Tao, Z. Competitive protein adsorption studied with atomic force microscopy and imaging ellipsometry. Colloids Surfaces B Biointerfaces 32, 1–10 (2003).

33. United States Environmental Protection Agency. Basic Information on PFAS. United States Environmental Protection Agency Available at: https://www.epa.gov/pfas/basic-information-pfas.

CHAPTER 3

FLUORINATED ZWITTERIONIC POLYMERS AS DYNAMIC SURFACE COATINGS

3.1 Introduction

The rapidly growing library of functional polymers, in combination with advances in controlled polymerization techniques, represents an exceptionally useful platform for controlling surface chemistry and topology.[1–3] For example, surfaces described by their "extreme wettability", meaning superhydrophilic or superhydrophobic, exhibit interesting and useful properties, including antifogging, self-cleaning, and controlled adhesion.[4–6] Functionalized surfaces equipped to interact selectively with compounds of interest are useful in separations and sensing.[7,8] Surfaces may also be engineered to mimic the wettability of exquisite structures in Nature, such as the lotus leaf (superhydrophobic)[9] or rose petal (large contact angle hysteresis).[10] In general, the ability of polymers to bridge the interface between a substrate and their surrounding environment tailors surface properties (wettability, adhesion, electronics, etc.) and provides a route to improved medical devices, implants, biosensors, and electronic devices.[11–13]

Synthetic polymers are prime candidates for selection as fouling resistant coatings, especially through the use of hydrophilic polymers, such as poly(ethylene oxide) (PEO) or polymer zwitterions.[14] Polymer zwitterions exhibit particularly outstanding performance, as their inner-salt structure promotes surface hydration that masks nonpolar biomolecule-surface interactions, thus exhibiting *fouling resistant* properties.[15] To date, phosphorylcholine (PC), sulfobetaine (SB), and carboxybetaine

(CB)-based structures represent the most frequently utilized examples of polymer zwitterions for surface modification.[16] Other approaches to achieve antifouling properties utilize fluoropolymers and silicone elastomers, each having low surface energy that weakens interactions with potential foulants, and thus enables *foulant release*.[17] Despite extensive research on such hydrophilic and fluorophilic materials, continued progress requires the discovery of new, innovative materials interfaces capable of responding to different environmental conditions. Recent studies have examined the combination of hydrophilic and fluorinated groups in surface modification. For example, Xu, *et al*. coated surfaces with polymers containing both trifluoromethyl and PEG side chains to afford synergistic non-fouling/fouling release behavior with proteins.[18] In some cases, modifying surfaces with amphiphilic polymers may enhance antifouling performance, and as such this approach is being examined in marine coatings and medical implants.[19,20]

In Chapter 2, the synthesis of novel fluorinated zwitterionic monomers was described, in which fluorinated groups were embedded directly into choline phosphate sub-units, giving fluorinated choline phosphates (FCPs). FCPs with 1H,1H,2H,2H-tridecafluoro-n-octyl (PFH-CP) pendent groups produced the non-aqueous soluble polymer **P2** by RAFT polymerization. In preliminary fouling experiments, performed by immersing **P2**-coated Si substrates into an aqueous protein solution, FCP coatings provided significant non-fouling properties; moreover, the coated substrates exhibited considerable hydrophobicity, with a measured water contact angle of 92^{o}. Described in Chapter 3 are efforts to gain a deeper appreciation of the impact of FCPs on surface properties. As illustrated in **Figure 3-1**, using surface-initiated atom transfer radical polymerization (SI-ATRP), Au substrates were modified with polymer zwitterions, fluorinated polymers, or FCPs. The combination of zwitterionic and fluorocarbon groups in the FCP structure afforded surfaces with distinctly different properties relative to PMPC or fluoropolymer-grafted substrates, including notably high contact angle hysteresis values that suggest dynamic surface rearrangement. Using surface plasmon resonance (SPR) techniques, BSA and lysozyme adsorption were examined, with results indicating a resistance to protein adsorption owing to FCP grafting. Overall, to our knowledge this work describes the first example of grafting fluorinated zwitterionic polymer brushes from surfaces and demonstrates the potential of these functional substrates as antifouling materials.

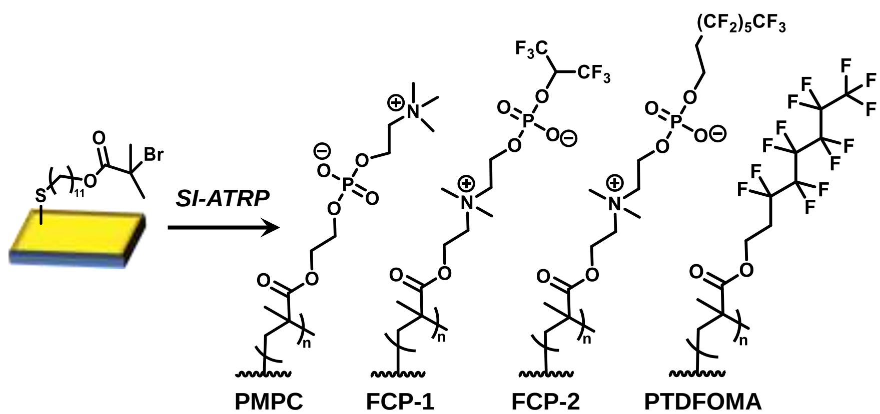

Figure 3-1. Schematic representation of grafting PMPC, FCP-1, FCP-2 and PTDFOMA from Au substrates by SI-ATRP.

3.2 Preparation of polymer grafted substrates

A gold-coated Si wafer was functionalized suitably for ATRP, using literature preparations,[22] and employed for SI-grafting of zwitterionic, fluorinated, and “fluorozwitterionic” polymers, as shown in **Figure 3-1**.[21] SI-ATRP was performed by placing the substrates in 7 mL glass vials containing 0.3-0.5 M monomer solutions in trifluoroethanol (TFE) at room temperature for 1-4 hrs, with CuBr and bipyridine, yielding PMPC-, FCP-1-, and FCP-2-grafted substrates. PTDFOMA grafting was performed similarly, employing a 0.8 M trifluorotoluene (TFT) solution of monomer at 60 ^{o}C, with CuBr and 4,4′-dinonyl-2,2′-bipyridyl (dNbpy). The presence of polymer on the substrates was confirmed by X-ray photoelectron spectroscopy (XPS), noting for example the presence of C, N, O, F, and P in the XPS survey scan of FCP-2 (**Figure 3-2a**) at elemental percentages that agreed with theoretical values (C 46.15%, N 2.56%, O 15.38%, F 33.33%, P 2.56%). In the high-resolution C_{1s} spectrum of FCP-2, peak deconvolution revealed the distinct carbon atoms (**Figure 3-2b**) at 284.8 eV ($\underline{C}$-C), 286 eV ($\underline{C}$-N), 286.7 eV ($\underline{C}H_2$-O), 288.6 eV ($\underline{C}$=O), 290.4 eV (-CF_2-$\underline{C}F_2$-CH_2), 291.4 eV ($\underline{C}F_2$), and 293.6 eV ($\underline{C}F_3$). Similar scans performed on FCP-1, PMPC and PTDFOMA-grafted substrates (**Figure 3-2(c-h)**) verified the presence of the desired polymers. The thickness of the polymer layers on each substrate, measured by ellipsometry (and calculated using the Cauchy model[23]) to be ~40-60 nm, suggests considerable extents of grafting and as such the presence of sufficient polymer coverage to modify surface properties and perform comparative evaluations across this set of samples. these grafted polymer chains were considered to be in the brush regime,[24] with grafting densities estimated to be 0.12, 0.30, 0.28 and 0.18 chains/nm^2 for PMPC-, FCP-1-, FCP-2- and PTDFOMA-modified surfaces, respectively (see Chapter 6.3 for calculations).

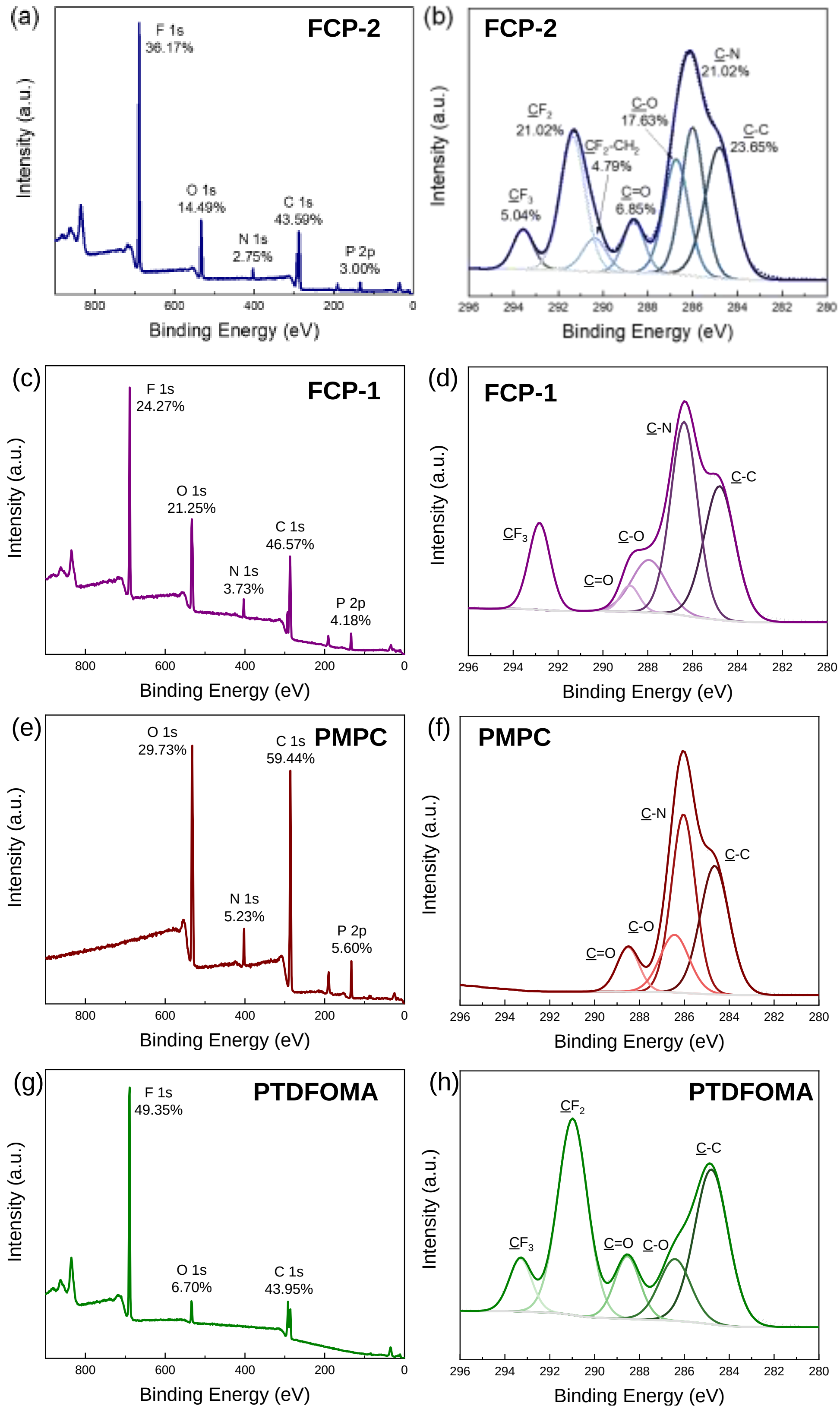

Figure 3-2. XPS spectra of FCP-2-, FCP-1-, PMPC- and PTDFOMA-grafted Au: (a), (c), (e) and (g) survey spectra and (b), (d), (f) and (h) C1s scan.

3.3 Characterization of wettability and surface energy

Wettability characteristics (*i.e.*, hydro- and fluorophilicity) of the polymer-modified substrates were evaluated by contact angle measurements, using water (in air) and trifluorotoluene (in water) as probe fluids. As shown in **Figure 3-3(a-d)** and **Table 3-1**, the PMPC-functionalized substrates exhibited very small contact angles, typically ~15^{o}, due to the extensive hydrophilicity of this polymer zwitterion; in contrast, the fluorocarbon-rich PTDFOMA grafted substrates repelled water, yielding contact angles of ~120^{o}. Substrates grafted with fluorinated zwitterions **FCP-1** and **FCP-2** had water contact angles intermediate between these extremes, measuring 69^{o} for **FCP-1** and 85^{o} for **FCP-2**. Thus, the effect of merging zwitterionic and fluorocarbon moieties in the pendant groups effectively alters the typical wetting properties of each: i.e., fluorocarbon polymers take on appreciable hydrophilicity, while polymer zwitterions gain an unusually high degree of hydrophobicity. Interestingly, when performing contact angle measurements with TFT in water, all zwitterion-containing substrates repelled the droplet with high contact angles (>140^{o}, **Figure 3-3(e-g)**), while the PTDFOMA-grafted surface was wet by TFT (contact angle ~31^{o}).

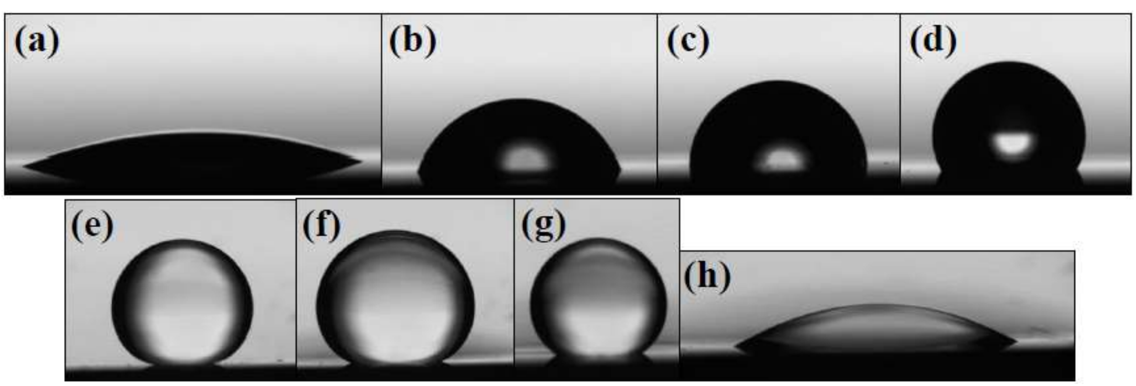

Figure 3-3. Photographs from static contact angle measurements of water on grafted substrates: (a) PMPC; (b) FCP-1; (c) FCP-2; and (d) PTDFOMA. Similar experiments using TFT as the probe fluid shown in (e) PMPC; (f) FCP-1; (g) FCP-2; and (h) PTDFOMA.

Solid-vapor (sv) surface energies (γ_{SV}, sum of the dispersive (γ_{SV}^d) and polar (γ_{SV}^p) components) were calculated using Young's equation (**Equation 3-1**) and the Owens-Wendt equation (**Equation 3-2**), employing the known surface energy (γ_{LV}) of

$$\gamma_{SV} = \gamma_{SL} + \gamma_{LV}\cos\theta \qquad \textbf{Equation 3-1}$$
$$\gamma_{LV}(1+\cos\theta) = 2(\gamma_{SV}^d\gamma_{LV}^d)^{1/2} + 2(\gamma_{SV}^p\gamma_{LV}^p)^{1/2} \qquad \textbf{Equation 3-2}$$

three test liquids—water, diiodomethane, and glycerol—and measurements of their contact angles (θ) on each surface in air (**Table 3-1**). The contact angle values of diiodomethane on PMPC- FCP-1-, FCP-2-, and PTDFOMA-modified surfaces in air were measured as 21°, 68°, 72°, and 100°, respectively; a similar trend was seen when using glycerol (38°, 72°, 90°, and 108° on PMPC- FCP-1-, FCP-2-, and PTDFOMA). These data produce surface energies of 70.4, 34.2, 23.4, and 9.3 mJ/m^2 for PMPC-, FCP-1-, FCP-2- and PTDFOMA-modified substrates, respectively, confirming the dominant impact of the fluorine-rich PTDFOMA on surface energy, and the role of the zwitterion in modulating surface energy. The calculated γ_{SV} and the observed water contact angles and surface/water interfacial energies (γ_{SL}) reported in **Table 3-1** were determined using

Table 3-1. Surface wettability and surface energy values of PMPC, FCP-1, FCP-2, and PTDFOMA-grafted substrates.

	PMPC	FCP-1	FCP-2	PTDFOMA
water, static (°)	14.8 ± 6.8	68.5 ± 1.9	85.3 ± 0.6	119.6 ± 0.1
water, advancing (°)	14.5 ± 0.5	79.3 ± 2.3	114.7 ± 3.8	125.0 ± 0.7
water, receding (°)	< 10	16.7 ± 1.5	24.7 ± 1.1	77.2 ± 1.5
diiodomethane, static (°)	21.2 ± 4.0	67.7 ± 1.0	72.3 ± 3.2	99.7 ± 1.0
glycerol, static (°)	37.7 ± 2.1	72.2 ± 1.3	90.2 ± 7.3	108.4 ± 0.6
TFT in water, static (°)	160.5 ± 2.1	154.7 ± 1.4	142.3 ± 1.7	30.9 ± 0.9
dispersive component γ_s^d (mJ/m^2)	40.9 ± 3.4	20.5 ± 1.1	17.6 ± 2.9	8.9 ± 0.4
polar component γ_s^p (mJ/m^2)	29.5 ± 1.3	13.7 ± 1.4	5.8 ± 0.2	0.4 ± 0.1
surface free energy γ_{SV} (mJ/m^2)	70.4 ± 4.8	34.2 ± 0.3	23.4 ± 2.7	9.3 ± 0.4
Water/surface interfacial free energy γ_{SL} (mJ/m^2)	0.3	7.5 ± 2.0	17.4 ± 1.9	45.3 ± 0.5

Equation 3-1. The PMPC-grafted substrates exhibited exceptionally low γ_{SL} values 0.3 mJ/m^2, while γ_{SL} values of FCP-1-, FCP-2- and PTDFOMA-grafted surfaces were calculated to be 7.5, 17.4, and 45.3 mJ/m^2, respectively. The lower γ_{SL} of PMPC-, FCP-1-, and FCP-2-modified surfaces hindered spreading of TFT in water (TFT/water interfacial energy = 33.8 mJ/m^2), resulting in high contact angles, while the PTDFOMA-modified surface showed the expected wettability when probed with TFT.

The wetting behavior described to this point suggests that the zwitterionic and fluorinated components of FCP-1 and FCP-2 are sensitive to their surrounding environment. Conformational rearrangement of fluorinated polymers has been discussed by Takahara on thin films of poly(fluoroalkyl acrylate)s, which may reorient to present carbonyl groups to the water interface.[25,26] In addition, Wooley reported PEG-containing hyperbranched fluoropolymers, where the PEG and fluorinated domains reorganized in response to the surrounding liquid, giving nanoscale complexity and non-fouling properties.[27–29] In our work, the fluorinated groups of FCP-1 and FCP-2 must strongly prefer the air interface, in accord with the apolar and self-associating nature of fluorocarbons. However, when immersed in water, the strong hydrophilicity of the zwitterionic groups induces their segregation to the polymer-water interface, imparting a significant degree of hydrophilicity (fluorophobicity) to substrates modified with FCP-1 and FCP-2.

Our findings are further supported by dynamic water contact angle measurements, in which large contact angle hysteresis values were observed for FCP-1 (~60°) and FCP-2 (~90°)-grafted surfaces (**Table 3-1**). In these measurements, increasing the volume of water in the advancing measurement led to repulsion of the droplet (and correspondingly high contact angle) by fluorinated groups at the polymer-air interface (**Figure 3-4a**). The advancing angles were sensitive to fluorine content, with FCP-1 (79°) < FCP-2 (115°) < PTDFOMA (125°). The low receding angles of FCP-1 (17°) and FCP-2 (25°) are due to the preference of the zwitterionic units for the water-polymer interface (**Figure 3-4b**), which are absent in PTDFOMA (receding angle ~77°). When the substrates were oriented vertically, the drop resisted sliding off of the FCP-2 surface, but traversed the PTDFOMA surface quickly. Such hydrophobic surfaces that retain water (i.e., exhibit large contact angle hysteresisvalues) mimic the surface wettability of rose petals and are interesting for studies in water transport. Surfaces with such property are typically obtained by manipulation of surface topology,[10,30] but here are achieved using the advantageous chemical structures of FCPs in combination with surface grafting techniques.

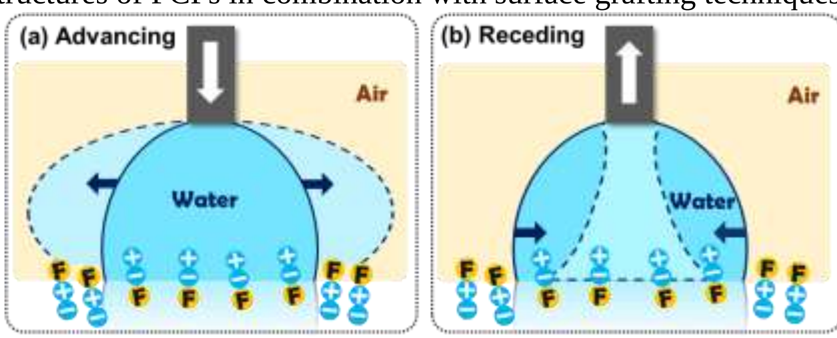

Figure 3-5. Schematic illustration FCP reorganization: (a) advancing and (b) receding contact angle measurements.

3.4 Protein resistance evaluation by SPR measurement

To examine protein adsorption on these polymer-modified substrates, SPR was employed (using the Biacore T200 system). These experiments are useful for assessing the change in the angle of minimum reflectivity (SPR angle) as a function of refractive index as it is altered upon analyte (i.e., protein) adherence or dissociation (**Figure 3-5a**).[31–35] Based on literature precedent,[36–38] our experimental design equated one response unit change (ΔRU) with 0.1 ng/cm^2 protein. These experiments were performed by first applying the protein solution (1 mg/mL) to the surfaces at a flow rate of 20 μL/min for 300 seconds, then rinsing the surfaces with PBS buffer for 300 seconds at 20 μL/min to remove any loosely adsorbed protein. As seen in **Figure 3-5b,** all of the polymer-grafted surfaces substantially reduced BSA adsorption relative to bare Au, giving ng/cm^2 values of 228.1 (bare gold), 56.2 (PTDFOMA), 36.8 (PMPC), 17.6 (FCP-2), and 9.5 (FCP-1); after rinsing with PBS, these values were reduced to 204.2, 42.6, 17.9, 3.6 and 0.6 ng/cm^2, respectively. FCP-1 and FCP-2 exhibited particularly impressive *adsorption resistance and foulant release* against BSA, with >75% reduction in BSA content after rinsing. In the lysozyme adsorption study, bare gold, PMPC-, FCP-1-, FCP-2- and PTDFOMA-modified surfaces had adsorption values of 152.3, 54.4, 51.3, 27.5, and 16.9 ng/cm^2, respectively, upon applying lysozyme solution; these values declined to 123.3, 36.9, 37.4, 13.6 and 10.6 ng/cm^2 after rinsing (**Figure 3-5c**). Notably, inclusion of the perfluorohexyl structure in FCP-2 effectively reduced lysozyme adhesion in comparison to PMPC, and 53% of the adsorbed lysozyme was removed after rinsing the FCP-2-modified surfaces, resulting in similar adsorption level as PTDFOMA-modified surface. In general, the combination of fluorinated and zwitterionic structures improved the antifouling properties of each structure, seen as reduced protein adhesion and enhanced foulant release.

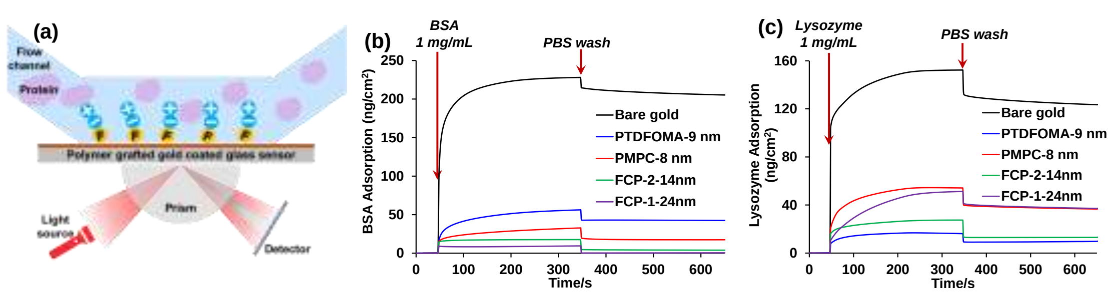

Figure 3-6. (a) Schematic illustration of SPR measurements; (b) BSA and (c) lysozyme adsorption on grafted substrates measured by SPR.

In summary, this Chapter has described the impact of grafting surfaces with fluorinated polymer zwitterions and specifically their unique wettability and anti-fouling attributes relative to conventional polymer zwitterions and polymeric fluorocarbons. The fluorinated zwitterionic polymers, FCP-1 and FCP-2, exhibited hydrophobicity in air and fluorophobicity in water, as well as notably high contact angle hysteresis values. These dynamic wetting behaviors suggest a dynamic reorganization of fluorinated and zwitterionic units in response to the contacting fluid environment. Remarkably, FCP-1- and FCP-2-grafted surfaces afforded comparable or greater protein resistance than the PMPC- and PTDFOMA- modified surfaces against BSA and lysozyme.

**Measurement and analysis of thickness and contact angle were performed by Dr. Zhefei Yang in the Emrick Group. XPS measurement and analysis of the modified surfaces was performed by James Nicolas Pagaduan in the Emrick Group.*

3.5 References

1. Sun, W., Liu, W., Wu, Z. & Chen, H. Chemical Surface Modification of Polymeric Biomaterials for Biomedical Applications. *Macromolecular Rapid Communications* **41**, 1900430 (2020).
2. Chen, W. L., Cordero, R., Tran, H. & Ober, C. K. 50th Anniversary Perspective: Polymer Brushes: Novel Surfaces for Future Materials. *Macromolecules* **50**, 4089–4113 (2017).
3. Elizabeth Welch, M. *et al.* Polymer Brushes as Functional, Patterned Surfaces for Nanobiotechnology. *Journal of Photopolymer Science and Technology* **25**, 53–56 (2012).
4. Si, Y., Dong, Z. & Jiang, L. Bioinspired Designs of Superhydrophobic and Superhydrophilic Materials. *ACS Central Science* **4**, 1102–1112 (2018).
5. Dong, T. & McCarthy, T. J. Superhydrophobic, Low-Hysteresis Patterning Chemistry for Water-Drop Manipulation. *ACS Applied Materials and Interfaces* **9**, 41126–41130 (2017).
6. Gao, L. & McCarthy, T. J. A perfectly hydrophobic surface ($\theta A/\theta R = 180°/180°$). *J Am Chem Soc* **128**, 9052–9053 (2006).

7. Bratek-Skicki, A. *et al.* Mixed Polymer Brushes for the Selective Capture and Release of Proteins. *Biomacromolecules* **20**, 778–789 (2019).

8. Srinivas, A. R. G. *et al.* Polymer Brush Functionalization of Polyurethane Tunable Nanopores for Resistive Pulse Sensing. *ACS Applied Polymer Materials* **3**, 279–289 (2021).

9. Ji, J., Fu, J. & Shen, J. Fabrication of a superhydrophobic surface from the amplified exponential growth of a multilayer. *Advanced Materials* **18**, 1441–1444 (2006).

10. Telford, A. M., Hawkett, B. S., Such, C. & Neto, C. Mimicking the wettability of the rose petal using self-assembly of waterborne polymer particles. *Chemistry of Materials* **25**, 3472–3479 (2013).

11. Pagaduan, J. N. *et al.* Electronic Tuning of Monolayer Graphene with Polymeric "Zwitterists." *ACS Nano* **15**, 2762–2770 (2021).

12. Li, B. *et al.* Trimethylamine N-oxide-derived zwitterionic polymers: A new class of ultralow fouling bioinspired materials. *Science Advances* **5**, 9562–9576 (2019).

13. Jesmer, A. H. *et al.* Graft-Then-Shrink: Simultaneous Generation of Antifouling Polymeric Interfaces and Localized Surface Plasmon Resonance Biosensors. *ACS Applied Materials and Interfaces* **13**, 52362–52373 (2021).

14. Lowe, S., O'Brien-Simpson, N. M. & Connal, L. A. Antibiofouling polymer interfaces: poly(ethylene glycol) and other promising candidates. *Polymer Chemistry* **6**, 198–212 (2014).

15. Chen, Z. Surface Hydration and Antifouling Activity of Zwitterionic Polymers. *Langmuir* **38**, 4483–4489 (2022).

16. Huang, H. *et al.* Strong Surface Hydration and Salt Resistant Mechanism of a New Nonfouling Zwitterionic Polymer Based on Protein Stabilizer TMAO. *J Am Chem Soc* **143**, 16786–16795 (2021).

17. Maan, A. M. C., Hofman, A. H., de Vos, W. M. & Kamperman, M. Recent Developments and Practical Feasibility of Polymer-Based Antifouling Coatings. *Advanced Functional Materials* **30**, 2000936 (2020).

18. Xu, B. *et al.* Semifluorinated Synergistic Nonfouling/Fouling-Release Surface. *ACS Applied Materials & Interfaces* **9**, 16517–16523 (2017).

19. Wu, H. X., Zhang, X. H., Huang, L., Ma, L. F. & Liu, C. J. Diblock Polymer Brush (PHEAA-b-PFMA): Microphase Separation Behavior and Anti-Protein Adsorption Performance. *Langmuir* **34**, 11101–11109 (2018).

20. Wu, H.-X., Tan, L., Yang, M.-Y., Liu, C.-J. & Zhuo, R.-X. Protein-resistance performance of amphiphilic copolymer brushes consisting of fluorinated polymers and polyacrylamide grafted from silicon surfaces. *RSC Advances* **5**, 12329–12337 (2015).

21. Zhou, L., Triozzi, A., Figueiredo, M. & Emrick, T. Fluorinated Polymer Zwitterions: Choline Phosphates and Phosphorylcholines. *ACS Macro Letters* **10**, 1204–1209 (2021).

22. Shah, R. R. *et al.* Using atom transfer radical polymerization to amplify monolayers of initiators patterned by microcontact printing into polymer brushes for pattern transfer. *Macromolecules* **33**, 597–605 (2000).

23. Xie, H., Wei, J. & Zhang, X. Characterisation of Sol-gel Thin Films by Spectroscopic Ellipsometry. *Journal of Physics: Conference Series* **28**, 95 (2006).

24. Wu, T., Efimenko, K. & Genzer, J. Combinatorial study of the mushroom-to-brush crossover in surface anchored polyacrylamide. *J Am Chem Soc* **124**, 9394–9395 (2002).

25. Honda, K. *et al.* Molecular Aggregation Structure of Poly(fluoroalkyl acrylate) Thin Films Evaluated by Synchrotron-sourced Grazing-incidence X-ray Diffraction. *Chemistry Letters* **34**, 1024–1025 (2005).

26. Honda, K., Morita, M., Otsuka, H. & Takahara, A. Molecular aggregation structure and surface properties of poly(fluoroalkyl acrylate) thin films. *Macromolecules* **38**, 5699–5705 (2005).

27. Pollack, K. A., Imbesi, P. M., Raymond, J. E. & Wooley, K. L. Hyperbranched Fluoropolymer-Polydimethylsiloxane-Poly(ethylene glycol) Cross-Linked Terpolymer Networks Designed for Marine and Biomedical Applications: Heterogeneous Nontoxic Antibiofouling Surfaces. *ACS Applied Materials & Interfaces* **6**, 19265–19274 (2014).

28. Imbesi, P. M. *et al.* Targeted surface nanocomplexity: two-dimensional control over the composition, physical properties and anti-biofouling performance of hyperbranched fluoropolymer–poly(ethylene glycol) amphiphilic crosslinked networks. *Polymer Chemistry* **3**, 3121–3131 (2012).

29. Gudipati, C. S., Creenlief, C. M., Johnson, J. A., Prayoncpan, P. & Wooley, K. L. Hyperbranched fluoropolymer and linear poly(ethylene glycol) based amphiphilic crosslinked networks as efficient antifouling coatings: An insight into the surface compositions, topographies, and morphologies. *Journal of Polymer Science, Part A: Polymer Chemistry* **42**, 6193–6208 (2004).

30. Wang, L., Wei, J. & Su, Z. Fabrication of surfaces with extremely high contact angle hysteresis from polyelectrolyte multilayer. *Langmuir* **27**, 15299–15304 (2011).

31. Zheng, X. *et al.* Antifouling property of monothiol-terminated bottle-brush poly(methylacrylic acid)-graft-poly(2-methyl-2-oxazoline) copolymer on gold surfaces. *Journal of Materials Chemistry B* **3**, 1921–1930 (2015).

32. Holmlin, R. E., Chen, X., Chapman, R. G., Takayama, S. & Whitesides, G. M. Zwitterionic SAMs that resist nonspecific adsorption of protein from aqueous buffer. *Langmuir* **17**, 2841–2850 (2001).

33. Dang, Y., Quan, M., Xing, C. M., Wang, Y. B. & Gong, Y. K. Biocompatible and antifouling coating of cell membrane phosphorylcholine and mussel catechol modified multi-arm PEGs. *Journal of Materials Chemistry B* **3**, 2350–2361 (2015).

34. St. Hill, L. R. *et al.* Antifouling Coatings Generated from Unsymmetrical Partially Fluorinated Spiroalkanedithiols. *ACS Applied Bio Materials* **4**, 1563–1572 (2021).

35. Xing, C. M. *et al.* Quantitative fabrication, performance optimization and comparison of PEG and zwitterionic polymer antifouling coatings. *Acta Biomaterialia* **59**, 129–138 (2017).

36. Yoshioka, K., Sato, Y., Tanaka, M., Murakami, T. & Niwa, O. Suppression of non-specific adsorption using densified tri(ethylene glycol) alkanethiols: monolayer characteristics evaluated by electrochemical measurements. *Anal Sci* **26**, 33–37 (2010).

37. de Mol, N. J. & Fischer, M. J. E. *Surface Plasmon Resonance: Methods and Protocols*. *Life Sciences* (2010). doi:10.1007/978-1-60761-670-2.

38. Zheng, X. *et al.* Antifouling property of monothiol-terminated bottle-brush poly(methylacrylic acid)-graft-poly(2-methyl-2-oxazoline) copolymer on gold surfaces. *Journal of Materials Chemistry B* **3**, 1921–1930 (2015).

CHAPTER 4

IMPACT OF FLUORINATED POLYMER ZWITTERIONS ON DNA PACKAGING: COLLOIDAL STABILITY AND BINDING STRENGTH

4.1 Introduction

Nucleic acids, such as DNA, mRNA and siRNA, have emerged as important therapeutics for diseases that cannot be treated effectively with conventional small molecule or protein drugs.[1] Developing safe and efficient delivery vectors is crucial for the ultimate success of nucleic acid-based therapy, and a wide array of carriers—including viral, lipid, and polymeric—have been examined for their biocompatibility and efficiency in delivering nucleic acids *in vitro* and *in vivo*.[2–4] Polymeric vectors have attracted considerable interest among researchers and clinicians owing to their advantages of relatively low immunogenicity, capacity to load large nucleic acids, and long shelf-life, relative to viral and lipid vectors.[5–7] Importantly, the versatile functionalities that polymers can accommodate provide a powerful pathway to tune their properties and construct delivery systems with attractive characteristics, such as targeted/responsive delivery, degradability, and imageability.[8–10]

Cationic polymers bind with nucleic acids through electrostatic interactions to form "polyplexes". Properties of the polyplex particles, including size, zeta potential and binding affinity, greatly influence cellular internalization, intracellular trafficking, and cargo unpacking, and thus play a key role in the therapeutic outcome.[11] Polyplex diameters typically ranges from sub-100 nm to several microns, and polyplexes usually exhibit larger size in salt- or serum-containing cell culture media due to aggregation.[4,12–

[15] Generally, particles smaller than 200 nm are desired for their extended *in vivo* circulation time and uptake,[16] and to be effective these particles should be colloidally stable in aqueous media so as to avoid unwanted aggregation or precipitation. Extensive research has shown that polyplexes with colloidal stability may achieve efficient transfection,[17–20] while several studies also indicated that polyplexes of larger size afforded higher transfection compared to the smaller ones (in the nano to micron range), attributed to better contact with cells due to the settling of larger particles.[14,15] In addition to polyplex size, studies by Han, *et al.* and others showed that optimal binding affinity for nucleic acids with polymers balanced cargo protection and release, and was important for achieving high transfection efficiency.[21,22]

Recent research activities have employed various chemical designs to achieve control over the complexation and self-assembly of polyplexes. Remarkably, the inclusion of hydrophobic, hydrophilic, and even fluorinated groups, improves the colloidal stability of polyplexes and tailors the binding strength between polymers and the nucleic acids, affording considerable enhancement of both safety and delivery efficiency.[23–25] Moreover, utilization of complex polymer architectures, such as comb, bottlebrush, and multiblock structures, has generated impressive transfection improvement, relative to conventional linear polymers.[4,23,26] In addition to chemically optimizing the polymer structures to enhance gene delivery, introducing additives such as PEG and pluronics to delivery systems also improves transfection,[27,28] though more detailed investigation is required to understand the impact of such additives on polyplex properties and activities.

The Emrick group previously reported a series of oligopeptide-grafted polyolefins as efficient DNA carriers.[10,26,29] The poly(cyclooctenes), grafted with reverse nuclear localization sequence (rNLS), specifically VKRKKKP, achieved transfection performance exceeding benchmark commercial reagents including PEI and lipofectamine, while maintaining >80% cell viability.[10] Inspired by the recent achievements of fluoropolymers in gene delivery, this thesis work examined the inclusion of fluorinated units into the rNLS polymers, which were then used to complex DNA. We found that adding fluorinated polymer zwitterions greatly improve the polyplex colloidal stability and reduced binding strength (**Figure 4-1**), likely due to interactions between the fluorinated groups. Addition of fluorinated polymer zwitterions greatly increased the colloidal stability of the polyplexes in cell culture media, while polyplex binding strength was tuned by the concentration of fluorinated polymer zwitterions and the structure of the cationic polymer itself. Moreover, fluorinated polymer zwitterions were utilized as surfactants in the preparation of perfluorooctyl bromide (PFOB) nanoemulsions, enhancing the potential of the delivery system in scenarios where both imaging ability and therapeutic delivery are desired.

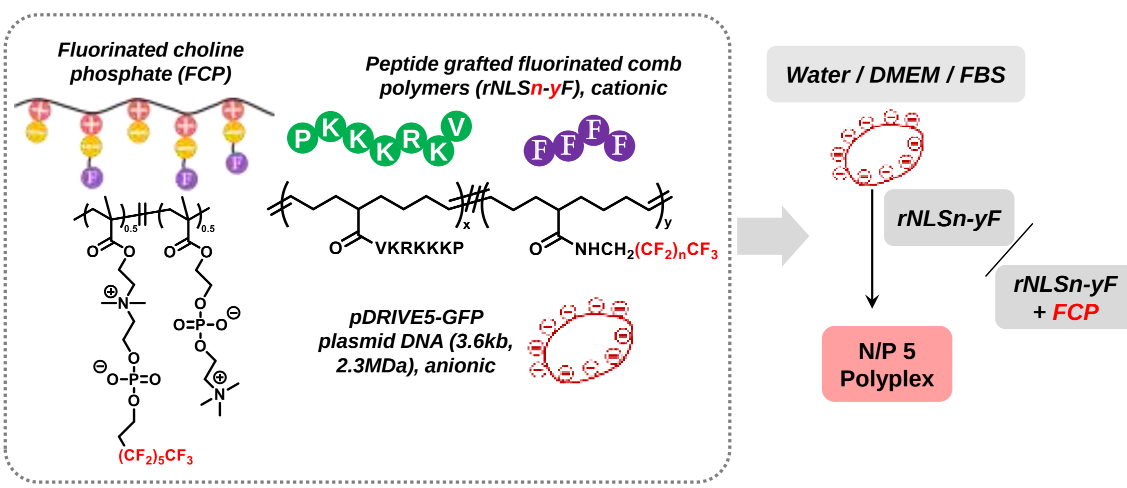

Figure 4-1. Packaging DNA with cationic poly(cyclooctenes) and FCPs.

4.2 Polymer Synthesis

Cyclooctene monomers (V-Fn, n=2, 3, 4, 5) with different lengths of fluorocarbon groups ($-CH_2(CF_2)_nCF_3$) were prepared by carbodiimide coupling using (1-ethyl-3-(3-dimethylaminopropyl)carbodiimide (EDC) as the coupling agent (**Figure 4-2**). 5-VK(Boc)R(Pbf)K(Boc)K(Boc)K(Boc)P-1-cyclooctene (rNLS-COE) was prepared as

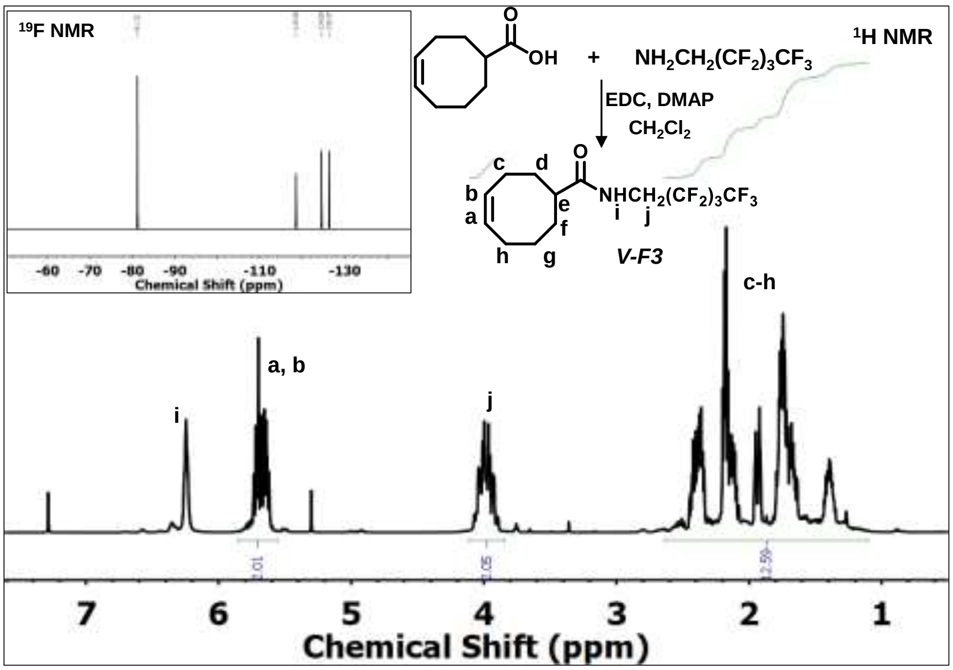

Figure 4-2. Synthesis and ^{1}H and ^{19}F (inset) NMR spectra of fluorinated cycooctene monomer V-F3 in $CDCl_3$.

previously reported.[10] The rNLS-COE monomer was copolymerized with the fluorinated cyclooctene monomer, by ring-opening metathesis polymerization (ROMP) using the 3-bromopyridine-substituted Grubbs Generation III catalyst,[10] giving typical monomer conversion of over 85%, as calculated from ^{1}H NMR of aliquots removed from the reaction mixture. The polymers were isolated by precipitation in diethyl ether and deprotected using trifluoroacetic acid, followed by removal of monomers and catalyst by dialysis. The polymers were obtained as white solids in 55-60% yield after lyophilization. Four groups of copolymers, **rNLSII**, **rNLSIII**, **rNLSIV**, and **rNLSV**, containing

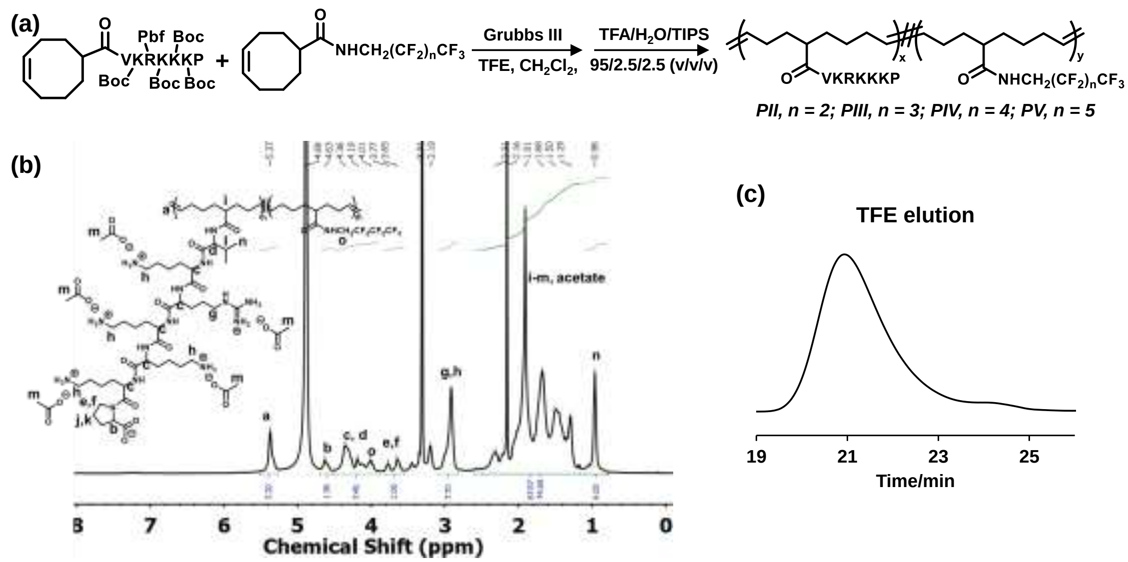

Figure 4-3. (a) Synthesis of polycyclooctene copolymers by ROMP; (b) ^1H NMR spectrum of **rNLSII** in CD_3OD; (c) GPC elution of **rNLSV** with TFE as mobile phase.

pendent fluorocarbon groups of various lengths and different incorporation percentage of the fluorocarbons, were prepared (**Figure 4-3a**). The actual incorporation of the fluorocarbon-substituted cycloctene monomers correlated closely with the targeted ratios, yielding polymers with 12-48 mol% incorporation of fluorinated groups, calculated from the ^1H NMR spectra of the polymers by comparing integration of -C$\underline{H_2}$$(CF_2)_nCF_3$ resonances at 3.80-4.36 ppm and -CH(C$\underline{H_3}$)$_2$ resonance at 0.86 ppm (**Figure 4-3b**). Polymer molecular weight was estimated to be ~50-65 kDa, with polydispersity of 1.4-1.7 (**Table 4-1**), using gel permeation chromatography (GPC) with TFE (containing 20 mM sodium trifluoroacetate) as eluent. The fluorinated choline phosphate polymer (FCP)

Table 4-1. Characterization data of **rNLSII-rNLSV**.

Polymers	Fluorinated unit mol%		$M_{w,GPC}$/kDa#	Đ
	Target	NMR*		
rNLSII-14F	10	14	59.8	1.40
rNLSIII-14F	10	14	57.0	1.52
rNLSIV-12F	10	12	59.6	1.43
rNLSV-16F	10	16	64.6	1.38
rNLSV-25F	20	25	59.9	1.38
rNLSV-35F	30	36	53.5	1.51
rNLSV-48F	40	48	54.5	1.52

used in this Chapter contained ~50 mol% incorporation of MPC and ~50 mol% of PFH-MCP, and was synthesized and characterized as described in Chapter 2. This series of polycyclooctenes combined with FCP provided a platform to study the effects of fluorocarbon length, incorporation of fluorocarbon and amount of FCP on key polyplex properties of colloidal stability and DNA binding affinity.

4.3 Polyplex formation and size

To achieve high transfection in *in vivo* or *in vitro* experiments, polyplexes must maintain their stability in biological environments. This section describes polyplexe stability in the DMEM solution, as well as in the presence of serum. Polyplexes of rNLSII–rNLSV and DNA with N/P = 5 were prepared by mixing the polymer solution with and the plasmid (pDRIVE5-GFP plasmid DNA, 3.6 kb) solution by vortexing, then measuring their size by dynamic light scattering (DLS). Polyplex diameter formed in water was ~70-100 nm and remained nearly constant within 24 hours, while the polyplexes prepared in DMEM media had initial diameter greater than 300 nm and increased to >700 nm within an hour under room temperature. Efficient binding of DNA

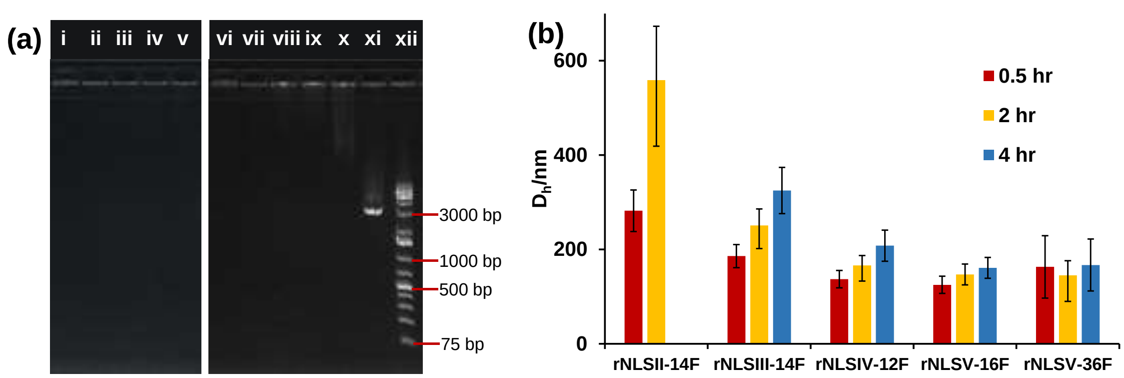

Figure 4-4. (a) Gel electrophoresis of polyplexes at N/P = 5 formed with (i) rNLSII-14F, (ii) rNLSIII-14F, (iii) rNLSIV-12F, (iv) rNLSV-16F and (v) rNLSV-36F, (vi)-(x) are formed in the presence of FCP for rNLSII-14F, rNLSIII-14F, rNLSIV-12F, rNLSV-16F and rNLSV-36F respectively; (b) hydrodynamic diameter of polyplexes prepared with rNLSII-rNLSV in the presence of FCP at different times.

by the polymer was confirmed by the absence of DNA band in gel electrophoresis (**Figure 4-4a**). To investigate the impact of FCP on the stability of the polyplexes against salt and serum, FCP was added to solutions of rNLSII-rNLSV, which were then mixed with the plasmid solution, to give a polyplex solution (DNA 10 µg/mL) with N/P = 5 and 0.125 mg/mL FCP. Successful polyplex formation in the presence of FCP was confirmed by gel electrophoresis. The presence of FCP did not influence the size of the polyplexes formed in water, again ~70-100 nm, which proved stable for 24 hours at room temperature. However, FCP had a significant impact on polyplex stability in DMEM, with some dependence on the fluorocarbon chain length (**Figure 4-4b**). For example, polyplex diameter prepared from rNLSII-14F/FCP formulation increased from ~280 nm to ~600 nm within two hours. Polyplexes prepared from rNLSIII-14F, rNLSIV-12F, rNLSV-16F and rNLSV-36F in the presence of FCP, showed initial size of ~130-190 nm.

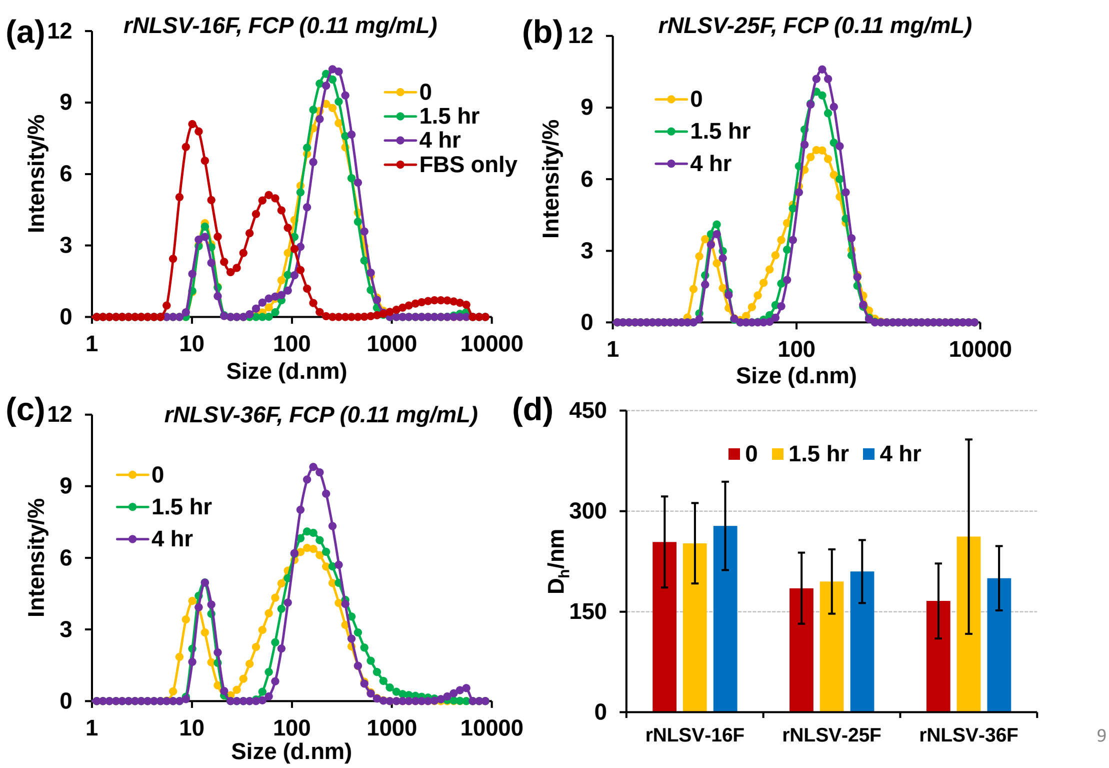

Figure 4-5. DLS intensity plot of polyplexes made with (a) rNLSV-16F, (b) rNLSV-25F, and (c) rNLSV-36F in the presence of FCP; (d) hydrodynamic diameter of polyplexes prepared with rNLSVs and FCP in 10% FBS DMEM.

In addition, rNLSIV-12F, rNLSV-16F and rNLSV-36F resulted in more stable polyplexes, with the size maintained smaller than 210 nm after four hours, while polyplexes made from rNLSIII-14F/FCP increased to 325 nm after four hours. The stability of the polyplexes formed with rNLSVs in the presence of FCP was further tested in DMEM solution containing 10% fetal bovine serum (FBS). As shown in **Figure 4-5 (a-c)**, DLS exhibited two size distributions: one at ~10 nm from the FBS; and the other at ~300 nm from the polyplexes. Addition of FBS caused the formation of larger polyplexes of ~200-250 nm, and the polyplexes remained stable over 4 hours, as indicated by a minimal change of their size (**Figure 4-5d**). Overall, at similar fluorocarbon content (~12-16 mol%), the cationic polycyclooctenes containing longer fluorocarbons (rNLSIV and rNLSV) afforded more stable polyplexes. When replacing FCP with PMPC or using rNLS polymers without fluorinated groups, this improved polyplex stability was not observed. Therefore, the ability of FCP to improve the stability of the polyplexes is attributed to the fluorine-fluorine interactions between FCP and the polyplexes.

The effect of FCP on polyplex zeta potential was examined at N/P = 5 with rNLSV-25F. As shown in **Figure 4-6**, N/P 5 polyplexes formed with only rNLSV-25F presented a zeta potential value of ~23 ± 4 mV, while the presence of FCP partially

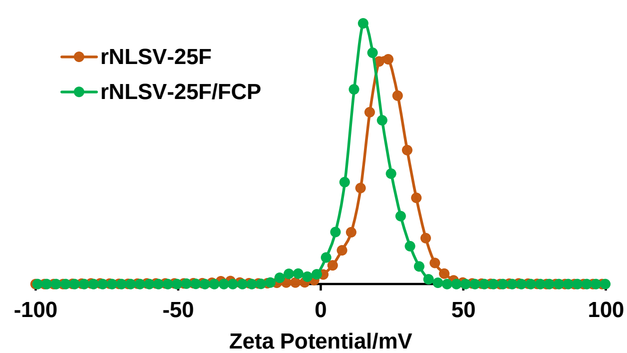

Figure 4-6. Zeta potential distribution of N/P 5 polyplexes formed with rNLSV-25F or rNLSV-25F/FCP in 10 mM NaCl. (DNA 20 μg/mL, FCP 0.125 mg/mL).

screened the cationic charges, reducing in zeta potential to ~17 ± 3 mV. This reduction of zeta potential may help alleviate cytotoxicity associate with cationic charges thus improving the safety of the delivery system.

4.4 Polyplex binding strength

The binding strength of polyplexes determines their ability to release polynucleotide cargo and thus is a key factor in successful transfection. This section examines the effects of FCP, and the structure of the poly(cyclooctenes), on binding affinity to DNA. Binding strength was evaluated using fluorescence assays: interaction of DNA with Picogreen (PG) produces enhanced fluorescence. The complexation of polymer with DNA excludes the dye from binding with DNA and causes fluorescence reduction. Addition of heparin, an anionic polyelectrolyte, which competes with DNA to bind to the polymers with DNA, results in DNA release from the polyplexes and fluorescence enhancement (**Figure 4-7a**). Thus, greater fluorescence intensity upon the addition of heparin indicates a weaker binding affinity for DNA. As shown in **Figure 4-7b**, FCP does not affect polyplex binding for polycyclooctenes with shorter fluorocarbons (rNLSII-rNLSIV), while for polyplexes formed with rNLSV-16F and rNLSV-36F, presence of FCP resulted in increase of fluorescence after incubation with heparin. Moreover, rNLS polymer (without fluorocarbon) and rNLSV containing 16, 26, 36 and 48 mol% fluorocarbon was mixed with FCP and used to prepare polyplexes, to examine the impact of fluorocarbon incorporation on binding strength (**Figure 4-7c**). FCP caused fluorescence enhancement (i.e., reduced binding strength) for polymers with higher fluorocarbon incorporation. The relative fluorescence values after heparin incubation for rNLS, rNLSV-16F, rNLSV-26F, rNLSV-36F and rNLSV-48F were 0.12, 0.19, 0.29, 0.4

and 0.43, respectively, and the difference in binding strength between rNLSV-36F and rNLSV-48F polyplexes was notably small. In addition, we found that for rNLSV-25F/FCP and rNLSV-36F/FCP polyplex formulations, the binding strength was sensitive to FCP concentration (**Figure 4-7d**). Increasing FCP concentration from 0.037 mg/mL to 0.11 mg/mL resulted in weaker binding, while further increasing the FCP concentration to 0.37 mg/mL showed no significant impact on binding. To summarize, inclusion of FCP in the polyplex solutions reduced the binding strength for rNLSV polymers, and this reduction was modulated by fluorocarbon incorporation percentage and the FCP amount in the polyplex formulation.

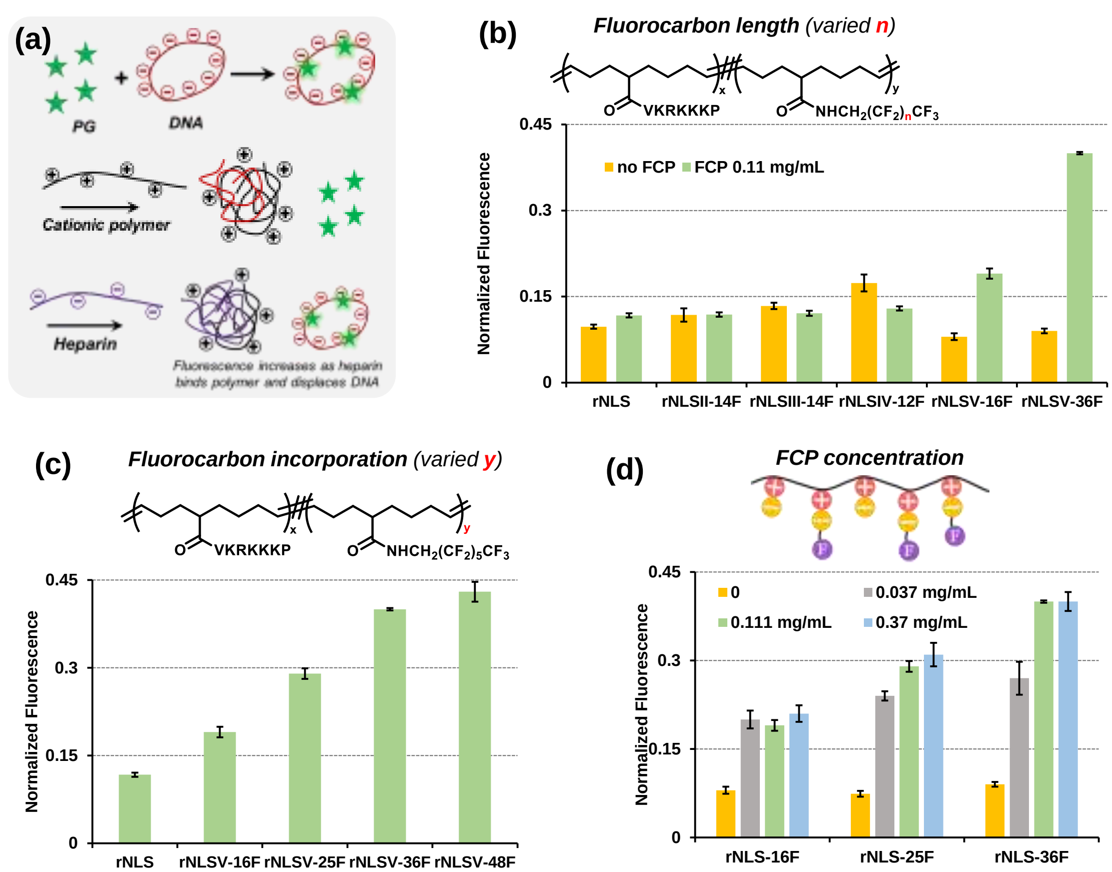

Figure 4-7. (a) Schematic of binding strength evaluation with Picogreen assay; impact of (b) adding FCP, (c) fluorocarbon incorporation percentage of rNLS polymers and (d) concentration of FCP on polyplex binding strength.

4.5 Polyplex nanoemulsion preparation and stability

Inclusion of FCP in the polyplex formulation significantly stabilized the polyplexes in the presence of salt and serum, and this formulation was further utilized to prepare PFOB nanoemulsions. Perfluorocarbon emulsions are used today in ultrasound imaging, ^{19}F magnetic resonance imaging, and therapeutic delivery. As described in Chapter 2, polymers with fluorinated choline phosphate groups exhibited an outstanding ability to reduce the interfacial tension of the perfluorohexane/water interface and stabilize perfluorohexane nanoemulsions. In this section, PFOB nanoemulsions were prepared by sonicating mixtures of PFOB with solution of rNLSV-36F and FCP. The nanoemulsions were then mixed with the DNA solution to yield a polyplex nanoemulsion. As shown in **Figure 4-8**, the initial size of the PFOB nanoemulsion was ~200 nm and remained stable over 120 hours, at both 7 ^{o}C and 37 ^{o}C. When mixing with DNA and forming N/P = 5 polyplex nanoemulsions, the system was relatively stable at 7 ^{o}C, and diameter increased from ~200 nm to ~300 nm over 120 hours. However, the polyplex nanoemulsion coalescenced at 37 ^{o}C, with gradual increase of diameter from ~200 nm to

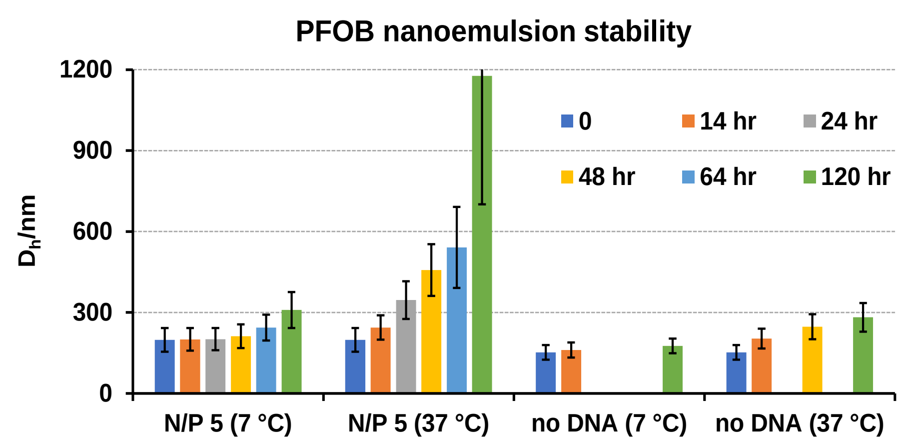

Figure 4-8. Hydrodynamic diameter of PFOB nanoemulsion over time. N/P 5 contains rNLSV-30F 10 ug/ml, FCP 250 ug/ml, PFOB 0.5 ul/ml, DNA 2 ug/ml, in DMEM media; no DNA formulation contains rNLSV-30F 10 ug/ml, FCP 250 ug/ml, PFOB 0.5 ul/ml, in DMEM media.

~600 nm over a 64-hour period. In general, the FCP/rNLSV-36F produced polyplex PFOB nanoemulsion with considerable stability and holds promise for therapeutic applications *in vivo* and *in vitro.*

To summarize, this Chapter described the synthesis of a new series of polycyclooctenes containing rNLS targeting peptides and fluorocarbon side chains. Remarkably, the combination of the fluorinated polymer zwitterion, FCP, and the fluorinated polycyclooctenes offered a platform to encapsulate DNA and form colloidally stable polyplexes under biologically relevant conditions. Moreover, the binding affinity for DNA was tuned by the structure of the polycyclooctenes and concentration of FCP. The presence of FCP in the polyplex formulation also contributed the added feature of stabilizing PFOB nanoemulsion, an important precursor to a successful gene delivery system.

4.6 References

1. Salameh, J. W. *et al.* Polymer-mediated gene therapy: Recent advances and merging of delivery techniques. *Wiley Interdiscip. Rev. Nanomedicine Nanobiotechnology* **12**, e1598 (2020).
2. Buck, T. M. & Wijnholds, J. Recombinant Adeno-Associated Viral Vectors (rAAV)-Vector Elements in Ocular Gene Therapy Clinical Trials and Transgene Expression and Bioactivity Assays. *Int. J. Mol. Sci. 2020, Vol. 21, Page 4197* **21**, 4197 (2020).
3. Quagliarini, E. *et al.* Microfluidic Formulation of DNA-Loaded Multicomponent Lipid Nanoparticles for Gene Delivery. *Pharm. 2021, Vol. 13, Page 1292* **13**, 1292 (2021).
4. Dalal, R. J., Kumar, R., Ohnsorg, M., Brown, M. & Reineke, T. M. Cationic Bottlebrush Polymers Outperform Linear Polycation Analogues for pDNA Delivery and Gene Expression. *ACS Macro Lett.* **10**, 886–893 (2021).
5. Kotterman, M. A., Chalberg, T. W. & Schaffer, D. V. Viral Vectors for Gene Therapy: Translational and Clinical Outlook. *Annu. Rev. Biomed. Eng.* **17**, 63–89 (2015).
6. Buck, J., Grossen, P., Cullis, P. R., Huwyler, J. & Witzigmann, D. Lipid-based

DNA therapeutics: Hallmarks of non-viral gene delivery. *ACS Nano* **13**, 3754–3782 (2019).

7. Kumar, R. *et al.* Polymeric Delivery of Therapeutic Nucleic Acids. *Chem. Rev.* **121**, 11527–11652 (2021).

8. Estabrook, D. A., Day, R. A. & Sletten, E. M. Redox-Responsive Gene Delivery from Perfluorocarbon Nanoemulsions through Cleavable Poly(2-oxazoline) Surfactants. *Angew. Chemie* **133**, 17502–17507 (2021).

9. Gao, J. *et al.* Photothermal-Enhanced Phase-Transition Nanodroplets for Ultrasound-Mediated Diagnosis and Gene Transfection. *ACS Biomater. Sci. Eng.* **5**, 1366–1377 (2019).

10. Parelkar, S. S. *et al.* Polymer-peptide delivery platforms: effect of oligopeptide orientation on polymer-based DNA delivery. *Biomacromolecules* **15**, 1328–1336 (2014).

11. Monnery, B. D. Polycation-Mediated Transfection: Mechanisms of Internalization and Intracellular Trafficking. *Biomacromolecules* **22**, 4060–4083 (2021).

12. Buckwalter, D. J., Sizovs, A., Ingle, N. P. & Reineke, T. M. MAG versus PEG: Incorporating a poly(MAG) layer to promote colloidal stability of nucleic acid/"click cluster" complexes. *ACS Macro Lett.* **1**, 609–613 (2012).

13. Ritt, N., Berger, S., Wagner, E. & Zentel, R. Versatile, Multifunctional Block Copolymers for the Self-Assembly of Well-Defined, Nontoxic pDNA Polyplexes. *ACS Appl. Polym. Mater.* **2**, 5469–5481 (2020).

14. Bono, N., Ponti, F., Mantovani, D. & Candiani, G. Non-Viral in Vitro Gene Delivery: It is Now Time to Set the Bar! *Pharmaceutics* **12**, 183 (2020).

15. Godbey, W. T., Wu, K. K. & Mikos, A. G. Size matters : Molecular weight affects the efficiency of poly (ethylenimine) as a gene delivery vehicle. *J. Biomed. Mater. Res.* **45**, 268–275 (1998).

16. Hoshyar, N., Gray, S., Han, H. & Bao, G. The effect of nanoparticle size on in vivo pharmacokinetics and cellular interaction. *Nanomedicine* **11**, 673 (2016).

17. Hemp, S. T., Smith, A. E., Bryson, J. M., Allen, M. H. & Long, T. E. Phosphonium-containing diblock copolymers for enhanced colloidal stability and efficient nucleic acid delivery. *Biomacromolecules* **13**, 2439–2445 (2012).

18. Diaz-Dussan, D., Peng, Y. Y., Kumar, P. & Narain, R. Oncogenic Epidermal Growth Factor Receptor Silencing in Cervical Carcinoma Mediated by Dynamic Sugar-Benzoxaborole Polyplexes. *ACS Macro Lett.* **9**, 1464–1470 (2020).

19. Smith, A. E., Sizovs, A., Grandinetti, G., Xue, L. & Reineke, T. M. Diblock glycopolymers promote colloidal stability of polyplexes and effective pDNA and siRNA delivery under physiological salt and serum conditions. *Biomacromolecules* **12**, 3015–3022 (2011).

20. Li, H., Cortez, M. A., Phillips, H. R., Wu, Y. & Reineke, T. M. Poly(2-deoxy-2-

methacrylamido glucopyranose)-b -Poly(methacrylate amine)s: Optimization of Diblock Glycopolycations for Nucleic Acid Delivery. *ACS Macro Lett.* **2**, 230–235 (2013).

21. Kim, K. *et al.* Controlling complexation/decomplexation and sizes of polymer-based electrostatic pDNA polyplexes is one of the key factors in effective transfection. *Colloids Surfaces B Biointerfaces* **184**, 110497 (2019).

22. Han, L., Tang, C. & Yin, C. Effect of binding affinity for siRNA on the in vivo antitumor efficacy of polyplexes. *Biomaterials* **34**, 5317–5327 (2013).

23. Jiang, Y., Lodge, T. P. & Reineke, T. M. Packaging pDNA by Polymeric ABC Micelles Simultaneously Achieves Colloidal Stability and Structural Control. *J. Am. Chem. Soc.* **140**, 11101–11111 (2018).

24. Ghobadi, A. F. *et al.* Dispersing Zwitterions into Comb Polymers for Nonviral Transfection: Experiments and Molecular Simulation. *Biomacromolecules* **17**, 546–557 (2016).

25. Wu, T., Wang, L., Ding, S. & You, Y. Fluorinated PEG-Polypeptide Polyplex Micelles Have Good Serum-Resistance and Low Cytotoxicity for Gene Delivery. *Macromol. Biosci.* **17**, 1–8 (2017).

26. Parelkar, S. S., Chan-seng, D. & Emrick, T. Reconfiguring polylysine architectures for controlling polyplex binding and non-viral transfection. *Biomaterials* **32**, 2432–2444 (2011).

27. Wu, C., Li, J., Wang, W. & Hammond, P. T. Rationally Designed Polycationic Carriers for Potent Polymeric siRNA-Mediated Gene Silencing. *ACS Nano* **12**, 6504–6514 (2018).

28. Liu, S. *et al.* Zwitterionic Phospholipidation of Cationic Polymers Facilitates Systemic mRNA Delivery to Spleen and Lymph Nodes. *J. Am. Chem. Soc.* **143**, 21321–21330 (2021).

29. Ghobadi, A. F. *et al.* Dispersing Zwitterions into Comb Polymers for Nonviral Transfection: Experiments and Molecular Simulation. *Biomacromolecules* **17**, 546–557 (2016).

CHAPTER 5

INSTALLING STRAIN-STIFFENING PROPERTIES INTO HYDROGELS VIA DYNAMIC SECONDARY CROSSLINKING

5.1 Introduction

Hydrogels are crosslinked three-dimensional polymer networks capable of retaining large amounts of water within their structures. These soft materials are suitable for numerous applications in biology and biomedical engineering, ranging from tissue engineering to cell culture platforms, owing to their mechanical tunability and water-rich structure.[1–3] Hydrogel modulus values can be tuned across a wide range by manipulating crosslinking density and polymer backbone chemistry.[4] However, realizing the full potential of hydrogels is generally constrained by a lack of access to post-synthetic modification of chemical and physico-mechanical properties. In addition, when subjected to constant deformations, conventional hydrogels lose structural integrity over time and ultimately fail.[5] In contrast, biological materials, such as collagen and fibrin, are force-responsive and show strain-stiffening behavior (*i.e.*, increasing stiffness when strained) which allows tissues to adapt to external forces and minimize associated force-induced damage.[6–9] Incorporating such properties into synthetic hydrogels would enhance their performance as they adapt to settings that involve dynamic stiffening.

Recent advances towards smart, dynamic hydrogels that alter their modulus effectively utilize external stimuli such as light, heat, pH, and enzymatic reactions.[10–13] However, there is an ongoing need to significantly expand the range of chemistries and conditions by which such dynamic systems can be achieved. As an alternative, mechanical force has been recognized as a useful tool to impart stimuli-responsiveness to hydrogels.[14,15] For example, strain-stiffening hydrogels have been achieved using polymers containing a semi-flexible backbone, whereby a mechanical load triggers polymer extension and packing, producing a “transient stiffening”. These deformation-induced effects are reversible and the system reverts to its original state when strain is removed.[16–20] Another strategy to design mechano-sensitive materials is to insert mechanophores into polymers, which transform applied mechanical forces to chemical reactions.[21–23] However, the forces required to activate these mechanochemical processes may be deleterious to materials properties due to chain scission reactions.[24] Hence, there is an opportunity to design polymers that will respond to milder forces, in a permanent and/or transient manner, and thereby overcome limitations of existing approaches.

Recently, Peyton and coworkers reported a novel approach to impart mechano-responsive stiffening properties to synthetic organogels, using polymers containing sterically hindered crosslinking sites, *i.e.*, “cryptic gels”.[25] Building on this concept for hydrophilic gels, this chapter describes sulfobetaine-based polymer zwitterions as “single-component” systems, in which the required crosslinking functionality—specifically 1,2-dithiolanes and allyl groups—are present as pendent groups on the same backbone (i.e., single-component systems). The strained cyclic disulfides of 1,2-ditholanes give them greater reactivity in thiol-disulfide exchange relative to conventional systems[26,27] and opens opportunities to prepare dynamic, self-healing structures.[26,28] Moreover, the polar hydrophilic nature of polymer zwitterions allows for embedding high concentrations of reactive allyl groups while maintaining aqueous solubility. As illustrated in **Figure 5-1** for these single-component systems, crosslinking *via* thiol-ene reactions and disulfide formation together contribute to hydrogel mechanics, in which thiol-ene “click” reactions (giving C-S bonds) define the primary network and stiffening is facilitated by interchain disulfide (S-S bond) formation. Such functional hydrogels are anticipated to be useful for next-generation applications that require mechano-responsive, dynamic strengthening with precise control over gel modulus.

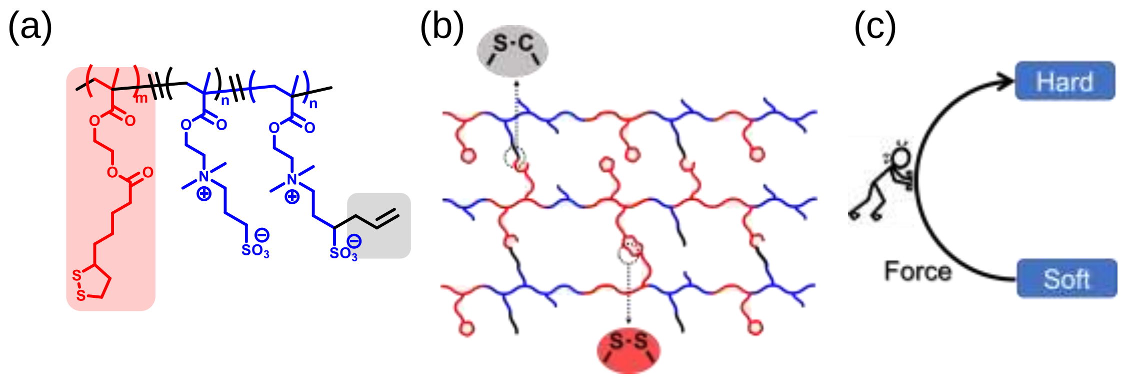

Figure 5-1. (a). Chemical structure of multifunctional polymer zwitterion that comprise (b). the force-responsive dynamic hydrogel network; (c). the dynamic network could switch from soft to stiff mechanical states through mechanical conditioning.

5.2 Synthesis of crosslinkable polymer precursors

The allyl-functionalized sulfobetaine methacrylate (allyl-SBMA) and dithiolane-containing methacrylate (HEMA-LA) monomers were prepared and characterized as reported previously.[29,30] Copolymerization of allyl-SBMA, HEMA-LA and [2-(methacryloyloxy)ethyl]dimethyl-(3-sulfopropyl)ammonium hydroxide (SBMA) was performed using reversible addition-fragmentation chain-transfer (RAFT) polymerization in trifluoroethanol (TFE) at 70 ^{o}C with 4-cyano-4-(phenylcarbonothioylthio)pentanoic acid (CPPA) serving as the chain-transfer agent (CTA) and 4,4’-azobis(4-cyanovaleric acid) (ACVA) as initiator (**Figure 5-2a**). Monomer conversion exceeded 70% in ~8 hours, yielding multigram quantities of copolymer samples, labeled **PI** in **Figure 5-2a**, in 60-70% isolated yields as pink solids after isolation. Successful incorporation of the allyl and dithiolane groups into the copolymers was confirmed by ^{1}H and ^{13}C NMR spectroscopy (**Figure 5-2(b-d)**), while polymer molecular weight was estimated by gel permeation chromatography (GPC), eluting in TFE (**Figure 5-2e**). Copolymers **PIA-PIC** were synthesized with varying mole percent of allyl-SBMA to investigate the impact of allyl incorporations on hydrogel mechanics. Holding HEMA-LA at 22-24 mole percent, allyl-SBMA mole percent values of 12 (**PI-A**), 26 (**PI-B**), and 31 (**PI-C**) were employed, and confirmed in the products by integration of ^{1}H NMR spectral resonances at 5.70, 2.56-3.25, and 0.47-2.44 ppm (**Figure**

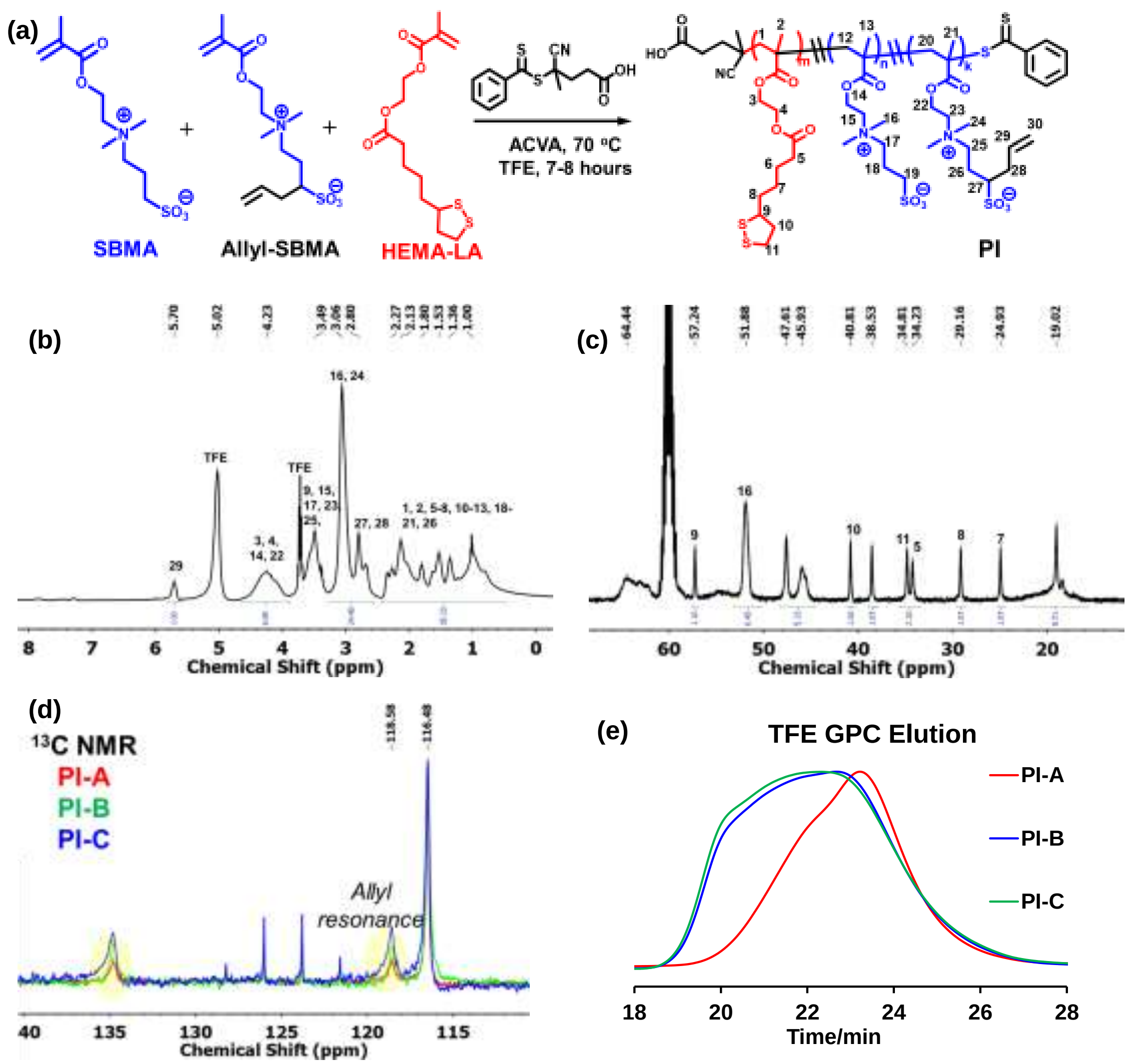

Figure 5-2. (a) Synthesis of functionalized polymer zwitterions **PI** with RAFT polymerization; (b) ^{1}H NMR of **PI** in TFE-d3; (c), (d) ^{13}C NMR of **PI** in D_2O; (e) GPC elution of **PIA-C** with TFE as mobile phase.

5-2a). The monomer ratios incorporated into the polymer structures correlated closely with the feed ratios employed (**Table 5-1**). The polydispersity index (PDI) (*i.e.*, M_w/M_n) values of the polymers broadened with allyl-SBMA content, likely due to involvement of pendent alkenes in the propagation mechanism, which becomes increasingly likely at higher alkene content.[30,31]

Table 5-1. Summary of polymer samples and molecular weight data.

Polymers		Alkene:LA:SB (mol%)[a]	M_n (kDa)[b]	PDI[b]
PI	**A**	12:23:65	21.2	1.39
	B	26:22:52	24.6	1.97
	C	31:24:45	24.7	2.08
PII		28:0:72	27.0	1.63
PIII		0:25:75	16.6	1.09

[a]Calculated from ^{1}H NMR signal integration. [b]Obtained by GPC analysis using trifluoroethanol as eluent (with 0.02 M sodium trifluoroacetate).

For comparative analysis, zwitterionic copolymers containing only pendent alkene (**PII**) or dithiolane moieties (**PIII**) were also prepared. The alkene incorporation of **PII** was calculated to be 28 mol %, judging from ^{1}H NMR integration (in 0.2 M NaCl D_2O solution) of the allyl resonance (C**<u>H</u>**=CH_2) at 5.97 ppm and the methylene (C(O)OC**<u>H2</u>**CH_2N) resonance at 4.56 ppm (**Figure 5-3a**). The ^{1}H NMR spectrum of **PIII**

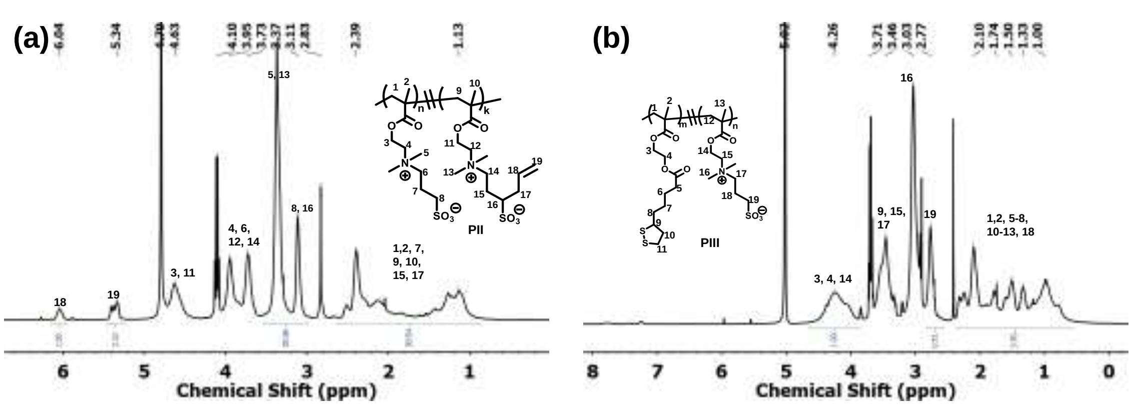

Figure 5-3. ^{1}H NMR spectra of (a) PII in D_2O and (b) PIII in TFE-d3.

shows 25 mol% inclusion of HEMA-LA from integration of resonances at 3.87-4.56 ppm and 0.58-2.35 ppm (**Figure 5-3b**).

5.3 Hydrogel preparation

Hydrogels prepared from the **PI** series by thiol-ene reactions utilized 33 wt% polymer solutions in 0.2 M $NaCl_{(aq)}$, employing 5 wt % tris(2-carboxyethyl) phosphine hydrochloride (TCEP-HCl) (to reduce disulfides to thiols) under UV-irradiation with lithium phenyl-2,4,6-trimethylbenzoylphosphinate (LAP) as initiator. As shown in **Figure 5-4a**, colorless, transparent hydrogels were prepared in cylindrical molds (5 mm diameter and 5 mm height), then washed with 0.2 M $NaCl_{(aq)}$ and finally immersed and swelled in the same aqueous environment.

Hydrogels from **PIA-PIC** were subjected to compressive rheology experiments to evaluate elastic modulus, using a rate of 20 µm/s . All of the formulations gave robust hydrogel materials, with the measured elastic modulus observed to be commensurate with the extent of alkene functionality that set the network structure (**Figure 5-4b**). Specifically, **PI-A** hydrogels possessed an elastic modulus of 45 ± 2.6 kPa, while **PI-B**

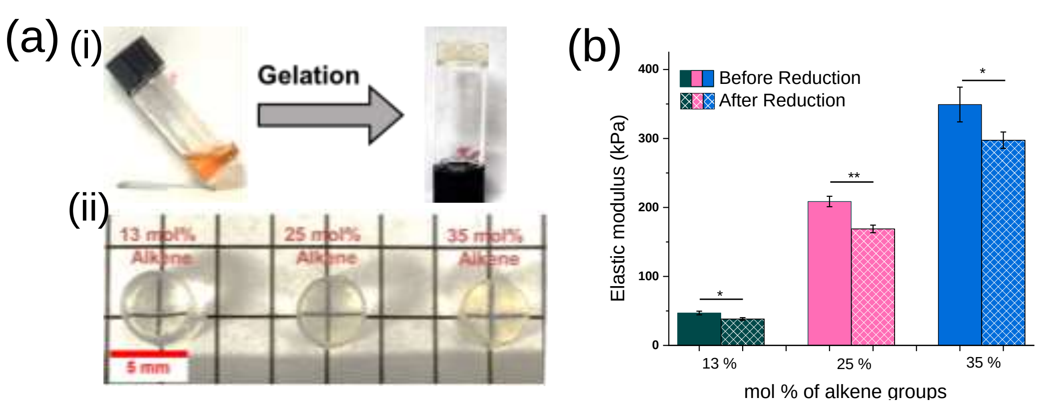

Figure 5-4. (a) Photographs showing (i) the sol-gel transition from polymer solution to hydrogel network and (ii) hydrogels synthesized in a cylindrical mold for cyclic compression experiments; (b) The elastic modulus of the as-synthesized hydrogels before and after chemical reduction.

and **PI-C** were significantly stronger due to their higher alkene incorporations, with measured values of ~209 ± 10 kPa and ~350 ± 25 kPa, respectively. Estimations of mesh size[34,35] of these hydrogel network also showed a dependence on the extent of allyl functionalities in the polymer employed. For hydrogels **PI-A**, **PI-B**, and **PI-C**, mesh sizes were each estimated to be ~1.7, 1.2, and 1.1 nm, which decreased as elastic modulus increased, suggesting that the primary network is predominantly produced by thiol-ene crosslinking. Moreover, the hydrogels remained intact, with a slight decrease of elastic modulus for these hydrogels, when subjected to chemical reduction.

Attempted gelation of **PII** in aqueous solution using PEG dithiol (M_n ~1 kDa) as a bifunctional crosslinker was unsuccessful, due to immiscibility of PEG and **PII**. **PIII** was crosslinked using the bifunctional thiol 2,2'-(ethylenedioxy)diethanethiol, resulting in opaque hydrogels containing only disulfide crosslinks. Notably, these hydrogels underwent a complete sol-to-gel transition when reduced with TCEP-HCl, while hydrogels prepared from **PI** (i.e., containing C-S crosslinks) remained intact. Inclusion of both the reactive allyl and dithiolane groups on the polymer backbone promoted gelation of **PI** in an aqueous environment, and the presence of both sulfide and disulfide crosslinking units enabled the networks to maintain mechanical integrity even after disulfide cleavage.

5.4 Strain-stiffening behavior of PI hydrogels

In evaluating the dynamic nature of the hydrogels, we envisioned the availability of the thiols to provide a mechanically tunable dynamic secondary network through disulfide interchain crosslinks. TCEP-HCl was used to reduce the disulfides, by immersing the hydrogels in the reducing solution for ~12 hrs, which liberates disulfide crosslinks and breaks the disulfides of 1,2-dithiolanes.[36] After reduction, the hydrogel was immersed into 0.1 M $H_2O_{2(aq)}$, resulting in oxidative reformation of disulfides. Interchain disulfide formation reestablishes crosslinking density and elastic modulus, while 1,2-dithiolane reformation does not strengthen the network. In the oxidative environment, the elastic modulus of the hydrogel increased over time (measured at 90-minute intervals) (**Figure 5-5a**). The rate at which this crosslinking occurred was influenced by the initial stiffness of the hydrogel. The weaker hydrogel (**PI-A**) showed a minimal increase of elastic modulus ($\Delta E \sim 14 \pm 0.7$ kPa) in 6 h over that of the fully reduced state. **PI-A** also had the largest mesh size (1.7 nm), which suggests that most of the thiols reverted to 1,2-dithiolanes rather than participate in crosslinking. In contrast, **PI-B** and **PI-C** hydrogels, with smaller mesh size, showed much larger increases in ΔE, $\sim 110 \pm 8$ kPa and $\sim 120 \pm 12$ kPa, respectively, compared to the fully reduced state (**Figure 5-5(b-c)**).

In addition to spontaneous stiffening, **PI** hydrogels exhibited accelerated stiffening in response to compressive strain, likely due to the role of interchain disulfide crosslinking. To study this effect, hydrogels were subjected to continuous cyclic compression of 20% strain at a rate of 20 μm/s in 0.1 M $H_2O_{2(aq)}$. ΔE, monitored at 45 min intervals under compression, increased minimally for **PI-A** hydrogels but significantly for **PI-B** and **PI-C**. Notably, the strain-induced conditions led to much greater modulus values relative to the unstrained samples. For **PI-B,** ΔE increased up to $\sim 430 \pm 5$ kPa, or nearly four-fold that of the unstrained system. **PI-C**, on the other hand, increased to 475 ± 27 kPa under strain. *Interestingly, the initial increase in ΔE was steeper for **PI-C** than **PI-B**, suggesting that strain-stiffening is indeed mediated by interchain* *disulfide formation, likely due to the smaller mesh size and increased probability of covalent bond formation in this system.*

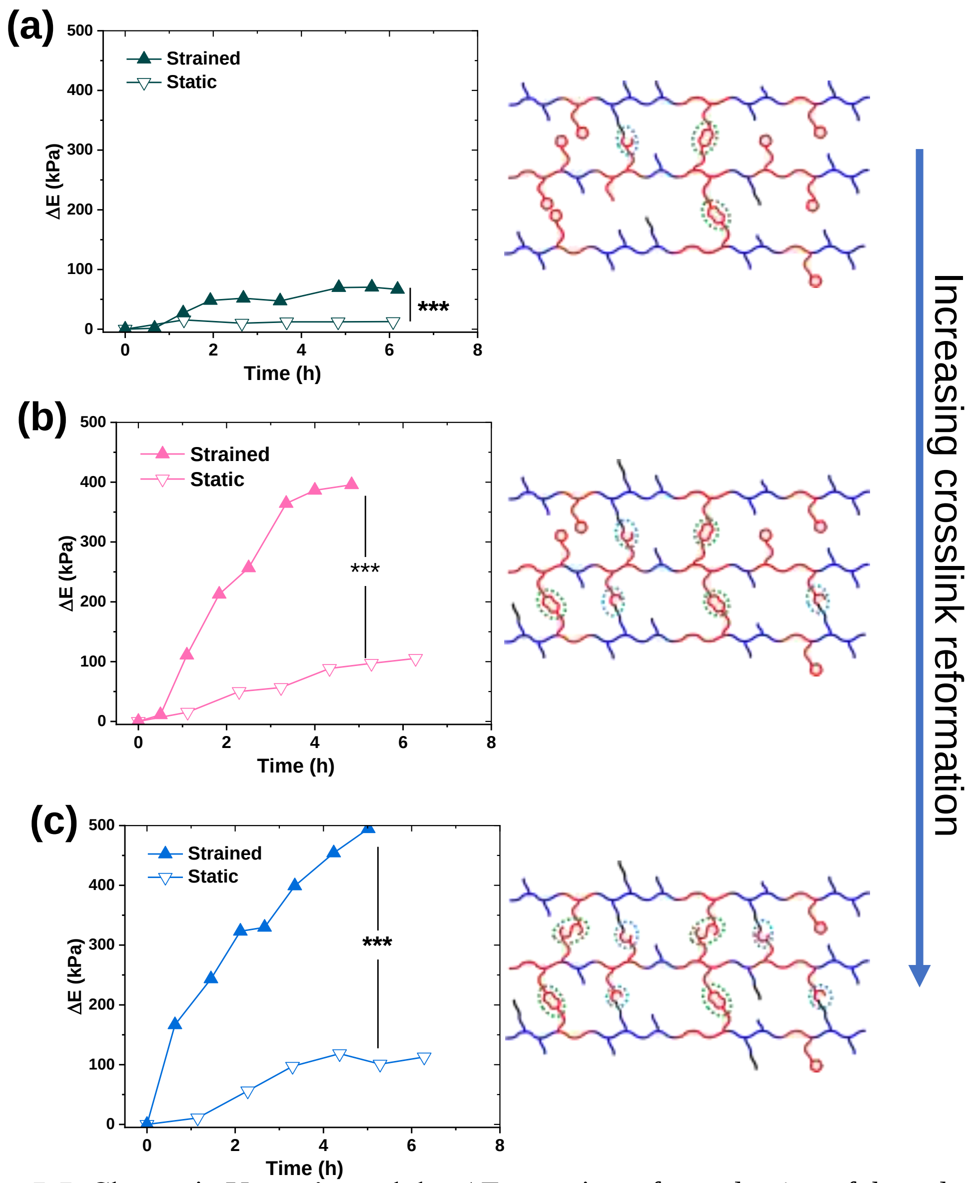

Figure 5-5. Change in Young's modulus ΔE over time after reduction of the gels with or without ~ 20 % cyclic compressive forces for (a) HI-A (b) HI-B and (c) HI-C. Next to each graph is a schematic to represent an envisaged network of strained hydrogels.

The alkene incorporation of the polymers determined the mesh size of the initial hydrogels, and further altered the rate of change and maximum magnitude of ΔE in the strain stiffening process. After gelation *via* thiol-ene reactopms, two types of free thiols remained 1,3-thiols that form thiolane rings[36] and those that are positioned gamma to C-

S sulfide units. The higher alkene incorporation in PI-B and PI-C led to a larger number of the latter type of thiols, whereas for PI-A, more 1,3-thiols prone to reverting to dithiolanes were present. Therefore, the free thiols in PI-B and PI-C are more likely to form interchain disulfide crosslinks than for PI-A. In addition, the smaller mesh size due to the initial higher crosslink density of PI-B and PI-C increased the probability of interchain disulfide formation. Overall, the thiols that are amenable to interchain crosslinking and smaller mesh size collectively contribute to the observed faster and larger increase of E values for PI-B and PI-C hydrogels under compressive strain.

Overall, in this chapter, novel functional zwitterionic polymers containing both 1,2-dithiolanes and alkene moieties were used to prepare hydrogels with dynamic networks responsive to redox conditions and mechanical force. In our polymer design, utilization of hydrophilic allyl-functionalized SBMA contributes aqueous solubility even when extents amounts of allyl groups are present. This unique, bifunctional design imparts gel-formation capability into the polymer structure without need for an external crosslinker. By appropriately tuning the reaction conditions, two types of crosslinking processes (permanent or dynamic) occur. The combination of permanent and dynamic crosslinks gives rise to the strain-stiffening features observed, for example, in the extracellular matrix of animal tissue. Under static conditions, the crosslinks associated with the permanent network (C-S bonds) define the mechanical state of the initial network and inhibit additional interchain (S-S) crosslinking. However, under cyclic strain, enhanced rates of disulfide crosslinking produce markedly greater stiffening of the network. Importantly, the rate of stiffening is not proportional to the availability of the free thiols but rather to mesh size of the primary network as defined by the permanent crosslinks.

The work in this chapter represents a collaboration with Dr. K. P. Sonu and Professor Shelly Peyton of the Chemical Engineering Department at UMASS Amherst. The mechanical properties of the hydrogels described in Sections 5.3 and 5.4 were characterized and analyzed by K. P. Sonu.

5.5 References

1. Lutolf, M. P. & Hubbell, J. A. Synthetic biomaterials as instructive extracellular microenvironments for morphogenesis in tissue engineering. *Nature Biotechnology 2005 23:1* **23**, 47–55 (2005).

2. Tibbitt, M. W. & Anseth, K. S. Hydrogels as extracellular matrix mimics for 3D cell culture. *Biotechnology and Bioengineering* **103**, 655–663 (2009).

3. Slaughter, B. V., Khurshid, S. S., Fisher, O. Z., Khademhosseini, A. & Peppas, N. A. Hydrogels in Regenerative Medicine. *Advanced Materials* **21**, 3307–3329 (2009).

4. April Kloxin, B. M. *et al.* Mechanical Properties of Cellularly Responsive Hydrogels and Their Experimental Determination. *Advanced Materials* **22**, 3484–3494 (2010).

5. Naficy, S., Brown, H. R., Razal, J. M., Spinks, G. M. & Whitten, P. G. Progress Toward Robust Polymer Hydrogels. *Australian Journal of Chemistry* **64**, 1007–1025 (2011).

6. Piechocka, I. K. *et al.* Multi-scale strain-stiffening of semiflexible bundle networks. *Soft Matter* **12**, 2145–2156 (2016).

7. Motte, S. & Kaufman, L. J. Strain stiffening in collagen I networks. *Biopolymers* **99**, 35–46 (2013).

8. Nia, H. T., Munn, L. L. & Jain, R. K. Physical traits of cancer. *Science (1979)* **370**, (2020).

9. Storm, C., Pastore, J. J., MacKintosh, F. C., Lubensky, T. C. & Janmey, P. A. Nonlinear elasticity in biological gels. *Nature 2005 435:7039* **435**, 191–194 (2005).

10. Yang, Z., Liang, G., Wang, L. & Xu, B. Using a kinase/phosphatase switch to regulate a supramolecular hydrogel and forming the supramolecular hydrogel in vivo. *J Am Chem Soc* **128**, 3038–3043 (2006).

11. Schild, H. G. Poly(N-isopropylacrylamide): experiment, theory and application. *Progress in Polymer Science* **17**, 163–249 (1992).

12. Yoshikawa, H. Y. *et al.* Quantitative evaluation of mechanosensing of cells on dynamically tunable hydrogels. *J Am Chem Soc* **133**, 1367–1374 (2011).

13. Lee, I. N. *et al.* Photoresponsive Hydrogels with Photoswitchable Mechanical Properties Allow Time-Resolved Analysis of Cellular Responses to Matrix Stiffening. *ACS Applied Materials and Interfaces* **10**, 7765–7776 (2018).

14. Kim, G. *et al.* High-intensity focused ultrasound-induced mechanochemical transduction in synthetic elastomers. *Proc Natl Acad Sci U S A* **116**, 10214–10222 (2019).

15. Chen, J. *et al.* Recent Advances in Mechano-Responsive Hydrogels for Biomedical Applications. *ACS Applied Polymer Materials* **2**, 1092–1107 (2020).

16. Fernandez-Castano Romera, M. *et al.* Strain Stiffening Hydrogels through Self-Assembly and Covalent Fixation of Semi-Flexible Fibers. *Angewandte Chemie* **129**, 8897–8901 (2017).

17. Wang, Y. *et al.* Biomimetic Strain-Stiffening Self-Assembled Hydrogels. *Angewandte Chemie* **132**, 4860–4864 (2020).

18. Erk, K. A., Henderson, K. J. & Shull, K. R. Strain Stiffening in Synthetic and Biopolymer Networks. *Biomacromolecules* **11**, 1358–1363 (2010).

19. Middleton, L. R. *et al.* Hierarchical Acrylic Acid Aggregate Morphologies Produce Strain-Hardening in Precise Polyethylene-Based Copolymers. *Macromolecules* **48**, 3713–3724 (2015).

20. Jaspers, M. *et al.* Ultra-responsive soft matter from strain-stiffening hydrogels. *Nature Communications 2014 5:1* **5**, 1–8 (2014).

21. Wang, J., Piskun, I. & Craig, S. L. Mechanochemical Strengthening of a Multi-mechanophore Benzocyclobutene Polymer. *ACS Macro Letters* **4**, 834–837 (2015).

22. Kim, G. *et al.* High-intensity focused ultrasound-induced mechanochemical transduction in synthetic elastomers. *Proc Natl Acad Sci U S A* **116**, 10214–10222 (2019).

23. Ramirez, A. L. B. *et al.* Mechanochemical strengthening of a synthetic polymer in response to typically destructive shear forces. *Nature Chemistry 2013 5:9* **5**, 757–761 (2013).

24. Willis-Fox, N., Rognin, E., Aljohani, T. A. & Daly, R. Polymer Mechanochemistry: Manufacturing Is Now a Force to Be Reckoned With. *Chem* **4**, 2499–2537 (2018).

25. Tran, Y. H., Rasmuson, M. J., Emrick, T., Klier, J. & Peyton, S. R. Strain-stiffening gels based on latent crosslinking. *Soft Matter* **13**, 9007–9014 (2017).

26. Scheutz, G. M. *et al.* Harnessing Strained Disulfides for Photocurable Adaptable Hydrogels. *Macromolecules* **53**, 4038–4046 (2020).

27. Scheutz, G. M. *et al.* Synthesis of functional 1,2-dithiolanes from 1,3-bis-: Tert -butyl thioethers. *Organic and Biomolecular Chemistry* **18**, 6509–6513 (2020).

28. Zhang, X. & Waymouth, R. M. 1,2-Dithiolane-Derived Dynamic, Covalent Materials: Cooperative Self-Assembly and Reversible Cross-Linking. *J Am Chem Soc* **139**, 3822–3833 (2017).

29. Chen, X., Lawrence, J., Parelkar, S. & Emrick, T. Novel zwitterionic copolymers with dihydrolipoic acid: Synthesis and preparation of nonfouling nanorods. *Macromolecules* **46**, 119–127 (2013).

30. Chang, C. C., Letteri, R., Hayward, R. C. & Emrick, T. Functional sulfobetaine polymers: Synthesis and salt-responsive stabilization of oil-in-water droplets. *Macromolecules* **48**, 7843–7850 (2015).

31. Jun, M., Cheng, C., Sun, G. & Wooley, K. L. Well-defined polymers bearing pendent alkene functionalities via selective RAFT polymerization. *Macromolecules* **41**, 9080–9089 (2008).

32. Richbourg, N. R. & Peppas, N. A. The swollen polymer network hypothesis: Quantitative models of hydrogel swelling, stiffness, and solute transport. *Progress in Polymer Science* **105**, 101243 (2020).

33. Flory, P. J. Molecular Theory of Rubber Elasticity. *Polymer Journal 1985 17:1* **17**, 1–12 (1985).

34. Canal, T. & Peppas, N. A. Correlation between mesh size and equilibrium degree of swelling of polymeric networks. *Journal of Biomedical Materials Research* **23**, 1183–1193 (1989).

35. Richbourg, N. R., Ravikumar, A. & Peppas, N. A. Solute Transport Dependence on 3D Geometry of Hydrogel Networks. *Macromolecular Chemistry and Physics* **222**, 2100138 (2021).

36. Liu, Y. *et al.* Dithiolane-Crosslinked Poly(ε-caprolactone)-Based Micelles: Impact of Monomer Sequence, Nature of Monomer, and Reducing Agent on the Dynamic Crosslinking Properties. *Macromolecules* **53**, 7009–7024 (2020).

CHAPTER 6

EXPERIMENTAL SECTION

6.1 Materials

Acetonitrile (ACN) (anhydrous, 99.8%), 4,4′-azobis(4-cyanovaleric acid) (98%, ACVA), 4-cyano-4-(phenylcarbonothioylthio)pentanoic acid (CPPA) (>97%), 2-(dimethylamino)ethyl methacrylate (DMAEMA) (98%), 2-methacryloyloxyethyl phosphorylcholine (MPC), trimethylamine (TEA), 11-Mercapto-1-undecanol (97%), bromine (≥99.99%), α-bromoisobutyryl bromide (98%), CuBr (99.999%), 2,2′-bipyridyl (bpy, ≥99%), 4,4′-dinonyl-2,2′-dipyridyl (dNbpy, 97%), ethyl α-bromoisobutyrate (EBiB, 98%), α, α, α-trifluorotoluene (anhydrous, ≥99%), monopotassium phosphate, bovine serum albumin (BSA, ≥98), lysozyme [2-(Methacryloyloxy)ethyl]dimethyl-(3-sulfopropyl)ammonium hydroxide (95%, SBMA), allyl bromide (99%), and n-butyllithium (2.5 M in hexanes), lithium phenyl-2,4,6-trimethylbenzoylphosphinate (≥95%, LAP) 1,5-cyclooctadiene (99 %), hydrobromic acid (33 weight % in acetic acid), 3-bromopyridine (99%), ethyl vinyl ether (99%), 2nd generation Grubbs catalyst ((1,3-bis(2,4,6-trimethylphenyl)-2-imidazolidinylidene) dichloro(phenylmethylene)(tricyclohexylphosphine) ruthenium), triisopropylsilane (TIPS, 99%), and 1,3-propanesultone (31, 98 %), heparin (ammonium salt from porcine intestinal mucosa), fetal bovine serum (FBS), and gold coated silicon wafers (99.999% (Au), layer thickness 1000 Å, 99.99% (Ti, adhesion layer)) and 3 Å molecular sieves were purchased from Sigma Aldrich. Diethyl ether (anhydrous), sodium chloride, potassium chloride, disodium phosphate, methanol, acetone, glacial acetic acid (ACS certified), hydrochloric acid (certified ACS plus), dialysis tubing (Spectra/Por®, regenerated cellulose membranes with a molecular weight cut-off of 6000-8000 g/mol), and 15 mL Millipore Ultra-15 Centrifugal Filter Unit Ultrafiltration Centrifugal Tube (MWCO 3000 or 10000) were purchased from Fisher Scientific. Fmoc-Val-OH (≥ 98%), Fmoc-Lys(Boc)-OH (≥ 98%), Fmoc-Arg(Pbf)-OH (≥ 98%), Fmoc-Pro-OH (≥ 98%), 1-hydroxybenzotriazole (HOBt, ≥98%) hydrate, O-(benzotriazol-1-yl)-N,N,N',N'-tetra-methyluronium hexafluorophosphate (HBTU, ≥ 98%), piperidine (≥ 99%), diisopropylethylamine (DIPEA, ≥ 99%), trifluoroacetic acid (TFA, ≥ 99%) and 2-chlorotrityl chloride resin (1.0-1.6 mmol/g, 100-200 mesh) were purchased from Creosalus. Ethylene chlorophosphate (ECP) was purchased from Alfa Aesar and purified by Kugelrohr distillation. 1,1,1,3,3,3-Hexafluoro-2-propanol (HFIP), 2,2,2-trifluoroethanol (TFE), 1H,1H,2H,2H-perfluoro-1-octanol (PFO), 1-(3-dimethylaminopropyl)-3-ethylcarbodiimide hydrochloride (EDC, > 98.0 %) and methanol-d4 were purchased from Oakwood Chemical. Chloroform-d and TFE-d3 were purchased from Cambridge Isotope Laboratories. 4-Methoxyphenol (MEHQ) was purchased from Acros Organics. 1H,1H,2H,2H-Tridecafluoro-n-octyl methacrylate (TDFOMA, stabilized with HQ + MEHQ, >98.0%) and 1H,1H,2H,2H-tridecafluoro-n-octyl acrylate (TDFOA) was purchased from TCI. Quant-iT™ PicoGreen® (200s assays) double stranded DNA reagent were purchased from Thermo Fisher Scientific. Plasmid DNA (pDRIVE5-GFP) was a gift from Dr. Figueiredo Lab at Purdue University. SIA kit Au from Cytiva was used to prepare chips for surface plasmon resonance study to characterize protein adsorption. MPC was washed with diethyl ether and dried *in vacuo*. Dichloromethane (DCM) and triethylamine (TEA) were dried by reflux and distillation over calcium hydride before use. Milli-Q water was obtained from Barnstead™

MicroPure™ Water Purification System and used for contact angle measurements and protein adsorption experiments. TDFOMA was purified by passing through a basic alumina plug. 2-{2-(Methacryloyloxy)ethyldimethylammonium}ethyl n-butyl phosphate (**MBP**) was synthesized following a published procedure.[1] Spectra/Por7 dialysis membranes (3.5 kDa MWCO, pretreated RC tubing) were purchased from VWR. Frozen HEK293 and MDA-MB-231 cells were purchased from ATCC. The cells were placed in Corning Falcon® 75 cm^2 tissue culture flasks and grown in Corning™ DMEM with L-glutamine, 4.5 g/L glucose and sodium pyruvate supplemented with Fisherbrand™ research grade fetal bovine serum and Gibco™ penicillin streptomycin. Cells were grown in a VWR 2310 incubator at 37 °C and 5% CO_2. Gibco™ trypsin-EDTA (0.25%) with phenol red was used to separate cells from tissue culture flasks. Detached cells were consolidated using an Eppendorf 5804R centrifuge. Cell densities were quantified using a Cellometer Mini purchased from Nexcelom Bioscience using ThermoFisher trypan blue solution (0.4%). Cells were placed on flat-bottomed, 96 well cell culture plates purchased from Chemglass Life Sciences. Cell viabilities were quantified using the Promega CellTiter-Glo™ Luminescent Cell Viability Assay Kit and luminescence values were recorded on a BMG Labtech POLARstar OPTIMA plate reader. Polymer solutions dissolved in growth media were filtered using a sterile Millex-GP 0.22 µm syringe filter manufactured by Merck Millipore Ltd.

6.2 Instrumentation

NMR spectra were acquired on a Bruker Avance-500 spectrometer (500 MHz for ^{1}H, 126 MHz for 13C, 202 MHz for 31P, and 470 MHz for 19F) or a Bruker Avance-400 machine (400 MHz for 1H, 101 MHz for 13C, 162 MHz for 31P, and 376 MHz for 19F). Gel permeation chromatography (GPC) was operated at 40 °C using 20 mM sodium trifluoroacetate in TFE as eluent at a flow rate of 1 mL/min on an Agilent 1200 series system equipped with the following: an isocratic pump, an autosampler, Polymer Standards Service (PSS) PFG guard column (8 × 50 mm), three PSS PFG analytical linear M columns (8 × 300 mm, particle size 7 μm), refractive index (RI) detection, and calibration against PMMA standards. GPC samples were filtered through a 0.45 μm PTFE filter prior to analysis. High resolution mass spectral data were obtained on a Thermo Orbitrap Fusion mass spectrometer. Dynamic light scattering (DLS) was performed on a Malvern Zetasizer NanoZS (data represent three replicate measurements). Tensiometry (DataPhysics OCA 15 plus) was performed in pendant drop mode to measure the interfacial tension of PFH and the polymer solution (1 mg/mL). Based on the shape of the drop, the interfacial tension between the liquids was calculated using the Young-Laplace equation and the software on the instrument. Water contact angle measurements were performed using the sessile drop method (OCA-15-plus, Dataphysics) or Biolin Scientific theta attension optical tensiometer. Images of PFH droplets were recorded using an optical microscope (Olympus CKX 41 equipped with an Olympus EP 50 digital camera). A G3P-8 spincoater from Specialty Coating System was employed for preparing polymer-coated Si substrates. J.A. Woollam RC2 spectroscopic ellipsometer was used to measure polymer coating thickness on the substrate. X-ray Photoelectron Spectroscopy (XPS) was carried out using a Thermo Scientific™ Nexsa Surface Analysis System with a monochromatic aluminum Kα X-ray source (1486.6 eV). The flood gun was turned on during all measurements to prevent charging. All data were collected using a 72-W focused X-ray beam with a spot size of 400 μm at a base pressure of 5×10^{-7} millibar or lower. Survey scans were obtained with a pass energy of 200 eV and a step size of 1 eV. Narrow scans were obtained with a pass energy of 50 eV and a step size of 0.1 eV. The elemental compositions were calculated using the Thermo Avantage software package (v5.9925). Shirley-type smart background subtraction method was applied to the raw narrow scans. The peaks were deconvoluted using a Lorentzian-Gaussian product function (L/G mix = 30%) and integrated at their full widths at half maximum for quantification. Protein adsorption was measured *via* surface plasmon resonance (SPR) study with a BIACORE T200 system at 25 ^{o}C.

6.3 Methods

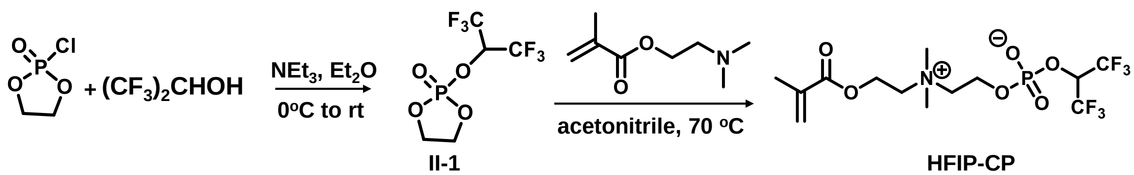

Synthesis of HFIP-MCP. HFIP was dried over 3 Å molecular sieves for 90 min. Anhydrous diethyl ether (110 mL), TEA (6.2 mL, 1.05 equiv.), and HFIP (8.44 g, 1.05 equiv.) were added to a three-neck round bottom flask equipped with a dropping funnel. A solution of ECP (6.84 g, 1.0 equiv.) in ether (40 mL) was added to the dropping funnel. The ECP solution was added dropwise to the HFIP solution, cooled in a 0 ^{o}C ice bath, over 45 minutes. Then, the ice bath was removed and the mixture was stirred at room temperature for 2 hours. The resultant white suspension was filtered through a short column of dry Celite and solvent was removed by rotary evaporation then on a vacuum line. Compound **II-1** (*i.e.*, the precursor to **HFIP-CP**) (11.18 g) was obtained as white solid in 85% yield. ^{1}H NMR (500 MHz, $CDCl_3$): δ 4.60-4.46 (m, 4H), 5.27-5.26 (m, 1H); ^{19}F NMR (470 MHz, $CDCl_3$) δ -74.46 (d, $^{3}J_{CF}$ = 5.8 Hz); ^{31}P NMR (202 MHz, $CDCl_3$) δ

17.30; ^{13}C NMR (126 MHz, $CDCl_3$) δ 66.85 (d, $^2J_{CP}$ = 3.0 Hz), 72.31(m), -$\underline{C}F_3$ signals observed between 130-110 ppm.

DMAEMA and MEHQ (0.01g of MEHQ per g of DMAEMA) were added to anhydrous ACN to give a solution of 0.125g/mL DMAEMA in ACN, and the solution was dried over 3 Å molecular sieves for 24 hours. The DMAEMA solution (51 mL, 41 mmol) was added to the flask containing **II-1** (11.2 g, 41 mmol). The mixture was stirred at 70 °C for 110 hours, then cooled to room temperature. Addition of ether (100 mL) to the solution caused a white solid precipitate to form. The mixture was stored at -20 °C for 4 hours after which the solid was isolated by vacuum filtration, then washed with ACN and diethyl ether, and dried *in vacuo*. **HFIP-CP** (13 g) was obtained as a white solid in 70% yield. ^1H NMR (CD_3OD, 500 MHz): δ 6.19-6.12 (m, 1H), 5.75-5.70 (m, 1H), 5.32-5.20 (m, 1H), 4.70-4.59 (m, 2H), 4.39-4.28 (m, 2H), 3.91-3.83 (m, 2H), 3.81-3.71 (m, 2H), 3.28 (s, 6H), 1.98 (m, 3H); ^{19}F NMR (470 MHz, CD_3OD) δ -75.73 (d, $^3J_{CF}$ = 6.1 Hz); ^{31}P NMR (202 MHz, CD_3OD) δ -3.11; ^{13}C NMR (126 MHz, CD_3OD) δ 166.17, 135.64, 125.90, 71.04, 64.64, 63.84, 59.41, 57.67, 51.45, 16.95. HRMS-ESI calculated mass for **HFIP-CP**, $C_{13}H_{20}F_6NO_6P$, calcd $[M+Na]^+$ 454.0825, found 454.0829.

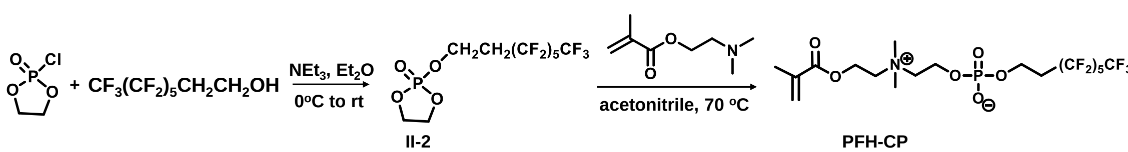

Synthesis of PFH-CP. Anhydrous diethyl ether (110 mL), TEA (6.0 mL, 1.02 equiv.), and PFO (15.7 g, 1.0 equiv.) were added to a three-neck round bottom flask equipped with a dropping funnel. ECP (6.13 g, 1.0 equiv.) and anhydrous diethyl ether (40 mL) were added to the dropping funnel. The ECP solution was added dropwise over 45 minutes to the PFO solution that was stirring in an ice-water bath; then, the cooling bath was removed and mixture was stirred for an additional 2 hours at room temperature. The white suspension was filtered through a short column of dry Celite and the solvent was removed by rotary evaporation then by vacuum pump. Compound **II-2** (*i.e.*, the precursor to **PFH-CP**) (18.15 g) was obtained as white solid in 92% yield. ^{1}H NMR (500 MHz, $CDCl_3$): δ 2.65-2.46 (m, 2H), 4.55-4.28 (m, 6H); ^{19}F NMR (470 MHz, $CDCl_3$) δ -80.82, -113.72, -121.88, -122.87, -123.61, -126.17; ^{31}P NMR (202 MHz, $CDCl_3$) δ 17.35; ^{13}C NMR (126 MHz, $CDCl_3$) δ 32.11 (m), 60.54 (m), 66.11 (d, $^{2}J_{CP}$ = 2.6 Hz), -$(\underline{C}F_2)_5\underline{C}F_3$ signals (weak) from 100-120 ppm.

DMAEMA and MEHQ (0.01 g MEHQ per g DMAEMA) were added to anhydrous ACN to give a solution of 0.125 g/mL DMAEMA in ACN, and the solution was dried over 3 Å molecular sieves for 24 hours. Then, the DMAEMA in ACN solution (48.6 mL, containing 39 mmol DMAEMA) was added to the flask containing **II-2** (18.1 g, 39.0 mmol). This mixture was stirred at 70 ^{o}C for 110 hours, during which time a white solid precipitate was observed. The reaction mixture was allowed to cool to room temperature, causing further precipitation of a white solid. Diethyl ether (100 mL) was added to the solution and the mixture was kept in a -20 ^{o}C freezer for ~4 hours. The solid was isolated by vacuum filtration, then washed with ACN and diethyl ether and dried *in vacuo*, to give **PFH-CP** (12 g) as white solid in 50% yield. ^{1}H NMR (CD_3OD, 400 MHz): δ 6.21-6.12 (m, 1H), 5.77-5.69 (m, 1H), 4.72-4.61 (m, 2H), 4.36-4.27 (m, 2H), 4.25-4.16 (q, J = 6.5 Hz, 2H), 3.94-3.84 (m, 2H), 3.81-3.70 (m, 2H), 3.29 (s, 6H), 2.72-2.52 (tt, J = 19.2, 6.2Hz, 2H), 1.98 (m, 3H); ^{19}F NMR (376 MHz, CD_3OD) δ -82.46, -114.54, -122.88, -123.88, -124.68, -127.35; ^{31}P NMR (162 MHz, CD_3OD) δ -0.68; ^{13}C NMR (101 MHz, CD_3OD) δ 167.59, 137.07, 127.26, 66.08, 66.19, 60.23, 59.16, 58.90, 52.93, 33.19, 18.36,

-($\underline{C}F_2$)$_5\underline{C}F_3$ peaks were not observed. HRMS-ESI calculated mass for **PFH-CP**, $C_{18}H_{23}F_{13}NO_6P$, calcd $[M+Na]^+$ 650.0949, found 650.0947.

Example procedure for the homopolymerization of HFIP-CP. **HFIP-CP** (2.0 g, 4.6 mmol), CPPA (26.3 mg, 0.094 mmol), ACVA (5.0 mg, 0.018 mmol) and TFE (3.6 mL) were added to a 20 mL glass vial that was sealed with a rubber septum, and the solution was purged with $N_{2(g)}$ for ~25 minutes. The solution was then stirred at 70 ^oC for 13 hours after which the reaction vial was immersed into $N_{2(l)}$. ^1H NMR spectroscopy (performed on aliquots taken from the reaction mixture) was used to assess monomer conversion by integrating the olefin signal of the monomer against the methine resonance of the polymer. A monomer conversion of 94% was obtained for this specific polymerization, and typical monomer conversion was in the 80-90+% range. The solution was precipitated into 40 mL diethyl ether and the precipitate was dissolved in water, which was dialyzed against water for 2 days (MWCO 3.5 kDa), then lyophilized for 2 days to provide **P1** (1.65 g) in 81% yield as pink solid. TFE GPC: M_n = 6.8 kDa, Đ = 1.23. ^1H NMR (CD_3OD, 500 MHz): 5.41-5.17 (br, 1H), 4.71-4.20 (br, 4H), 4.18-3.60 (br, 4H), 3.57-3.10 (br, 6H), 2.46-0.64 (br, 5H); ^{19}F NMR (470 MHz, CD_3OD) δ -75.43 (br); ^{31}P NMR (202 MHz, CD_3OD) δ -3.20 (br).

Example procedure for the homopolymerization of PFH-CP. **PFH-CP** (2.50 g, 3.98 mmol), CPPA (22.1 mg, 0.079 mmol), ACVA (4.2 mg, 0.015 mmol) and TFE (3.6 mL) were added to a 20 mL glass vial sealed with a rubber septum, and the solution was purged with $N_{2(g)}$ for 20-25 minutes. The solution was stirred at 70 ^oC for 13 hours, after which the vial was submerged into $N_{2(l)}$. Aliquots taken from the solution during the polymerization were characterized by ^1H NMR spectroscopy to assess monomer conversion by integrating the alkene signal of the monomer against the resonances arising from the polymer backbone. A monomer conversion of 88% was obtained for this polymerization (typical monomer conversion is 80-90+%). TFE was added to the reaction solution, which was then precipitated into a mixture of acetone and diethyl ether. The precipitate was separated by centrifugation and redissolved in TFE, the precipitated into acetone once and diethyl ether once. **P2** (1.6 g) was obtained as pink solid in ~80% yield after drying *in vacuo*. TFE GPC: M_n = 13.1 kDa, Đ = 1.25. ^{1}H NMR (CF_3CD_2OD, 500 MHz) δ 4.51-6.68 (br, 16H), 2.41-0.2 (br, 7H); ^{19}F NMR (470 MHz, CD_3OD) δ -82.79, -114.89, -122.94, -124.03, -125.11, -127.56; ^{31}P NMR (202 MHz, CD_3OD) δ -1.15.

Synthesis of random copolymers from MPC and PFH-CP (P3). To a solution of MPC (0.28 g, 0.96 mmol) in TFE (1.7 mL) in a 7 mL glass vial was added **PFH-CP** (0.60 g, 0.96 mmol), affording a homogenous solution after vortexing. CPPA (10.5 mg, 0.037 mmol) and ACVA (2.1 mg, 0.007 mmol) were then added and the solution was purged with $N_{2(g)}$ for 20 minutes then stirred at 70 °C for 14 hours. The polymerization was terminated by opening the vial to air. Small aliquots were removed from the solution and ^{1}H NMR spectroscopy was used to determine monomer conversion by integration of alkene resonances of the monomer against methylene group signals of the polymer. A monomer conversion of 97% was obtained for this specific polymerization (typical monomer conversion is 90+%). The solution was precipitated into diethyl ether and the precipitate was dissolved in water, then dialyzed against water for two days (MWCO 3.5 kDa) and finally lyophilized for two days to provide **P3** (0.7 g) in ~80% yield as a pink solid. TFE GPC: M_n= 20.5 kDa. ^{1}H NMR (CD_3OD, 500 MHz) δ 4.64-3.62 (br), 3.52-3.15 (br), 2.77-2.49 (br), 2.45-0.68 (br); ^{19}F NMR (470 MHz, CD_3OD) δ -82.45, -114.47,

-122.86, -123.91, -124.65, -127.35; ^{31}P NMR (202 MHz, CD_3OD) δ -0.60, -0.83. Samples of **P3** containing different amounts of MPC were prepared using a similar procedure but adjusting monomer feed ratios.

Synthesis of random copolymers from MPC and TDFOA (P4). MPC (0.20 g, 0.69 mmol) was dissolved in TFE (1.4 mL) in a 7 mL vial, to which TDFOA (0.279 g, 0.67 mmol) was added dropwise, followed by CPPA (7.6 mg, 0.027 mmol) and ACVA (1.3 mg, 0.005 mmol). The resultant solution was purged with $N_{2(g)}$ for 20 minutes then heated at 70 ^oC for 14 hours, after which the mixture was allowed to cool to room temperature and the vial opened to the air. ^1H NMR spectroscopy was employed to determine monomer conversion of 88%. The polymer-containing product solution was precipitated in diethyl ether and the precipitate was isolated by centrifugation. The precipitate was then dissolved in water and concentrated using an ultrafiltration centrifugal tube (MWCO 3.5 kDa) and the obtained concentrated material was diluted with water. This concentration-dilution process was repeated for four times and the collected material was lyophilized. **P4** (~0.40 g) was obtained as pink solid in 83% yield. TFE GPC: M_n= 17.3 kDa. ^1H NMR (CD_3OD, 500 MHz): 4.53-3.96 (br),3.81-3.62 (br), 3.40-3.20 (br), 2.81-0.80 (br).

Preparation of the polyMPC macroCTA reagent. MPC (2.53 g, 8.57 mmol) and CDPA (0.137 g, 0.34 mmol) was dissolved in TFE (6 mL) in a 20 mL glass vial and ACVA (4.6 mg, 0.016 mmol) was added to the solution. The solution was purged with $N_{2(g)}$ for 30 minutes and heated with stirring at 70 ^oC for 11 hours, after which the vial was submerged in $N_{2(l)}$. A monomer conversion of 92% was obtained. The resultant solution was precipitated in diethyl ether and the precipitate was dissolved in water then purified by dialysis for 2 days (MWCO 3.5 kDa), followed by lyophilization to yield the polyMPC macroCTA (2.2 g) as yellow solid in 88% yield. TFE GPC: M_n= 15.0 kDa. M_n determined by ^{1}H NMR spectroscopy ($M_{n,NMR}$) was used for mass calculations subsequent chain extensions.

Chain extension of polyMPC macroCTA with TDFOA (P5). The polyMPC macroCTA (0.40 g, 0.05 mmol) was dissolved in methanol (0.6 mL) and TFE (0.3 mL) in a 7 mL glass vial. A solution of TDFOA (0.533 g, 1.27 mmol) in TFE (0.3 mL) was added dropwise to the stirring polyMPC solution and ACVA (2.3 mg, 0.008 mmol) was added. The solution was purged with $N_{2(g)}$ for 30 minutes then stirred at 70 ^oC for 4 hours. The reaction was quenched by immersion of the glass vial into $N_{2(l)}$. A small aliquot was taken from the solution and ^{1}H NMR spectroscopy was used to determine monomer conversion by integrating the alkene peaks of the monomer against the methylene peaks of the polymer, indicating a 93% monomer conversion. The solution was precipitated in diethyl ether and the precipitate was redissolved in methanol then precipitated again in diethyl ether. The final precipitate was dried *in vacuo* to give **P5** (0.8 g) as a light yellow solid in 85% yield. TFE GPC: M_n= 16.5 kDa. ^{1}H NMR (CD_3OD, 500 MHz): 4.58-4.01 (br),3.80-3.66 (br), 3.50-3.19 (br), 2.90-0.68 (br).

Chain extension of polyMPC macroCTA with PFH-CP (P6). The polyMPC macroCTA (0.30 g, 0.04 mmol) was dissolved in methanol (0.45 mL) in a 7 mL glass vial. TFE (0.9 mL) was added, followed by **PFH-CP** (0.607 g, 0.97 mmol) and ACVA (2.3 mg, 0.008 mmol). The resultant solution was purged with $N_{2(g)}$ for 25 minutes and heated with stirring to 70 ^oC for 8 hours. The vial was then immersed $N_{2(l)}$. A small aliquot was taken from the solution and ^{1}H NMR spectroscopy was used to determine monomer conversion by integrating the olefin resonances of the monomer against the methylene signals of the polymer (monomer conversion ~95%). The solution was precipitated in diethyl ether and the recovered solid was dissolved in a methanol/water (4/6 v/v) mixture, which was concentrated by ultracentrifugation (MWCO 10.0 kDa); the obtained concentrate was diluted with a methanol/water (4/6 v/v) mixture and this concentration-dilution process was repeated four times, with water used for dilution in the last two cycles. The final concentrate was dried by lyophilization to yield **P6** as slightly yellow solid (0.72 g, 80% yield). GPC (eluent = TFE): M_n= 17.7 kDa. ^{1}H NMR (CD_3OD, 500 MHz): 4.64-3.65 (br), 3.45-3.20 (br), 2.79-2.50 (br), 2.36-0.70 (br); ^{19}F NMR (470 MHz, CD_3OD) δ -82.53, -114.53, -122.91, -123.96, -124.69, -127.42; ^{31}P NMR (202 MHz, CD_3OD) δ -0.48, -0.89.

Chain extension of polyMPC macroCTA with MBP (P7). The polyMPC macroCTA (0.32 g, 0.04 mmol) was dissolved in methanol (0.6 mL) in a 7 mL glass vial. TFE (0.6 mL) was added, followed by **MBP** (0.36 g, 1.03 mmol) and ACVA (2.3 mg). The solution was purged with $N_{2(g)}$ for 25 minutes then stirred with heating at 70 ^oC for 6 hours. A small aliquot taken from the solution was used to determine monomer conversion, using ^{1}H NMR spectroscopy and integrating the olefin resonances of the monomer against the methylene signals of the polymer (monomer conversion = 93%). The solution was precipitated in diethyl ether and the recovered solid was dissolved in a methanol/water (4/6 v/v) mixture, which was concentrated by ultracentrifugation (MWCO 10 kDa); the obtained concentrate was diluted with water. This concentration-dilution procedure was repeated four times and the final concentrate was lyophilized to yield **P7** as a slightly yellow solid (0.43 g, 63% yield). GPC (eluent = TFE): M_n= 19.4 kDa. ^{1}H NMR (CD_3OD, 500 MHz): 4.72-3.68 (br), 3.48-3.16 (br), 2.19-0.81 (br); ^{31}P NMR (202 MHz, CD_3OD) δ -0.22, -0.46.

Surface procedures for Chapter 3.

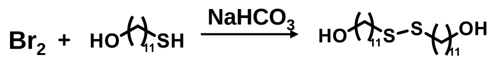

1 2

Synthesis of the disulfide alcohol 2[2]

11-Mercapto-1-undecanol (1) (3.6 g, 17.6 mmol) was dissolved in 132 mL dry DCM in a round-bottom flask, followed by addition of 17.6 mL of 10% $NaHCO_3$ solution. Bromine (0.45 mL, 8.7 mmol) was slowly added using a dropping funnel under stirring. After 40-min reaction, the organic phase was collected using a separatory funnel, and the aqueous phase was washed with 50 mL DCM twice. The organic phase was combined and dried over anhydrous $MgSO_4$, followed by solvent removal with evaporation, yielding the pure product (2) in 72% yield.

^{1}H NMR (500 MHz, $CDCl_3$, δ, ppm): 3.64 (t, J = 6.7 Hz, 4H), 2.68 (t, J = 6.5 Hz, 4H), 1.2-1.7 (m, 52H).

Synthesis of the disulfide initiator 3[2]

2 3

The disulfide diol (2) (2.59 g, 6.4 mmol) was dissolved in 159 mL dry DCM in a flame-dried round-bottom flask, followed by addition of dry TEA (4.44 mL, 31.8 mmol). α-Bromoisobutyryl bromide (1.89 mL, 15.3 mmol) was slowly added using a dropping funnel while the mixture was stirred at 0°C under N_2 atmosphere. After 1-h stirring at 0°C, the mixture was stirred for another 2 h at room temperature to complete the reaction. The mixture was then washed with 1 M Na_2CO_3 saturated with NH_4Cl, followed by drying over anhydrous $MgSO_4$ and solvent evaporation. After further purification with column (hexane/ethyl acetate = 13/1), the pure disulfide initiator (3) was collected as a pale yellow, viscous liquid in 58% yield.

^{1}H NMR (500 MHz, $CDCl_3$, δ, ppm): 4.16 (t, J = 6.6 Hz, 4H), 2.67 (t, J = 7.4 Hz, 4H), 1.92 (s, 12H), 1.66 (m, 8H), 1.21-1.43 (m, 30H).

^{13}C NMR (500 MHz, $CDCl_3$, δ, ppm): 171.85, 66.26, 56.13, 39.28, 30.92, 29.58, 29.33, 29.28, 28.64, 28.46, 25.90.

ESI-MS: m/z calc.: 704.7; found: 727.2 (M + Na+).

Au substrate functionalization with ATRP initiator.

Au substrates were cut into 1×1.2 cm pieces, and cleaned by bath sonication in acetone and isopropanol for 10 min each, followed by drying under N_2 (g). After further cleaning via 30-min UV/Ozone treatment (Jelight 342 UVO cleaner), the substrates were immersed in 2 mM ethanolic solution of the disulfide initiator for 24 h. Afterwards, the substrates were rinsed extensively with ethanol and dried under $N_{2(g)}$ for further modification.

Preparation of polymer-grafted Au substrates via surface-initiated atom transfer polymerization (SI-ATRP).

A) Grafting ***PMPC***. In a 7 mL vial, 0.25 g MPC was dissolved with 1.5 mL TFE, and the initiator- immobilized Au substrate was added to the vial. The monomer solution was purged with $N_{2(g)}$ solution for 10 minutes, then 165 µL solution of CuBr (2 mg/mL)/bpy (12 mg/mL) in methanol was added to the monomer solution, which was purged with $N_{2(g)}$ for another 10 minutes. The reaction was left at room temperature under $N_{2(g)}$ for ~3 hours, after which the substrates were taken out of the solution, rinsed with methanol, water, and acetone, and dried with air.

B) Grafting ***FCP-1***. In a 7 mL vial, 0.25 g HFIP-MCP was dissolved with 1.4 mL TFE, and the initiator immobilized Au substrate was added to the vial. The monomer solution was purged with $N_{2(g)}$ solution for 10 minutes, then 115 µL solution of CuBr (2 mg/mL)/bpy (12 mg/mL) in methanol was added to the monomer solution, which was purged with $N_{2(g)}$ for another 10 minutes. The reaction was left at room temperature under $N_{2(g)}$ for ~1.5 hours, after which the substrates were taken out of the solution, rinsed with methanol, TFE, water, and acetone, and dried with air.

C) Grafting ***FCP-2***. In a 7 mL vial, 0.5 g PFH-MCP was dissolved with 1 mL TFE, and the initiator immobilized Au substrate was added to the vial. The monomer solution was purged with $N_{2(g)}$ solution for 10 minutes, then 150 µL solution of CuBr (2 mg/mL)/bpy (12 mg/mL) in methanol was added to the monomer solution, which was purged with $N_{2(g)}$ for another 10 minutes. The reaction was left at room temperature under $N_{2(g)}$ for ~3 hours, after which the substrates were taken out of the solution, rinsed with methanol, TFE, water, and acetone, and dried with air.

D) Grafting ***PTDFOMA***. In a 7 mL vial, 0.4 mL TDFOMA was mixed with 1.3 mL TDFOMA, the initiator immobilized Au substrate was added to the vial, and 3 mg CuBr and 45 mg dNbpy was added to the solution. The solution was purged with $N_{2(g)}$ solution for ~20-25 minutes, after which the reaction was carried out at 60 ^{o}C. After ~10 hours, the substrates were taken out of the solution, rinsed with trifluorotoluene, TFE, water, and acetone, and dried with air.

Allyl SBMA and **HEMA-LA** used in Chapter 5 were prepared according to procedures published by Chang *et al*.[3]

Example procedure for PI synthesis

SBMA (1.5 g), allyl-SBMA (1.5 g), HEMA-LA (1.1 g), and CPPA (0.064 g), ACVA (0.01 g) and TFE (8mL) were added to a 25 mL round bottom flask, and the solution was purged with N_2 (g) for ~20-25 minutes. The solution was then stirred at 70 ^oC for 7-8 hours. The polymerization was terminated by stopping heating and exposing the solution to air. ^1H NMR spectroscopy in 0.2 M NaCl D_2O (performed on aliquots taken from the reaction mixture) was used to estimate monomer conversion by integrating the olefin signals of the monomers against the resonances of polymers at 0.5-2.5 ppm, 3.8-4.6 ppm and 5.7 ppm. A monomer conversion of ~80-90% was typically obtained for this polymerization. The solution was precipitated into 35 mL methanol, and the precipitate was separated by centrifugation and redissolved in TFE. The precipitate was precipitated in methanol twice more and diethyl ether once. The final precipitate was dried *in vacuo* to provide PI (3 g) in 75% yield as a pink solid (typical polymerization yield was ~65-80%).

Fabrication of the hydrogels

PI hydrogels preparation. 225 mg PI was dissolved in 410 μL 0.2 M $NaCl_{(aq)}$ and the polymer solution was incubated with 45 mg TCEP-HCl at 37 ^oC for 2 hours, then ~2-3 mg LAP and 45 μL triethylamine(added to neutralize the solution for dissolving LAP) was added to the solution, which was transferred to the cylindrical silicone molds with the diameter of 0.5 mm and the height of 0.5 mm. The solution was exposed to 365 nm UV for 2 hours, affording transparent and colorless hydrogels. The hydrogels were washed and equilibrated with 0.2 M $NaCl_{(aq)}$ before further experiments and characterizations.

Gelation of PIII. 225 mg PIII was dissolved in 450 μL 0.2 M $NaCl_{(aq)}$, to which 2,2′-(ethylenedioxy)diethanethiol was added. The solution was heated at 70 °C for 12 hours, resulting in the formation of opaque hydrogels.

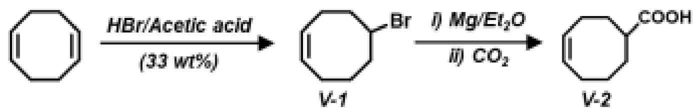

5-Bromo-1-cyclooctene (V-1) was prepared according to previously reported procedures.[4]

Synthesis of 5- carboxylic acid-1-cyclooctene (V-2). *All glassware used in the reaction was flame-dried three times under vacuum.* Magnesium (3.17 g) and 60 mL dry diethyl ether were added to a three-neck round bottom flask equipped with a condenser and dropping funnel. V-1 (20 g) and 60 mL dry diethyl ether were added to the dropping funnel. V-1 solution was then dropwise added to the magnesium, and the solution in the flask turned opaque and started refluxing. The mixture was stirred under room temperature for 4 hours, after which a greatly excess amount of dry ice (~10 g) was added to the reaction, and the reaction was stirred under room temperature for another 4 hours. 1 M $HCl_{(aq)}$ (50 mL) was added to quench the reaction, and the organic layer and the acidic aqueous layer were separated. The organic layer was extracted with 0.2 M $NaOH_{(aq)}$ (200mL) three times, the aqueous extractions were combined and acidified with 10M $HCl_{(aq)}$ to pH < 2, and the acidified aqueous extraction was extracted with dichloromethane (200mL) three times. The dichloromethane extractions underwent rotary evaporation and were then dried *in vacuo*, affording V-2 (3.3 g) as light-yellow liquid in ~20% yield. ^{1}H NMR ($CDCl_3$, 500 MHz): δ = 11.17 (s, 1H), 5.43-5.88 (m, 2H), 0.9-2.70 (m,11 H).

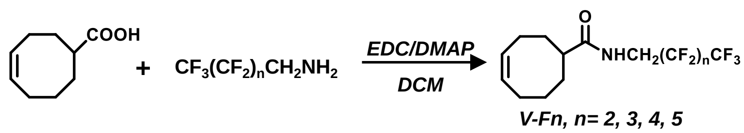

Synthesis of V-F2. *All glassware used in the reaction was flame-dried three times under vacuum.* V-2 (2.07 g), 1H, 1H-heptafluorobutylamine (2.50 g), EDC (2.65 g) and DMAP (0.32 g) were added to 90 mL DCM in a three-neck round bottom flask. The reaction was stirred for over 8 hours at room temperature, and the obtained solution was passed through a basic alumina plug. DCM was removed by rotary evaporation and vacuum dry to give V-F2 (3.5 g) as a white solid in 83% yield. V-F3, V-F4 and V-F5 were prepared by similar procedures.

V-F2: ^{1}H NMR ($CDCl_3$, 500 MHz): δ = 5.48-5.91 (m, 2H), 3.79-4.16 (m, 2H), 1.06-2.81 (m,11 H).

V-F3: ^{1}H NMR ($CDCl_3$, 500 MHz): δ = 6.17-6.27 (m, 1H), 5.45-5.88 (m, 2H), 3.74-4.13 (m, 2H), 0.98-2.78 (m,11 H).

V-F4: ^{1}H NMR ($CDCl_3$, 500 MHz): δ = 6.02-6.14 (m, 1H), 5.40-5.80 (m, 2H), 3.76-4.18 (m, 2H), 0.85-2.65 (m,11 H).

V-F5: ^{1}H NMR ($CDCl_3$, 500 MHz): δ = 6.16-6.30 (m, 1H), 5.43-5.88 (m, 2H), 3.74-4.21 (m, 2H), 0.96-2.78 (m,11 H).

Cyclooct-4-ene-1-VK(Boc)R(Pbf)K(Boc)K(Boc)K(Boc)P (rNLS-COE) was successfully prepared according to previously reported procedures,[4] confirmed by ^{1}H NMR spectroscopy and high-resolution ESI mass spectrometry.

Example procedure of copolymerization of V-Fn and rNLS-COE by ring opening metathesis polymerization (ROMP). *Grubbs III catalyst with 5-bromopyridine substituent was prepared according to reported procedures.* V-F2 (6 mg) and rNLS-COE (0.25 g) were added to a 7-mL glass vial and dissolved with 0.5 mL TFE. The obtained monomer solution was then degassed by three rounds of freeze-pump-thaw to remove oxygen from the reaction. Degassed (by three times freeze-pump-thaw) catalyst solution (58.8 µL, 50 mg/mL Grubbs III in DCM) was added to the monomer solution. The polymerization proceeded at room temperature for 2 hours under $N_{2(g)}$ and was quenched by addition of ethyl vinyl ether (0.1 mL), which was stirred for another 15 minutes. The reaction was precipitated in diethyl ether (45 mL), centrifuged, decanted and vacuum dried. The precipitate was dissolved in 5 mL deprotection solution (TFA/water/TIPS 95/2.5/2.5 v/v/v) and the solution was stirred at room temperature for 3 hours, to remove the protection groups. The reaction mixture was added to diethyl ether (45 mL), then centrifuged, decanted and vacuum dried. The obtained solid was dissolved in water, which was then dialyzed against water, 30% acetic $\text{acid}_{(aq)}$ and water (three times). Polymer rNLSII-14F (120 mg) was obtained as a white solid after lyophilization in ~60 % yield.

Relaxation time measurements. Relaxation measurements were performed on 10 mg/mL polymer solutions in PBS/D_2O (90/10, v/v) on a Bruker 500 MHz NMR spectrometer. The T_1 relaxation values of the polymers were measured using a standard inversion–recovery pulse sequence. T_2 was measured using a Carr–Purcell–Meilboom–Gill (CPMG) pulse sequence.[5,6]

^{19}F MR Imaging. ^{19}F MR images of polymer solutions were acquired on a 11.74 Tesla Agilent Direct Drive MRI. Polymer solutions, loaded in 5 mm NMR, were placed in 3D printed holder inside of a custom-built ^{19}F one-turn solenoid coil (25 mm ID). Fast spin echo sequence (TE = 4.9 ms, TR = 500 ms, echo train length = 2, 48 x 48 matrix size, 32 averages, acquisition time = 6 min 25 sec) was used to obtain T_1 weighted images. A multi echo spin echo sequence (TE = 6.5 ms, TR = 4000 ms, TE spacing = 6.5 ms, 16 echoes, 4 averages, 48 x 48 matrix size, acquisition time = 12 min 48 sec) was used to produce a series of images with different T_2 weightings.

Optical microscopy of PFH droplets stabilized by P3 (2 mg/mL) in water. PFH droplets were prepared by mixing PFH (100 µL) in **P3** (3 mL, 2 mg/mL) solution by vortexing (using vortex mixer from Chemglass Life Sciences) for 10-30 seconds. The droplet solution was added to a glass microscope slide and the image was recorded by optical microscopy with a 4x objective. The **P3** sample used in these experiments had a 45 mol% incorporation of MPC.

Preparation of PFH nanoemulsions. To a solution of polymer (8 mg) in water (4 mL) was added 20 µL of PFH. The mixture was placed in ice bath and sonicated using a Branson 150 probe sonicator under pulse mode (45 seconds on; 30 seconds off) at an amplitude of 35-40% for 2-3 min (total on time). Nanoemulsion size and stability were recorded as a function of time using DLS. The nanoemulsions were vortexed before the measurement to redisperse any sedimented droplets. The **P3** sample used in these experiments had a 45 mol% incorporation of MPC. The $M_{n,GPC}$ of the **P1** sample used here is ~6.7 kDa.

Preparation of polymer-coated Si substrates. Si substrates were cleaned by sonicating for 10 minutes in water then rinsing with methanol and acetone. The polymer was applied from a 25 mg/mL polymer solution (**P2** in TFE, polystyrene (PS) or poly(methyl methacrylate) (PMMA) in THF) by spin coating at 2000 rpm for 1 minute, then drying the coated substrate on a hot plate at 80 ^{o}C for 2 minutes.

Exposure of substrates to FITC-BSA. The coated substrates prepared as described above were immersed in 1 mg/mL FITC-BSA solution for 20 hours, then rinsed with pH 7.4 PBS buffer (~20 mL) and water (~600 mL). PS and PMMA were used as positive controls and bare substrate without exposure to the protein solution was utilized as a 'blank' substrate. Fluorescence analysis was performed using a Nikon A1R confocal microscope with 488 nm laser excitation. NIH ImageJ software (http://imagej.nih.gov/ij/) was employed to obtain the mean fluorescence intensity (MFI) of each image, indicative of the presence of protein that had adsorbed to the surface.

Cell culture and biocompatibility experiments and analysis. Cytotoxicity experiments analyzing the effect of the polymers on live cells were performed using HEK293 human embryonic kidney cells and MDA-MB231 human breast adenocarcinoma cells purchased from ATCC. Each polymer was dissolved in growth media consisting of DMEM supplemented with 10% FBS and 1% penicillin/streptomycin. The polymer was vortexed and then sterilized by filtration using a 0.22 µm syringe filter. 4,000 cells per well in 100 µL of growth medium were seeded onto a 96-well plate and placed in the incubator at 37 °C and 5% CO_2 overnight. The medium was removed and replaced with new polymer-containing media (from 0.05 to 5 mg/mL). Each experiment was compared to a control sample containing refreshed growth medium. Experiments associated with particular conditions were performed in triplicate and incubated for 48 hours. Cell viability was quantified using CellTiter-Glo luminescent viability assays (Promega). Luminescence values were obtained from a POLARstar OPTIMA plate reader. All conditions were normalized to the control luminescent values. To determine if there was a statistically significant difference between the experimental and control samples, a single factor ANOVA with an α=0.05 was performed. If the ANOVA revealed a statistically significant difference between the conditions, Tukey's Honestly Significant Difference and Bonferroni post hoc analysis tests were performed to determine which conditions were different than the controls. All statistical analysis was performed in Microsoft Excel.

**Thickness and contact angle measurements were performed by Dr. Zhefei Yang in the Emrick Group.*

Ellipsometry. Polymer coating thickness values were determined by ellipsometry using a J.A. Woollam RC2 spectroscopic ellipsometer. The measurement was conducted at varying angles of incidence (45°, 50°, 55°, 60°, 65°). The thickness of polymer coatings were calculated by fitting experimental data with the Cauchy equation (**Equation S1**),

$$n = A + \frac{B}{\lambda^2} \qquad \textbf{Equation S1}$$

where n is the refractive index, λ is the light wavelength in μm, A and B are constants with value of 1.5 and 0.01, respectively.

Calculation of grafting density. Grafting density of the polymer chains on the surface was calculated according to reported procedures,[7] using **Equation S2**, where d is the density of the polymers (1.30 g/cm^3)[8], L_d is the thickness of the polymers on the surface measured by ellipsometry, and N_A is the Avogadro's number. EBiB was added to the reaction and M_n of the free polymers in solution (measured by gel permeation chromatography with TFE (contains 20 mM sodium trifluoroacetate) as eluent, calibrated against poly(methyl methacrylate) standards) was assumed to be the same as that for polymers grafted on the surface.

$$\sigma = \frac{dL_d N_A \times 10^{-21}}{M_n} \qquad \textbf{Equation S2}$$

Contact angle measurements. The contact angle measurement was conducted using a Biolin Scientific theta attension optical tensiometer. For the static contact angle, a 2.5-μL probe liquid droplet was released onto the surface, followed by 1-min measurements at 2.3 frames per second to obtain the average results. Measurements on three different spots were collected for each sample to obtain the average value and standard deviation.

The dynamic contact angle was measured by changing volume of an existing droplet on the surface. A 2.5-μL probe liquid droplet was released onto the surface, with the needle in direct contact with the droplet. The vertical position of the needle was adjusted to keep the contact angle identical with the static contact angle. Then the probe liquid was injected at a rate of 0.2 μL/s using an auto-dispenser. The advancing contact angle was determined by averaging contact angles during the process in which the length of baseline increased, the droplet volume increased while the contact angle kept constant. Similarly, the receding contact angle was determined during withdrawal of fluid from the droplet at a rate of 0.2 μL/s. When the length of baseline decreased, the droplet volume decreased and the contact angle kept constant, the contact angles were collected and averaged to achieve the receding contact angle.

Protein adsorption experiments. Protein adsorption was measured *via* SPR study with a BIACORE T200 system at 25 ^{o}C. SPR sensors modified with PMPC, FCP-1, FCP-2, and PTDFOMA, and unmodified SPR sensor were tested with BSA and Lysozyme in PBS buffer (137 mM NaCl, 2.7 mM KCl, 2 mM KH_2PO_4, and 10 mM Na_2HPO_4, pH 7.4). In each measurement, three start-up cycles were run for system equilibration before the protein adsorption assay. For protein adsorption measurement, PBS buffer first flowed through the sensor for 50 seconds, a protein solution (1 mg/mL BSA or lysozyme in PBS buffer) then flowed through surface for 300 seconds, followed by rinsing with PBS buffer for 300 seconds to remove loosely bound proteins.

**Dr K.P. Sonu in the Peyton Group from Chemical Engineering Department at UMASS Amherst performed the characterization and analysis of hydrogel properties following procedures described below.*

Characterization of Hydrogels prepared in Chapter 5

Swelling Studies. **S**welling studies were conducted in pure water, 0.1 M and 0.2 M NaCl aqueous solutions. The hydrogels were allowed to stand in the respective solution for at least 24 hours to reach equilibrium swelling. The swollen weight (W_s) of the hydrogel was determined by weighing the swollen hydrogel. The same hydrogels were then subjected freeze drying for overnight to determine the dry weight (W_d) of the polymer network. The weight fraction of the polymer in the swollen gel, r is defined as below:

$$\mathbf{r} = \frac{W_d}{W_s} \qquad (1)$$

Initial Polymer Volume Fraction (φ_o) is the volumetric concentration of polymer in water before gelation. We determined $\boldsymbol{\varphi_o}$ from weights and volume of the initial polymer solution before subjecting to gelation conditions.

$$\boldsymbol{\varphi_o} = \frac{V_{polymer}}{V_{polymer+water}} \qquad (2)$$

where $V_{polymer}$ is the volume of the polymer in the polymer solution ($V_{polymer} = V_{totol} - V_{water}$) and $V_{polymer+water}$ is the total volume of the polymer solution.

Relaxed and Swollen Polymer Volume Fraction (φ_r and φ_s). The relaxed state polymer volume fraction (φ_s) is defined as the volumetric concentration of the polymer just after gelation before swelling the hydrogel. The swollen polymer volume fraction (φ_s) defines the volumetric concentration of polymer in the hydrogel at the equilibrium swelling state.

$$\boldsymbol{\varphi}_{\mathbf{r}} = \frac{\boldsymbol{V_d}}{\boldsymbol{V_r}} \qquad (3)$$

$$\boldsymbol{\varphi}_{\boldsymbol{s}} = \frac{\boldsymbol{V_d}}{\boldsymbol{V_s}} \qquad (4)$$

where V_d is the volume of the dry network, V_r is the volume of relaxed state, and the V_s is the volume of swollen state.

V_r and V_s are determined by using buoyancy-based measurements where V is determined as follow:

$$\boldsymbol{V} = \frac{\boldsymbol{m - m'}}{\boldsymbol{\rho_{ns}}} \qquad (5)$$

where m is the mass of the hydrogel and m' is the apparent mass of the hydrogel when immersed in heptane. ρ_{ns} is the density of heptane (0.6837 g/mL).

Mesh Size calculations. The mesh size (ξ, nm) is the average linear distance between two adjacent crosslink junctions. It is determined using the following equation:

$$\boldsymbol{\xi} = \boldsymbol{\varphi}_{\boldsymbol{s}}^{-\frac{1}{3}} \left[\left(\mathbf{1} - \frac{\mathbf{2}}{\boldsymbol{f}}\right) \boldsymbol{l}^{\mathbf{2}} \boldsymbol{C}_{\propto} \boldsymbol{\lambda} \boldsymbol{N_j}\right]^{\frac{1}{2}} \qquad (6)$$

where $\boldsymbol{\varphi}_{\boldsymbol{s}}$ is swollen polymer volume fraction, $\boldsymbol{f}$ is junction functionality (which is 4 in our hydrogels), $\boldsymbol{l}$ is average bond length in the polymer backbone, $\boldsymbol{C}_{\propto}$ is Flory's characteristic ratio (which is taken as 8.1 which is for PMMA that is structurally closest to our polymer system). $\boldsymbol{\lambda}$ number of backbone bonds in the polymer repeating unit (2 for our polymer), and $\boldsymbol{N_j}$ is degree of polymerization between junctions. The mesh size calculations were carried out with help of an online calculator at https://hydrogeldesign.com/the-model/mesh-transport/.

Elastic Modulus Experimental Determination: After 24 h of swelling with 0.2 M $NaCl_{(aq)}$, the hydrogel was placed between the parallel plates of a rheometer (TA Instruments, USA) to perform compressive stress-strain mechanical measurements. The hydrogel was compressed by moving the top-plate at a rate of 20 μm/s in air and the initial linear region (0- 5 %) of stress-strain curve was used to determine the elastic moduli. The cross-sectional area of the hydrogels was determined by using the digital caliper (Fisherbrand™ Traceable™) of ±0.03 mm accuracy.

Strain-induced Stiffening Experiments. The hydrogel was taken from the reduction solution right before the mechanical conditioning. The hydrogel was placed in a petri-dish containing 0.2 M $NaCl_{(aq)}$ to avoid drying. The petri-dish with hydrogel was placed between the parallel plates for rheometer. The top-plate was lower such that the hydrogel was confined between the bottom of the petri-dish and top-plate. Compression and tension cycles are performed at 20 μm/s with 0-25 % strain. At pre-determined time intervals, the elastic modulus of the hydrogel was determined in air. The conditioning and elastic modulus determination cycles continued for 6 h.

Statistical Analysis. Statistical analysis was performed by using OriginPro 2020. Data are reported as mean ± standard deviation. Statistical significance of difference between the relevant pairs (in terms of P-values) was calculated by using Tukey post-test. $P \leq 0.05$ represented as single asterisk (*), $P \leq 0.01$ as double asterisk (**), $P \leq 0.001$ as triple asterisk (***) and $P \leq 0.0001$ as quadruple asterisk (****). $P > 0.05$ is considered insignificant.

Size and zeta potential measurements of polyplexes. N/P 30 polymer stock solution was prepared by diluting N/P 200 polymer stock solution with water or DMEM (relative to [DNA] = 20 µg/mL) (N/P ratio calculation was performed according to reported procedures[9]). DNA stock solution (400 µg/mL) was diluted to 20 µg/mL with water or DMEM. N/P 5 polyplexes were formed by vortexing the mixture 15 µL N/P 30 polymer stock solution, 75 µL water or DMEM and 90 µL DNA solution (20 µg/mL) were mixed, vortexed and equilibrated at room temperature for ~40-60 minutes. To evaluate the stability of the polyplexes in the presence of serum, 20 µL FBS was added to the polyplexes prepared in DMEM after equilibration. For polyplex formulations containing FCP, FCP was added into the N/P 30 solution, which was used in the subsequent experiments for polyplex preparation. Polyplexes size in water or DMEM at different times was recorded with DLS over three measurements on the same sample, and the intensity-average size were reported. Zeta potentials were calculated using the Smoluchowski approximation and were reported as the average over three measurements on the same sample.

Heparin-induced polyplex decomplexation Picogreen® assay. PicoGreen® 20X solution was prepared by diluting the purchased PicoGreen® solution 1000 times with DNase free water. N/P 30 polymer stock solution (17 µL), DNase free water (83 µL), and DNA solution (100 µL, 20 µg/mL) were mixed and equilibrated for four hours at room temperature to obtain N/P 5 polyplex solution. PicoGreen® 20X solution (20 µL) was added to the polyplex solution which was then equilibrated at room temperature for 10 minutes. Heparin solution (20 µL, 0.75 unit/ µL, 1 mg heparin = 200 units) was added to the polyplex/ PicoGreen® solution. The mixture was then added to three wells of a 96 well plate (75 µL). The well plate was incubated at 37ºC for 6 hours in total and fluorescence intensity of the samples were recorded at predetermined time points using BMG Labtech FLUOstar OPTIMA plate reader. The fluorescence intensity of the samples was normalized using the blank (containing no polymer or DNA) and the positive control (containing no polymers).

6.4 References

1. Hu, G., Parelkar, S. S. & Emrick, T. A facile approach to hydrophilic, reverse zwitterionic, choline phosphate polymers. *Polym. Chem.* **6**, 525–530 (2015).
2. Shah, R. R. *et al.* Using atom transfer radical polymerization to amplify monolayers of initiators patterned by microcontact printing into polymer brushes for pattern transfer. *Macromolecules* **33**, 597–605 (2000).
3. Chang, C. C., Letteri, R., Hayward, R. C. & Emrick, T. Functional sulfobetaine polymers: Synthesis and salt-responsive stabilization of oil-in-water droplets. *Macromolecules* **48**, 7843–7850 (2015).
4. Parelkar, S. S. *et al.* Polymer-peptide delivery platforms: effect of oligopeptide orientation on polymer-based DNA delivery. *Biomacromolecules* **15**, 1328–1336 (2014).
5. Carr, H. Y. & Purcell, E. M. Effects of Diffusion on Free Precession in Nuclear Magnetic Resonance Experiments. *Phys. Rev.* **94**, 630–638 (1954).
6. Meiboom, S. & Gill, D. Modified Spin-Echo Method for Measuring Nuclear Relaxation Times. *Rev. Sci. Instrum.* **29**, 688–691 (1958).
7. Kobayashi, M. *et al.* Wettability and antifouling behavior on the surfaces of superhydrophilic polymer brushes. *Langmuir* **28**, 7212–7222 (2012).
8. Yan, W. *et al.* Growing Polymer Brushes from a Variety of Substrates under Ambient Conditions by Cu0-Mediated Surface-Initiated ATRP. *ACS Appl. Mater. Interfaces* **11**, 27470–27477 (2019).
9. Letteri, R. A. Functional Hydrophilic Polymers for Solution Assembly and Non-Viral Gene Therapy. *Doctoral Dissertations* (2016). doi:https://doi.org/10.7275/8527458.0

BIBLIOGRAPHY

"Approved Cellular and Gene Therapy Products | FDA." https://www.fda.gov/vaccines-blood-biologics/cellular-gene-therapy-products/approved-cellular-and-gene-therapy-products (May 27, 2022).

"GTCT (FMS19)." https://a873679.fmphost.com/fmi/webd/GTCT (May 27, 2022).

"PFAS Treatment in Drinking Water and Wastewater – State of the Science | US EPA." https://www.epa.gov/research-states/pfas-treatment-drinking-water-and-wastewater-state-science

April Kloxin, By M, Christopher J Kloxin, Christopher N Bowman, Kristi S Anseth, A M Kloxin, C J Kloxin, C N Bowman, and K S Anseth. 2010. 'Mechanical Properties of Cellularly Responsive Hydrogels and Their Experimental Determination'. Advanced Materials 22 (31): 3484–94. https://doi.org/10.1002/ADMA.200904179.

Arumugam, Madan Kumar et al. 2021. "Beneficial Effects of Betaine: A Comprehensive Review." Biology 2021, Vol. 10, Page 456 10(6): 456. https://www.mdpi.com/2079-7737/10/6/456/htm

Bai, Ying et al. 2016. "Functional Droplets That Recognize, Collect, and Transport Debris on Surfaces." Science Advances 2(10). https://www.science.org/doi/10.1126/sciadv.1601462

Bhuchar, Neha, Zhicheng Deng, Kazuhiko Ishihara, and Ravin Narain. 2011. "Detailed Study of the Reversible Addition-Fragmentation Chain Transfer Polymerization and Co-Polymerization of 2-Methacryloyloxyethyl Phosphorylcholine." Polymer Chemistry 2(3): 632–39.

Bono, Nina, Federica Ponti, Diego Mantovani, and Gabriele Candiani. 2020. "Non-Viral in Vitro Gene Delivery: It Is Now Time to Set the Bar!" Pharmaceutics 12(2): 183.

Bouard, D., N. Alazard-Dany, and F. L. Cosset. 2009. "Viral Vectors: From Virology to Transgene Expression." British Journal of Pharmacology 157(2): 153–65.

Bratek-Skicki, Anna, Vanina Cristaudo, Jérôme Savocco, Sylvain Nootens, Pierre Morsomme, Arnaud Delcorte, and Christine Dupont-Gillain. 2019. "Mixed Polymer Brushes for the Selective Capture and Release of Proteins." Biomacromolecules 20(2): 778–89. https://pubs.acs.org/doi/full/10.1021/acs.biomac.8b01353

Brown, Marcel U, Alexandria Triozzi, and Todd Emrick. 2021. "Polymer Zwitterions with Phosphonium Cations." Cite This: J. Am. Chem. Soc 143: 6532. https://doi.org/10.1021/jacs.1c00793.

Buck, Jonas et al. 2019. "Lipid-Based DNA Therapeutics: Hallmarks of Non-Viral Gene Delivery." ACS Nano 13(4): 3754–82.

Buck, Thilo M., and Jan Wijnholds. 2020. "Recombinant Adeno-Associated Viral Vectors (RAAV)-Vector Elements in Ocular Gene Therapy Clinical Trials and Transgene Expression and Bioactivity Assays." International Journal of Molecular Sciences 2020, Vol. 21, Page 4197 21(12): 4197. https://www.mdpi.com/1422-0067/21/12/4197/htm

Buckwalter, Daniel J., Antons Sizovs, Nilesh P. Ingle, and Theresa M. Reineke. 2012. "MAG versus PEG: Incorporating a Poly(MAG) Layer to Promote Colloidal Stability of Nucleic Acid/"click Cluster" Complexes." ACS Macro Letters 1(5): 609–13.

Bulcha, Jote T. et al. 2021. "Viral Vector Platforms within the Gene Therapy Landscape." Signal Transduction and Targeted Therapy 6(1): 53. http://dx.doi.org/10.1038/s41392-021-00487-6.

Caffery, Breanne, Jeoung Soo Lee, and Angela A. Alexander-Bryant. 2019. "Vectors for Glioblastoma Gene Therapy: Viral & Non-Viral Delivery Strategies." Nanomaterials 9(1): 105.

Canal, Tiziana, and Nikolaos A. Peppas. 1989. 'Correlation between Mesh Size and Equilibrium Degree of Swelling of Polymeric Networks'. Journal of Biomedical Materials Research 23 (10): 1183–93. https://doi.org/10.1002/JBM.820231007.

Carr, H Y, and E M Purcell. 1954. "Effects of Diffusion on Free Precession in Nuclear Magnetic Resonance Experiments." Physical Review 94(3): 630–38. https://link.aps.org/doi/10.1103/PhysRev.94.630.

Chang, Chia-Chih, Rachel Letteri, Ryan C Hayward, and Todd Emrick. 2015. "Functional Sulfobetaine Polymers: Synthesis and Salt-Responsive Stabilization of Oil-in-Water Droplets." Macromolecules 48(21): 7843–50. https://doi.org/10.1021/acs.macromol.5b01861.

Chen, Jingsi, Qiongyao Peng, Xuwen Peng, Linbo Han, Xiaogang Wang, Jianmei Wang, and Hongbo Zeng. 2020. 'Recent Advances in Mechano-Responsive Hydrogels for Biomedical Applications'. ACS Applied Polymer Materials 2 (3): 1092–1107. https://doi.org/10.1021/ACSAPM.0C00019.

Chen, Sheng-Han, Kyoko Fukazawa, Yuuki Inoue, and Kazuhiko Ishihara. 2019. "Photoinduced Surface Zwitterionization for Antifouling of Porous Polymer Substrates." Langmuir 35(5): 1312–19. https://doi.org/10.1021/acs.langmuir.8b01089.

Chen, Wei Liang, Roselynn Cordero, Hai Tran, and Christopher K. Ober. 2017. '50th Anniversary Perspective: Polymer Brushes: Novel Surfaces for Future Materials'. Macromolecules 50 (11): 4089–4113. https://doi.org/10.1021/acs.macromol.7b00450.

Chen, Xiangji et al. 2012. "PolyMPC–Doxorubicin Prodrugs." Bioconjugate Chemistry 23(9): 1753–63. https://doi.org/10.1021/bc200667s.

Chen, Xiangji, Jimmy Lawrence, Sangram Parelkar, and Todd Emrick. 2013. "Novel Zwitterionic Copolymers with Dihydrolipoic Acid: Synthesis and Preparation of Nonfouling Nanorods." Macromolecules 46(1): 119–27. https://doi.org/10.1021/ma301288m.

Chen, Xiangji, Samantha McRae, Sangram Parelkar, and Todd Emrick. 2009. "Polymeric Phosphorylcholine−Camptothecin Conjugates Prepared by Controlled Free Radical Polymerization and Click Chemistry." Bioconjugate Chemistry 20(12): 2331–41. https://doi.org/10.1021/bc900339x.

Chen, Zhan. 2022. 'Surface Hydration and Antifouling Activity of Zwitterionic Polymers'. Langmuir 38 (15): 4483–89. https://doi.org/10.1021/ACS.LANGMUIR.2C00512.

Chopra, Amitabh M et al. 2017. "Polymer Coating Embolism from Intravascular Medical Devices — a Clinical Literature Review." Cardiovascular Pathology 30: 45–54. https://www.sciencedirect.com/science/article/pii/S1054880717301175.

Couturaud, Benoit et al. 2019. "Supramolecular Fluorine Magnetic Resonance Spectroscopy Probe Polymer Based on Passerini Bifunctional Monomer." ACS Macro Letters 8(11): 1479–83. https://doi.org/10.1021/acsmacrolett.9b00626

Dalal, Rishad J. et al. 2021. "Cationic Bottlebrush Polymers Outperform Linear Polycation Analogues for PDNA Delivery and Gene Expression." ACS Macro Letters 10: 886–93.

Dang, Yuan, Miao Quan, Cheng Mei Xing, Yan Bing Wang, and Yong Kuan Gong. 2015. 'Biocompatible and Antifouling Coating of Cell Membrane Phosphorylcholine and Mussel Catechol Modified Multi-Arm PEGs'. Journal of Materials Chemistry B 3 (11): 2350–61. https://doi.org/10.1039/c4tb02140a.

Day, Rachael A. et al. 2020. "Systematic Study of Perfluorocarbon Nanoemulsions Stabilized by Polymer Amphiphiles." ACS Applied Materials and Interfaces 12(35): 38887–98.

Diaz-Dussan, Diana, Yi Yang Peng, Piyush Kumar, and Ravin Narain. 2020. "Oncogenic Epidermal Growth Factor Receptor Silencing in Cervical Carcinoma Mediated by Dynamic Sugar-Benzoxaborole Polyplexes." ACS Macro Letters 9(10): 1464–70. https://pubs.acs.org/doi/full/10.1021/acsmacrolett.0c00599

Dong, Dianyu et al. 2022. "High-Strength and Fibrous Capsule–Resistant Zwitterionic Elastomers." Science Advances 7(1): eabc5442. https://doi.org/10.1126/sciadv.abc5442.

Dong, Ting, and Thomas J. McCarthy. 2017. "Superhydrophobic, Low-Hysteresis Patterning Chemistry for Water-Drop Manipulation." ACS Applied Materials and Interfaces 9(47): 41126–30. https://pubs.acs.org/doi/full/10.1021/acsami.7b15739

Dunbar, Cynthia E. et al. 2018. "Gene Therapy Comes of Age." Science 359(6372): eaan4672.

Elizabeth Welch, M., Youyong Xu, Hongjun Chen, Norah Smith, Michele E. Tague, Héctor D. Abruña, Barbara Baird, and Christopher K. Ober. 2012. 'Polymer Brushes as Functional, Patterned Surfaces for Nanobiotechnology'. Journal of Photopolymer Science and Technology 25 (1): 53–56. https://doi.org/10.2494/PHOTOPOLYMER.25.53.

Erk, Kendra A., Kevin J. Henderson, and Kenneth R. Shull. 2010. 'Strain Stiffening in Synthetic and Biopolymer Networks'. Biomacromolecules 11 (5): 1358–63. https://doi.org/10.1021/BM100136Y.

Estabrook, Daniel A, Amanda F Ennis, Rachael A Day, and Ellen M Sletten. 2019. "Controlling Nanoemulsion Surface Chemistry with Poly(2-Oxazoline) Amphiphiles." Chemical Science 10(14): 3994–4003. http://dx.doi.org/10.1039/C8SC05735D.

Estabrook, Daniel A., Rachael A. Day, and Ellen M. Sletten. 2021. "Redox-Responsive Gene Delivery from Perfluorocarbon Nanoemulsions through Cleavable Poly(2-oxazoline) Surfactants." Angewandte Chemie 133(32): 17502–7.

Etayash, Hashem, and Robert E W Hancock. 2021. "Host Defense Peptide-Mimicking Polymers and Polymeric-Brush-Tethered Host Defense Peptides: Recent Developments, Limitations, and Potential Success." Pharmaceutics 13(11).

Fernandez-Castano Romera, Marcos, René P. M. Lafleur, Clément Guibert, Ilja K. Voets, Cornelis Storm, and Rint P. Sijbesma. 2017. 'Strain Stiffening Hydrogels through Self-Assembly and Covalent Fixation of Semi-Flexible Fibers'. Angewandte Chemie 129 (30): 8897–8901. https://doi.org/10.1002/ANGE.201704046.

Fu, Changkui et al. 2020a. "Low-Fouling Fluoropolymers for Bioconjugation and In Vivo Tracking." Angewandte Chemie 132(12): 4759–65. https://onlinelibrary.wiley.com/doi/full/10.1002/ange.201914119

Fujii, Sayaka et al. 2022. "Preparation of Biocompatible Poly(2-(Methacryloyloxy)Ethyl Phosphorylcholine) Hollow Particles Using Silica Particles as a Template." Langmuir. https://pubs.acs.org/doi/full/10.1021/acs.langmuir.2c00423

Gao, Jinbiao et al. 2019. "Photothermal-Enhanced Phase-Transition Nanodroplets for Ultrasound-Mediated Diagnosis and Gene Transfection." ACS Biomaterials Science and Engineering 5(3): 1366–77.

Gao, Lichao, and Thomas J. McCarthy. 2006. "A Perfectly Hydrophobic Surface (ΘA/ΘR = 180°/180°)." Journal of the American Chemical Society 128(28): 9052–53. https://pubs.acs.org/doi/full/10.1021/ja062943n

Ghobadi, Ahmadreza F. et al. 2016. "Dispersing Zwitterions into Comb Polymers for Nonviral Transfection: Experiments and Molecular Simulation." Biomacromolecules 17(2): 546–57

Ginn, Samantha L. et al. 2018. "Gene Therapy Clinical Trials Worldwide to 2017: An Update." Journal of Gene Medicine 20(5): e3015.

Godbey, W T, Kenneth K Wu, and Antonios G Mikos. 1998. "Size Matters : Molecular Weight Affects the Efficiency of Poly (Ethylenimine) as a Gene Delivery Vehicle." Journal of Biomedical Materials Research 45(3): 268–75. https://onlinelibrary.wiley.com/doi/10.1002/(SICI)1097-4636(19990605)45:3%3C268::AID-JBM15%3E3.0.CO;2-Q

Gudipati, Chakravarthy S., C. Michael Creenlief, Jeremiah A. Johnson, Pornpimol Prayoncpan, and Karen L. Wooley. 2004. 'Hyperbranched Fluoropolymer and Linear Poly(Ethylene Glycol) Based Amphiphilic Crosslinked Networks as Efficient Antifouling Coatings: An Insight into the Surface Compositions, Topographies, and Morphologies'. Journal of Polymer Science, Part A: Polymer Chemistry 42 (24): 6193–6208. https://doi.org/10.1002/POLA.20466.

Han, Lu, Cui Tang, and Chunhua Yin. 2013. "Effect of Binding Affinity for SiRNA on the in Vivo Antitumor Efficacy of Polyplexes." Biomaterials 34(21): 5317–27.

Hemp, Sean T. et al. 2012. "Phosphonium-Containing Diblock Copolymers for Enhanced Colloidal Stability and Efficient Nucleic Acid Delivery." Biomacromolecules 13(8): 2439–45. https://pubs.acs.org/doi/full/10.1021/bm300689f

Higaki, Yuji et al. 2017. "Effect of Charged Group Spacer Length on Hydration State in Zwitterionic Poly(Sulfobetaine) Brushes." Langmuir 33(34): 8404–12. https://pubs.acs.org/doi/full/10.1021/acs.langmuir.7b01935

Hill, Lydia R. St., John W. Craft, Pawilai Chinwangso, Hung Vu Tran, Maria D. Marquez, and T. Randall Lee. 2021. 'Antifouling Coatings Generated from Unsymmetrical Partially Fluorinated Spiroalkanedithiols'. ACS Applied Bio Materials 4 (2): 1563–72. https://doi.org/10.1021/acsabm.0c01409.

Hill, Megan R., R. Nicholas Carmean, and Brent S. Sumerlin. 2015. "Expanding the Scope of RAFT Polymerization: Recent Advances and New Horizons." Macromolecules 48(16): 5459–69.

Holmlin, R. Erik, Xiaoxi Chen, Robert G. Chapman, Shuichi Takayama, and George M. Whitesides. 2001. 'Zwitterionic SAMs That Resist Nonspecific Adsorption of Protein from Aqueous Buffer'. Langmuir 17 (9): 2841–50. https://doi.org/10.1021/la0015258.

Honda, Koji, Hirohiko Yakabe, Tomoyuki Koga, Sono Sasaki, Osami Sakata, Hideyuki Otsuka, and Atsushi Takahara Ãy. 2005. 'Molecular Aggregation Structure of Poly(Fluoroalkyl Acrylate) Thin Films Evaluated by Synchrotron-Sourced Grazing-Incidence X-Ray Diffraction'. Chemistry Letters 34 (7): 1024–25. https://doi.org/10.1246/cl.2005.1024.

Honda, Koji, Masamichi Morita, Hideyuki Otsuka, and Atsushi Takahara. 2005. "Molecular Aggregation Structure and Surface Properties of Poly(Fluoroalkyl Acrylate) Thin Films." Macromolecules 38(13): 5699–5705. https://pubs.acs.org/doi/full/10.1021/ma050394k

Hoshyar, Nazanin, Samantha Gray, Hongbin Han, and Gang Bao. 2016. "The Effect of Nanoparticle Size on in Vivo Pharmacokinetics and Cellular Interaction." Nanomedicine 11(6): 673. /pmc/articles/PMC5561790/

Hu, Gaojie, and Todd Emrick. 2016. "Functional Choline Phosphate Polymers." Journal of the American Chemical Society 138(6): 1828–31.

Hu, Gaojie, Sangram S. Parelkar, and Todd Emrick. 2015. "A Facile Approach to Hydrophilic, Reverse Zwitterionic, Choline Phosphate Polymers." Polymer Chemistry 6(4): 525–30.

Hu, Huamin et al. 2019. "Perfluorocarbon-Based O2 Nanocarrier for Efficient Photodynamic Therapy." Journal of Materials Chemistry B 7(7): 1116–23. https://pubs.rsc.org/en/content/articlehtml/2019/tb/c8tb01844h

Huang, Hao et al. 2021. "Strong Surface Hydration and Salt Resistant Mechanism of a New Nonfouling Zwitterionic Polymer Based on Protein Stabilizer TMAO." Journal of the American Chemical Society 143(40): 16786–95. https://pubs.acs.org/doi/full/10.1021/jacs.1c08280

Huang, Yuran et al. 2017a. "Polymer-Stabilized Perfluorobutane Nanodroplets for Ultrasound Imaging Agents." Journal of the American Chemical Society 139(1): 15–18. https://pubs.acs.org/doi/full/10.1021/jacs.6b08800

Imbesi, Philip M., John A. Finlay, Nick Aldred, Michael J. Eller, Simcha E. Felder, Kevin A. Pollack, Alexander T. Lonnecker, et al. 2012. 'Targeted Surface Nanocomplexity: Two-Dimensional Control over the Composition, Physical Properties and Anti-Biofouling Performance of Hyperbranched Fluoropolymer–Poly(Ethylene Glycol) Amphiphilic Crosslinked Networks'. Polymer Chemistry 3 (11): 3121–31. https://doi.org/10.1039/C2PY20317K.

Inoue, Yuuki et al. 2005. "Synthesis of Sequence-Controlled Copolymers from Extremely Polar and Apolar Monomers by Living Radical Polymerization and Their Phase-Separated Structures." Journal of Polymer Science Part A: Polymer Chemistry 43(23): 6073–83. https://doi.org/10.1002/pola.21095.

Ishihara, K., and N. Nakabayashi. 1996. "Preparation of Phospholipid Polymers and Their Properties as Polymer Hydrogel Membranes." Proceedings of the Controlled Release Society 22(23): 787–88.

Ishihara, Kazuhiko. 2015. "Highly Lubricated Polymer Interfaces for Advanced Artificial Hip Joints through Biomimetic Design." Polymer Journal 2015 47:9 47(9): 585–97. https://www.nature.com/articles/pj201545

Jaspers, Maarten, Matthew Dennison, Mathijs F.J. Mabesoone, Frederick C. MacKintosh, Alan E. Rowan, and Paul H.J. Kouwer. 2014. 'Ultra-Responsive Soft Matter from Strain-Stiffening Hydrogels'. Nature Communications 2014 5:1 5 (1): 1–8. https://doi.org/10.1038/ncomms6808.

Jesmer, Alexander H. et al. 2021. "Graft-Then-Shrink: Simultaneous Generation of Antifouling Polymeric Interfaces and Localized Surface Plasmon Resonance Biosensors." ACS Applied Materials and Interfaces 13(44): 52362–73. https://pubs.acs.org/doi/full/10.1021/acsami.1c14930

Ji, Jian, Jinhong Fu, and Jicong Shen. 2006. 'Fabrication of a Superhydrophobic Surface from the Amplified Exponential Growth of a Multilayer'. Advanced Materials 18 (11): 1441–44. https://doi.org/10.1002/ADMA.200502453.

Jiang, Yaming, Timothy P. Lodge, and Theresa M. Reineke. 2018. "Packaging PDNA by Polymeric ABC Micelles Simultaneously Achieves Colloidal Stability and Structural Control." Journal of the American Chemical Society 140(35): 11101–11.

Jun, Ma, Chong Cheng, Guorong Sun, and Karen L. Wooley. 2008. "Well-Defined Polymers Bearing Pendent Alkene Functionalities via Selective RAFT Polymerization." Macromolecules 41(23): 9080–89. https://pubs.acs.org/doi/full/10.1021/ma802057u

Kasper, Jonathan J et al. 2016. "A Library of Fluorinated Electrophiles for Chemical Tagging and Materials Synthesis." The Journal of Organic Chemistry 81(17): 8095–8103. https://doi.org/10.1021/acs.joc.6b01572.

Kim, Gun et al. 2019. "High-Intensity Focused Ultrasound-Induced Mechanochemical Transduction in Synthetic Elastomers." Proceedings of the National Academy of Sciences of the United States of America 116(21): 10214–22. www.pnas.org/cgi/doi/10.1073/pnas.1901047116

Kim, Kyoungnam et al. 2019. "Controlling Complexation/Decomplexation and Sizes of Polymer-Based Electrostatic PDNA Polyplexes Is One of the Key Factors in Effective Transfection." Colloids and Surfaces B: Biointerfaces 184: 110497.

Kobayashi, Motoyasu et al. 2012. "Wettability and Antifouling Behavior on the Surfaces of Superhydrophilic Polymer Brushes." Langmuir 28(18): 7212–22.

Kotterman, Melissa A, Thomas W Chalberg, and David V Schaffer. 2015. "Viral Vectors for Gene Therapy: Translational and Clinical Outlook." Annual Review of Biomedical Engineering 17(1): 63–89. http://www.annualreviews.org/doi/10.1146/annurev-bioeng-071813-104938.

Kumar, Ramya et al. 2021. "Polymeric Delivery of Therapeutic Nucleic Acids." Chemical Reviews 121(18): 11527–652.

Kumarasamy, Elango et al. 2020. "Ionic Fluorogels for Remediation of Per-and Polyfluorinated Alkyl Substances from Water." ACS Central Science 6(4): 487–92. https://pubs.acs.org/doi/full/10.1021/acscentsci.9b01224

Lee, I. Ning et al. 2018. "Photoresponsive Hydrogels with Photoswitchable Mechanical Properties Allow Time-Resolved Analysis of Cellular Responses to Matrix Stiffening." ACS Applied Materials and Interfaces 10(9): 7765–76. https://pubs.acs.org/doi/full/10.1021/acsami.7b18302

Letteri, Rachel A et al. 2017. "Forming Sticky Droplets from Slippery Polymer Zwitterions." Advanced Materials 29(38): 1702921. https://onlinelibrary.wiley.com/doi/full/10.1002/adma.201702921

Letteri, Rachel A. 2016. Doctoral Dissertations "Functional Hydrophilic Polymers for Solution Assembly and Non-Viral Gene Therapy." https://scholarworks.umass.edu/dissertations_2/751

Lewoczko, Evan M. et al. 2021. “Effects of N-Substituents on the Solution Behavior of Poly(Sulfobetaine Methacrylate)s in Water: Upper and Lower Critical Solution Temperature Transitions.” ACS Applied Polymer Materials 3(2): 867–78. https://pubs.acs.org/doi/full/10.1021/acsapm.0c01191

Li, Bowen et al. 2018. “Revealing the Immunogenic Risk of Polymers.” Angewandte Chemie International Edition 57(42): 13873–76. https://onlinelibrary.wiley.com/doi/full/10.1002/anie.201808615

Li, Bowen et al. 2019. “Trimethylamine N-Oxide–Derived Zwitterionic Polymers: A New Class of Ultralow Fouling Bioinspired Materials.” Science Advances 5(6): eaaw9562. http://advances.sciencemag.org/content/5/6/eaaw9562.abstract.

Li, Haibo et al. 2013. “Poly(2-Deoxy-2-Methacrylamido Glucopyranose)-b - Poly(Methacrylate Amine)s: Optimization of Diblock Glycopolycations for Nucleic Acid Delivery.” ACS Macro Letters 2(3): 230–35. https://pubs.acs.org/doi/full/10.1021/mz300660t

Liu, Shuai et al. 2021. “Zwitterionic Phospholipidation of Cationic Polymers Facilitates Systemic MRNA Delivery to Spleen and Lymph Nodes.” Journal of the American Chemical Society 143(50): 21321–30.

Liu, Yanna, Mies J van Steenbergen, Zhiyuan Zhong, Sabrina Oliveira, Wim E Hennink, and Cornelus F van Nostrum. 2020. ‘Dithiolane-Crosslinked Poly(ε-Caprolactone)-Based Micelles: Impact of Monomer Sequence, Nature of Monomer, and Reducing Agent on the Dynamic Crosslinking Properties’. Macromolecules 53 (16): 7009–24. https://doi.org/10.1021/acs.macromol.0c01031.

Lohmann, Rainer, Ian T Cousins, Jamie C DeWitt, et al. 2020. “Are Fluoropolymers Really of Low Concern for Human and Environmental Health and Separate from Other PFAS?” Environmental Science & Technology 54(20): 12820–28. https://doi.org/10.1021/acs.est.0c03244.

Lowe, Sean, Neil M. O’Brien-Simpson, and Luke A. Connal. 2014. ‘Antibiofouling Polymer Interfaces: Poly(Ethylene Glycol) and Other Promising Candidates’. Polymer Chemistry 6 (2): 198–212. https://doi.org/10.1039/C4PY01356E.

Lutolf, M. P., and J. A. Hubbell. 2005. ‘Synthetic Biomaterials as Instructive Extracellular Microenvironments for Morphogenesis in Tissue Engineering’. Nature Biotechnology 2005 23:1 23 (1): 47–55. https://doi.org/10.1038/nbt1055.

Lv, Jia et al. 2015. “Fluorination on Polyethylenimine Allows Efficient 2D and 3D Cell Culture Gene Delivery.” Journal of Materials Chemistry B 3(4): 642–50.

Lv, Jia, and Yiyun Cheng. 2021. “Fluoropolymers in Biomedical Applications: State-of-the-Art and Future Perspectives.” Chemical Society Reviews 50(9): 5435–67.

Maan, Anna M C, Anton H Hofman, Wiebe M de Vos, and Marleen Kamperman. 2020. “Recent Developments and Practical Feasibility of Polymer-Based Antifouling Coatings.” Advanced Functional Materials 30(32): 2000936. https://doi.org/10.1002/adfm.202000936.

Machtakova, M, H Therien-Aubin, and K Landfester. 2022. “Polymer Nano-Systems for the Encapsulation and Delivery of Active Biomacromolecular Therapeutic Agents.” CHEMICAL SOCIETY REVIEWS 51(1): 128–52.

Malloggi, C. et al. 2015. “Comparative Evaluation and Optimization of Off-the-Shelf Cationic Polymers for Gene Delivery Purposes.” Polymer Chemistry 6(35): 6325–39.

Matyjaszewski, Krzysztof. 2012. “Atom Transfer Radical Polymerization (ATRP): Current Status and Future Perspectives.” Macromolecules 45(10): 4015–39. https://pubs.acs.org/doi/full/10.1021/ma3001719

Meiboom, S, and D Gill. 1958. “Modified Spin-Echo Method for Measuring Nuclear Relaxation Times.” Review of Scientific Instruments 29(8): 688–91. https://doi.org/10.1063/1.1716296.

Middleton, L. Robert et al. 2015. “Hierarchical Acrylic Acid Aggregate Morphologies Produce Strain-Hardening in Precise Polyethylene-Based Copolymers.” Macromolecules 48(11): 3713–24. https://pubs.acs.org/doi/abs/10.1021/acs.macromol.5b00797

Mol, Nico J de, and Marcel J E Fischer. 2010. Surface Plasmon Resonance: Methods and Protocols. Life Sciences. https://doi.org/10.1007/978-1-60761-670-2.

Monnery, Bryn D. 2021. “Polycation-Mediated Transfection: Mechanisms of Internalization and Intracellular Trafficking.” Biomacromolecules 22(10): 4060–83.

Moro, Toru et al. 2004. “Surface Grafting of Artificial Joints with a Biocompatible Polymer for Preventing Periprosthetic Osteolysis.” Nature Materials 2004 3:11 3(11): 829–36. https://www.nature.com/articles/nmat1233

Motte, Stéphanie, and Laura J. Kaufman. 2013. ‘Strain Stiffening in Collagen I Networks’. Biopolymers 99 (1): 35–46. https://doi.org/10.1002/BIP.22133.

Mukai, Masaru et al. 2020. “Synthesis and Hydration Behavior of a Hydrolysis-Resistant Quasi-Choline Phosphate Zwitterionic Polymer.” Biomacromolecules 21(6): 2125–31. https://doi.org/10.1021/acs.biomac.0c00120.

Mukai, Masaru, Yuji Higaki, Tomoyasu Hirai, and Atsushi Takahara. 2018. “Separation of Endo-Cyclic 2-Methacryloyloxyethyl Choline Phosphate by Anion Exchange Approach.” Chemistry Letters 47(12): 1509–11.

Naficy, Sina, Hugh R. Brown, Joselito M. Razal, Geoffrey M. Spinks, and Philip G. Whitten. 2011. ‘Progress Toward Robust Polymer Hydrogels’. Australian Journal of Chemistry 64 (8): 1007–25. https://doi.org/10.1071/CH11156.

Nia, Hadi T., Lance L. Munn, and Rakesh K. Jain. 2020. “Physical Traits of Cancer.” Science 370(6516). https://www.science.org/doi/abs/10.1126/science.aaz0868

Pagaduan, James Nicolas, Nicholas Hight-Huf, Avdhoot Datar, Yehiel Nagar, Michael Barnes, Doron Naveh, Ashwin Ramasubramaniam, Reika Katsumata, and Todd Emrick. 2021. 'Electronic Tuning of Monolayer Graphene with Polymeric "Zwitterists"'. ACS Nano 15 (2): 2762–70. https://doi.org/10.1021/acsnano.0c08624.

Pardi, Norbert, Michael J. Hogan, Frederick W. Porter, and Drew Weissman. 2018. "MRNA Vaccines-a New Era in Vaccinology." Nature Reviews Drug Discovery 17(4): 261–79. http://dx.doi.org/10.1038/nrd.2017.243.

Parelkar, Sangram S. et al. 2014. "Polymer-Peptide Delivery Platforms: Effect of Oligopeptide Orientation on Polymer-Based DNA Delivery." Biomacromolecules 15(4): 1328–36.

Parelkar, Sangram S, Delphine Chan-seng, and Todd Emrick. 2011. "Reconfiguring Polylysine Architectures for Controlling Polyplex Binding and Non-Viral Transfection." Biomaterials 32(9): 2432–44. http://dx.doi.org/10.1016/j.biomaterials.2010.12.004.

Patra, Diptendu et al. 2022. "Unique Random-Block Polymer Architecture for Site-Specific Mitochondrial Sequestration-Aided Effective Chemotherapeutic Delivery and Enhanced Fluorocarbon Segmental Mobility-Facilitated 19F Magnetic Resonance Imaging." Biomacromolecules. https://pubs.acs.org/doi/full/10.1021/acs.biomac.2c00188

Perrier, Sébastien. 2017. "50th Anniversary Perspective: RAFT Polymerization - A User Guide." Macromolecules 50(19): 7433–47.

Piechocka, Izabela K., Karin A. Jansen, Chase P. Broedersz, Nicholas A. Kurniawan, Fred C. MacKintosh, and Gijsje H. Koenderink. 2016. 'Multi-Scale Strain-Stiffening of Semiflexible Bundle Networks'. Soft Matter 12 (7): 2145–56. https://doi.org/10.1039/C5SM01992C.

Piotrowski-Daspit, Alexandra S., Amy C. Kauffman, Laura G. Bracaglia, and W. Mark Saltzman. 2020. "Polymeric Vehicles for Nucleic Acid Delivery." Advanced Drug Delivery Reviews 156: 119–32. https://doi.org/10.1016/j.addr.2020.06.014.

Pollack, Kevin A, Philip M Imbesi, Jeffery E Raymond, and Karen L Wooley. 2014. 'Hyperbranched Fluoropolymer-Polydimethylsiloxane-Poly(Ethylene Glycol) Cross-Linked Terpolymer Networks Designed for Marine and Biomedical Applications: Heterogeneous Nontoxic Antibiofouling Surfaces'. ACS Applied Materials & Interfaces 6 (21): 19265–74. https://doi.org/10.1021/am505296n.

Quagliarini, Erica et al. 2021. "Microfluidic Formulation of DNA-Loaded Multicomponent Lipid Nanoparticles for Gene Delivery." Pharmaceutics 2021, Vol. 13, Page 1292 13(8): 1292. https://www.mdpi.com/1999-4923/13/8/1292/htm

Ralls, Alessandro, Pankaj Kumar, Mano Misra, and Pradeep L. Menezes. 2020. "Material Design and Surface Engineering for Bio-Implants." JOM 72(2): 684–96. https://link.springer.com/article/10.1007/s11837-019-03687-2

Ramirez, Ashley L.Black, Zachary S. Kean, Joshua A. Orlicki, Mangesh Champhekar, Sarah M. Elsakr, Wendy E. Krause, and Stephen L. Craig. 2013. 'Mechanochemical Strengthening of a Synthetic Polymer in Response to Typically Destructive Shear Forces'. Nature Chemistry 2013 5:9 5 (9): 757–61. https://doi.org/10.1038/nchem.1720.

Richbourg, Nathan R., Akhila Ravikumar, and Nicholas A. Peppas. 2021. "Solute Transport Dependence on 3D Geometry of Hydrogel Networks". Macromolecular Chemistry and Physics 222 (16): 2100138. https://doi.org/10.1002/MACP.202100138.

Ripps, Harris, and Wen Shen. 2012. "Review: Taurine: A 'Very Essential' Amino Acid." Molecular Vision 18: 2686. /pmc/articles/PMC3501277/

Ritt, Nicolas, Simone Berger, Ernst Wagner, and Rudolf Zentel. 2020. "Versatile, Multifunctional Block Copolymers for the Self-Assembly of Well-Defined, Nontoxic PDNA Polyplexes." ACS Applied Polymer Materials 2(12): 5469–81. https://pubs.acs.org/doi/full/10.1021/acsapm.0c00818

Sae-ung, Pornpen et al. 2017. "Antifouling Stripes Prepared from Clickable Zwitterionic Copolymers." Langmuir 33(28): 7028–35. https://doi.org/10.1021/acs.langmuir.7b01431.

Salameh, Janelle W. et al. 2020. "Polymer-Mediated Gene Therapy: Recent Advances and Merging of Delivery Techniques." Wiley Interdisciplinary Reviews: Nanomedicine and Nanobiotechnology 12(2): e1598. https://onlinelibrary.wiley.com/doi/full/10.1002/wnan.1598

Santa Chalarca, Cristiam F et al. 2018. "Building Supracolloidal Fibers from Zwitterion-Stabilized Adhesive Emulsions." Advanced Functional Materials 28(45): 1804325. https://onlinelibrary.wiley.com/doi/full/10.1002/adfm.201804325

Santa Chalarca, Cristiam F, and Todd Emrick. 2017. "Reactive Polymer Zwitterions: Sulfonium Sulfonates." Journal of Polymer Science Part A: Polymer Chemistry 55(1): 83–92. https://doi.org/10.1002/pola.28359.

Scheutz, Georg M., Jonathan L. Rowell, Fu Sheng Wang, Khalil A. Abboud, Chi How Peng, and Brent S. Sumerlin. 2020. 'Synthesis of Functional 1,2-Dithiolanes from 1,3-Bis-: Tert -Butyl Thioethers'. Organic and Biomolecular Chemistry 18 (33): 6509–13. https://doi.org/10.1039/d0ob01577f.

Scheutz, Georg M., Jonathan L. Rowell, S. Tori Ellison, John B. Garrison, Thomas E. Angelini, and Brent S. Sumerlin. 2020. 'Harnessing Strained Disulfides for Photocurable Adaptable Hydrogels'. Macromolecules 53 (10): 4038–46. https://doi.org/10.1021/acs.macromol.0c00604.

Schild, H. G. 1992. 'Poly(N-Isopropylacrylamide): Experiment, Theory and Application'. Progress in Polymer Science 17 (2): 163–249. https://doi.org/10.1016/0079-6700(92)90023-R.

Schlenoff, Joseph B. 2014. "Zwitteration: Coating Surfaces with Zwitterionic Functionality to Reduce Nonspecific Adsorption." Langmuir 30(32): 9625–36.

Schönemann, Eric et al. 2020. “Synthesis of Novel Sulfobetaine Polymers with Differing Dipole Orientations in Their Side Chains, and Their Effects on the Antifouling Properties.” Macromolecular Rapid Communications 41(1): 1900447. https://onlinelibrary.wiley.com/doi/full/10.1002/marc.201900447

Sedlacek, Ondrej et al. 2020. “Fluorinated Water-Soluble Poly(2-Oxazoline)s as Highly Sensitive 19F MRI Contrast Agents.” Macromolecules 53(15): 6387–95. https://doi.org/10.1021/acs.macromol.0c01228.

Shah, Rahul R., David Merreceyes, Marc Husemann, Ian Rees, Nicholas L. Abbott, Craig J. Hawker, and James L. Hedrick. 2000. “Using Atom Transfer Radical Polymerization to Amplify Monolayers of Initiators Patterned by Microcontact Printing into Polymer Brushes for Pattern Transfer.” Macromolecules 33(2): 597–605. https://pubs.acs.org/doi/full/10.1021/ma991264c

Shirley, Jamie L, Ype P De Jong, Cox Terhorst, and Roland W Herzog. 2020. “Immune Responses to Viral Gene Therapy Vectors.” Molecular Therapy 28: 709–22. https://doi.org/10.1016/j.ymthe.2020.01.001

Si, Yifan, Zhichao Dong, and Lei Jiang. 2018. “Bioinspired Designs of Superhydrophobic and Superhydrophilic Materials.” ACS Central Science 4(9): 1102–12. https://pubs.acs.org/doi/full/10.1021/acscentsci.8b00504

Slaughter, Brandon V., Shahana S. Khurshid, Omar Z. Fisher, Ali Khademhosseini, and Nicholas A. Peppas. 2009. ‘Hydrogels in Regenerative Medicine’. Advanced Materials 21 (32–33): 3307–29. https://doi.org/10.1002/ADMA.200802106.

Smith, Adam E. et al. 2011. “Diblock Glycopolymers Promote Colloidal Stability of Polyplexes and Effective PDNA and SiRNA Delivery under Physiological Salt and Serum Conditions.” Biomacromolecules 12(8): 3015–22. https://pubs.acs.org/doi/full/10.1021/bm200643c

Srinivas, Anupama Rao Gulur et al. 2021. “Polymer Brush Functionalization of Polyurethane Tunable Nanopores for Resistive Pulse Sensing.” ACS Applied Polymer Materials 3(1): 279–89. https://pubs.acs.org/doi/full/10.1021/acsapm.0c01087

Srivastava, Arvind, Krishna M.G. Mallela, Nandkumar Deorkar, and Ger Brophy. 2021. “Manufacturing Challenges and Rational Formulation Development for AAV Viral Vectors.” Journal of Pharmaceutical Sciences 110(7): 2609–24.

Storm, Cornelis, Jennifer J. Pastore, F. C. MacKintosh, T. C. Lubensky, and Paul A. Janmey. 2005. ‘Nonlinear Elasticity in Biological Gels’. Nature 2005 435:7039 435 (7039): 191–94. https://doi.org/10.1038/nature03521.

Sun, Wei, Wenying Liu, Zhaoqiang Wu, and Hong Chen. 2020. ‘Chemical Surface Modification of Polymeric Biomaterials for Biomedical Applications’. Macromolecular Rapid Communications 41 (8): 1900430. https://doi.org/10.1002/MARC.201900430.

Tan, Xiao et al. 2021. “Amphiphilic Perfluoropolyether Copolymers for the Effective Removal of Polyfluoroalkyl Substances from Aqueous Environments.” Macromolecules 54(7): 3447–57. https://pubs.acs.org/doi/full/10.1021/acs.macromol.1c00096

Tan, Xiao et al. 2022. “Revealing the Molecular-Level Interactions between Cationic Fluorinated Polymer Sorbents and the Major PFAS Pollutant PFOA.” Macromolecules 55(3): 1077–87. https://pubs.acs.org/doi/full/10.1021/acs.macromol.1c02435

Telford, A. M., B. S. Hawkett, C. Such, and C. Neto. 2013. “Mimicking the Wettability of the Rose Petal Using Self-Assembly of Waterborne Polymer Particles.” Chemistry of Materials 25(17): 3472–79. https://pubs.acs.org/doi/full/10.1021/cm4016386

Tenchov, Rumiana, Robert Bird, Allison E. Curtze, and Qiongqiong Zhou. 2021. “Lipid Nanoparticles from Liposomes to MRNA Vaccine Delivery, a Landscape of Research Diversity and Advancement.” ACS Nano 15(11): 16982–15.

Tennie, Iris K., and Andreas F.M. Kilbinger. 2020. “Polymeric 19F MRI Contrast Agents Prepared by Ring-Opening Metathesis Polymerization/Dihydroxylation.” Macromolecules 53(23): 10386–96.

Tibbitt, Mark W., and Kristi S. Anseth. 2009. ‘Hydrogels as Extracellular Matrix Mimics for 3D Cell Culture’. Biotechnology and Bioengineering 103 (4): 655–63. https://doi.org/10.1002/BIT.22361.

Tirotta, Ilaria et al. 2015. “19F Magnetic Resonance Imaging (MRI): From Design of Materials to Clinical Applications.” Chemical Reviews 115(2): 1106–29. https://pubs.acs.org/doi/full/10.1021/cr500286d

Tran, Yen H., Matthew J. Rasmuson, Todd Emrick, John Klier, and Shelly R. Peyton. 2017. ‘Strain-Stiffening Gels Based on Latent Crosslinking’. Soft Matter 13 (47): 9007–14. https://doi.org/10.1039/C7SM01888F.

United States Environmental Protection Agency. “Basic Information on PFAS.” United States Environmental Protection Agency. https://www.epa.gov/pfas/basic-information-pfas.

Waehler, Reinhard, Stephen J. Russell, and David T. Curiel. 2007. “Engineering Targeted Viral Vectors for Gene Therapy.” Nature Reviews Genetics 8(8): 573–87.

Wang, Junpeng, Ilya Piskun, and Stephen L. Craig. 2015. ‘Mechanochemical Strengthening of a Multi-Mechanophore Benzocyclobutene Polymer’. ACS Macro Letters 4 (8): 834–37. https://pubs.acs.org/doi/full/10.1021/acsmacrolett.5b00440

Wang, Liming, Jingjing Wei, and Zhaohui Su. 2011. ‘Fabrication of Surfaces with Extremely High Contact Angle Hysteresis from Polyelectrolyte Multilayer’. Langmuir 27 (24): 15299–304. https://pubs.acs.org/doi/full/10.1021/la2039448

Wang, Mingming, Hongmei Liu, Lei Li, and Yiyun Cheng. 2014. "A Fluorinated Dendrimer Achieves Excellent Gene Transfection Efficacy at Extremely Low Nitrogen to Phosphorus Ratios." Nature Communications 2014 5:1 5(1): 1–8. https://www.nature.com/articles/ncomms4053

Wang, Wenliang et al. 2016. "Tailor-Made PH-Responsive Poly(Choline Phosphate) Prodrug as a Drug Delivery System for Rapid Cellular Internalization." Biomacromolecules 17(6): 2223–32. https://doi.org/10.1021/acs.biomac.6b00455.

Wang, Xinyu et al. 2020. "In Vivo Tracking of Fluorinated Polypeptide Gene Carriers by Positron Emission Tomography Imaging." ACS applied materials & interfaces 12(41): 45763–71.

Wang, Yiming, Zhi Xu, Matija Lovrak, Vincent A. A. Sage, Kai Zhang, Xuhong Guo, Rienk Eelkema, Eduardo Mendes, and Jan H. Esch. 2020. 'Biomimetic Strain-Stiffening Self-Assembled Hydrogels'. Angewandte Chemie 132 (12): 4860–64. https://doi.org/10.1002/ANGE.201911364.

Ward, Sarah M, Matthew Skinner, Banishree Saha, and Todd Emrick. 2018. "Polymer–Temozolomide Conjugates as Therapeutics for Treating Glioblastoma." Molecular Pharmaceutics 15(11): 5263–76. https://doi.org/10.1021/acs.molpharmaceut.8b00766.

Wijekoon, Asanka, Natalie Fountas-Davis, and Nic D. Leipzig. 2013. "Fluorinated Methacrylamide Chitosan Hydrogel Systems as Adaptable Oxygen Carriers for Wound Healing." Acta Biomaterialia 9(3): 5653–64.

Willis-Fox, Niamh, Etienne Rognin, Talal A. Aljohani, and Ronan Daly. 2018. 'Polymer Mechanochemistry: Manufacturing Is Now a Force to Be Reckoned With'. Chem 4 (11): 2499–2537. https://doi.org/10.1016/J.CHEMPR.2018.08.001.

Wu, Chuanfeng, and Cynthia E. Dunbar. 2011. "Stem Cell Gene Therapy: The Risks of Insertional Mutagenesis and Approaches to Minimize Genotoxicity." Frontiers of Medicine 2011 5:4 5(4): 356–71. https://link.springer.com/article/10.1007/s11684-011-0159-1 (February 6, 2022).

Wu, Connie, Jiahe Li, Wade Wang, and Paula T. Hammond. 2018. "Rationally Designed Polycationic Carriers for Potent Polymeric SiRNA-Mediated Gene Silencing." ACS Nano 12(7): 6504–14.

Wu, Hai Xia, Xiao Hong Zhang, Lin Huang, Lu Fang Ma, and Chuan Jun Liu. 2018. "Diblock Polymer Brush (PHEAA-b-PFMA): Microphase Separation Behavior and Anti-Protein Adsorption Performance". Langmuir 34 (37): 11101–9. https://pubs.acs.org/doi/full/10.1021/acs.langmuir.8b02584

Wu, Hai-Xia, Lei Tan, Mei-Yan Yang, Chuan-Jun Liu, and Ren-Xi Zhuo. 2015. 'Protein-Resistance Performance of Amphiphilic Copolymer Brushes Consisting of Fluorinated Polymers and Polyacrylamide Grafted from Silicon Surfaces'. RSC Advances 5 (16): 12329–37. https://doi.org/10.1039/c4ra16036c.

Wu, Tao, Kirill Efimenko, and Jan Genzer. 2002. “Combinatorial Study of the Mushroom-to-Brush Crossover in Surface Anchored Polyacrylamide”. Journal of the American Chemical Society 124 (32): 9394–95. https://pubs.acs.org/doi/full/10.1021/ja027412n

Wu, Ting, Longhai Wang, Shenggang Ding, and Yezi You. 2017. “Fluorinated PEG-Polypeptide Polyplex Micelles Have Good Serum-Resistance and Low Cytotoxicity for Gene Delivery.” Macromolecular Bioscience 17(8): 1–8.

Xie, H., J. Wei, and X. Zhang. 2006. ‘Characterisation of Sol-Gel Thin Films by Spectroscopic Ellipsometry’. Journal of Physics: Conference Series 28 (1): 95. https://doi.org/10.1088/1742-6596/28/1/020.

Xie, Qingyi, Jiansen Pan, Chunfeng Ma, and Guangzhao Zhang. 2019. “Dynamic Surface Antifouling: Mechanism and Systems.” Soft Matter 15(6): 1087–1107.

Xing, Cheng Mei, Fan Ning Meng, Miao Quan, Kai Ding, Yuan Dang, and Yong Kuan Gong. 2017. ‘Quantitative Fabrication, Performance Optimization and Comparison of PEG and Zwitterionic Polymer Antifouling Coatings’. Acta Biomaterialia 59: 129–38. https://doi.org/10.1016/j.actbio.2017.06.034.

Xu, Binbin et al. 2017. “Semifluorinated Synergistic Nonfouling/Fouling-Release Surface.” ACS Applied Materials & Interfaces 9(19): 16517–23. https://doi.org/10.1021/acsami.7b03258.

Yan, Wenqing et al. 2019. “Growing Polymer Brushes from a Variety of Substrates under Ambient Conditions by Cu0-Mediated Surface-Initiated ATRP.” ACS Applied Materials and Interfaces 11(30): 27470–77. https://pubs.acs.org/doi/full/10.1021/acsami.9b09529

Yang, Zhimou, Gaolin Liang, Ling Wang, and Bing Xu. 2006. ‘Using a Kinase/Phosphatase Switch to Regulate a Supramolecular Hydrogel and Forming the Supramolecular Hydrogel in Vivo’. Journal of the American Chemical Society 128 (9): 3038–43. https://pubs.acs.org/doi/full/10.1021/ja057412y

Ying, Peiqing, Yong Yu, Gang Jin, and Zulai Tao. 2003. “Competitive Protein Adsorption Studied with Atomic Force Microscopy and Imaging Ellipsometry.” Colloids and Surfaces B: Biointerfaces 32(1): 1–10. https://www.sciencedirect.com/science/article/pii/S0927776502001339.

Yoshikawa, Hiroshi Y., Fernanda F. Rossetti, Stefan Kaufmann, Thomas Kaindl, Jeppe Madsen, Ulrike Engel, Andrew L. Lewis, Steven P. Armes, and Motomu Tanaka. 2011. ‘Quantitative Evaluation of Mechanosensing of Cells on Dynamically Tunable Hydrogels’. Journal of the American Chemical Society 133 (5): 1367–74. https://pubs.acs.org/doi/full/10.1021/ja1060615

Yoshioka, Kyoko, Yukari Sato, Mutsuo Tanaka, Teiichi Murakami, and Osamu Niwa. 2010. ‘Suppression of Non-Specific Adsorption Using Densified Tri(Ethylene Glycol) Alkanethiols: Monolayer Characteristics Evaluated by Electrochemical Measurements’. Analytical Sciences : The International Journal of the Japan Society for Analytical Chemistry 26 (1): 33–37. https://doi.org/10.2116/ANALSCI.26.33.

Yu, Xifei et al. 2013. “ATRP Synthesis of Poly(2-(Methacryloyloxy)Ethyl Choline Phosphate): A Multivalent Universal Biomembrane Adhesive.” Chemical Communications 49(61): 6831–33. https://pubs.rsc.org/en/content/articlehtml/2013/cc/c3cc41895b

Zhang, Cheng et al. 2018. “Elucidating the Impact of Molecular Structure on the 19F NMR Dynamics and MRI Performance of Fluorinated Oligomers.”

Zhang, Cheng et al. 2022. “Biological Utility of Fluorinated Compounds: From Materials Design to Molecular Imaging, Therapeutics and Environmental Remediation.” Chemical Reviews 122(1): 167–208. https://doi.org/10.1021/acs.chemrev.1c00632.

Zhang, Ershuai et al. 2020. “Fouling-Resistant Zwitterionic Polymers for Complete Prevention of Postoperative Adhesion.” Proceedings of the National Academy of Sciences of the United States of America 117(50): 32046–55. https://www.pnas.org/doi/abs/10.1073/pnas.2012491117

Zhang, Xiangyi, and Robert M. Waymouth. 2017. ‘1,2-Dithiolane-Derived Dynamic, Covalent Materials: Cooperative Self-Assembly and Reversible Cross-Linking’. Journal of the American Chemical Society 139 (10): 3822–33. https://pubs.acs.org/doi/full/10.1021/jacs.7b00039

Zheng, Xiajun et al. 2015. “Antifouling Property of Monothiol-Terminated Bottle-Brush Poly(Methylacrylic Acid)-Graft-Poly(2-Methyl-2-Oxazoline) Copolymer on Gold Surfaces.” Journal of Materials Chemistry B 3(9): 1921–30. www.rsc.org/materialsB.

Zhou, Le, Alexandria Triozzi, Marxa Figueiredo, and Todd Emrick. 2021. “Fluorinated Polymer Zwitterions: Choline Phosphates and Phosphorylcholines.” ACS Macro Letters 10(10): 1204–9. https://doi.org/10.1021/acsmacrolett.1c00451 (May 18, 2022).

Zhou, Ling Yan et al. 2020. “Novel Zwitterionic Vectors: Multi-Functional Delivery Systems for Therapeutic Genes and Drugs.” Computational and Structural Biotechnology Journal 18: 1980–99.